UNIVERSITÀ DEGLI STUDI DI MILANO

Scuola di Dottorato in Fisica, Astrofisica e Fisica Applicata

Dipartimento di Fisica

Corso di Dottorato in Fisica, Astrofisica e Fisica Applicata

Ciclo XXXIII

Ab-initio Calculation of the Rates of the Reactions between Volatile Organic Compounds in Wine and Cations for Mass Spectrometry

Settore Scientifico Disciplinare FIS/03

Supervisore: Prof. Nicola Manini

Co-supervisore: Dr. Franco Biasioli

Co-supervisore: Prof. Paolo Piseri

Coordinatore: Prof. Matteo Paris

Tesi di Dottorato di:

Manjeet Kumar

Anno Accademico 2019-2020

External Referees:
Jonathan Beauchamp
Giorgio Benedek

Commission of the final examination:

External Members:
Saskia Van Ruth
Luca Cappellin

Internal Member:
Nicola Manini

Final examination:

Date 18-12-2020

Università degli Studi di Milano, Dipartimento di Fisica, Milano, Italy

Dedicated to my parents

Cover illustration:

Volatile Organic Compounds responsible for producing cork-taint in a bottle of wine.

MIUR subjects:

FIS/03, FIS/07, CHIM/01, CHIM/10

PACS:

82.20.Pm, 33.15.Ms, 31.15.Ar

Abstract

Wine is a complex mixture housing many aroma and flavor compounds giving it a unique texture and bouquet. These volatile organic compounds (VOCs), if present near the sensory threshold limits, may contribute positively to wine quality; however, excessive amounts can detract from quality, and are considered as a fault in wine. It is believed that nearly 10% of the world's wine is affected from various types of faults.

The most common and potent wine taint is 2,4,6-trichloroanisole (2,4,6-TCA), commonly known as cork-taint molecule resulting from the cork stopper of wine bottles. 2,4,6-TCA produces intense 'musty', 'mouldy' 'earthy' smelling in wine.

Similar off-flavor smells are associated to compounds including geosmin and 2-methoxy-3,5-dimethylpyrazine. We studied 74 such VOCs frequently present in wine. Determining concentration of VOCs in wine requires detection techniques to be fast, in real time, and with a detection limit as low as few parts per trillion by volume. The most frequently used techniques based on direct injection mass spectrometry, namely proton transfer reaction mass spectrometry (PTR-MS) and selected ion flow tube mass spectrometry (SIFT-MS), are being successfully employed in the measurements of VOCs concentrations.

Quantification using these techniques usually relies on compound-by-compound instrument calibration. The calibration procedures are generally laborious and time consuming. The theoretical evaluation of the rate coefficients of ion-molecule reactions occurring in PTR-MS/SIFT-MS flow (drift) tubes is a practical alternative to calibration.

In this thesis, we compute and report the rate coefficients for ion-molecule reactions, relevant for different experimental conditions, such as varied temperature and electric fields inside the drift tube. We have used well-established models based on capture cross-section collision and classical trajectories. These models rely on physical properties such as electric dipole moment and polarizability of the volatile molecules. To compute these quantities we resorted to ab initio density functional theory.

Introduction

The flavor of food products determines their sensory qualities, whilst their appearance and color provide the first indicators of quality. Flavor and texture in food products are critical in confirming or undermining the initial impression of our perception of the food.

Wine is a popular food drink and has evolved as an integral part in our life, culture and diet since time immemorial. Over the years, the role of wine has evolved from cultural symbol to an important source of nutrition [1]. Two major components of wine are water and ethanol. The alcoholic content of wine is considered crucial to the stability, aging, and sensory properties of wine and produce multiple effects on taste and mouthfeel [2]. The alcohol in wine, mainly ethanol, produced during fermentation process, contributes to the formation of several volatile aromatic compounds (VOCs) including acetaldehyde, diacetyl, acetic acid and numerous other volatile compounds in wine. Apart from water and alcohol, many compounds typically present at trace level (< 10 g/L) are responsible for most of the flavor and color of wine and many key odorants are found at part-per-trillion (ng/L) concentrations.

It is worth mentioning that VOCs appear in wine are not unique to the wine but appear in coffee, beer, bread, spices, vegetables, cheese, and other foodstuffs. The VOCs in food and alcoholic beverages provide a flavor fingerprint that help us in recognizing hygienic foods and avoid poor or dangerous food choices. Wine flavor is characterized by the fine balance between number of different organic compounds. Above threshold concentration they deteriorate the quality of the wine and causing economic losses to the wineries and damage their reputation. A report published in 1983 by Nykänen and Suomalainen have reported around 1300 volatile compounds in wine and other alcoholic beverages [3]. Recent developments in various mass spectrometry techniques were able to detect tens of thousands chemical compounds in wine and the count might be even higher [4].

The VOCs play important role as they determine the flavor of grapes and wine made from it. Wine off-flavor and taint molecules produced can be classified by the following three stages of wine production: from grapes, during fermentation and while storage. The compounds present in grapes remain unchanged in the wine. Many new compounds form during alcoholic fermentation due to normal metabolism of sugars and amino acids. Other major sources such as improper storage and handling of wine, extraction from oak

and abiotic transformation of precursor compounds can also produce microbial spoilage or chemical tainting in wine. The most problematic and highly potent molecule present in wine is 2,4,6-trichloroanisole. It results from cork stopper of wine bottles, usually called cork-taint, produces intense 'musty', 'mouldy', and 'earthy' smells in the wine. Many terpenes such as 1,8-cineole and rotundone are responsible for 'spicy' and 'mint' like character to the wine. 4-ethylcatechol is another major spoilage compound associated with Dekkera/Brettanomyces yeast resembles 'horsey' aroma. Variety of sulfur compounds including dimethyl sulfide and disulfides produce smell like 'cooked cabbage', 'cooked corn', 'cooked tomato' or 'molasses' in many wines [5, 6].

Therefore, accurate measurement of such trace level VOCs demand appropriate analytic methods that are capable of separating and quantifying VOCs in a complex gas mixture, able to track concentrations that change rapidly over time and with high sensitivity and low detection range (pptv) [7]. The most frequently used techniques based on the direct injection mass spectrometry such as proton transfer reaction mass spectrometry (PTR-MS) and selected ion flow tube mass spectrometry (SIFT-MS) have been very successful in measuring VOCs concentrations. PTR-MS allows real-time monitoring of many VOCs with very low detection limit (pptv range) and with high sensitivity. SIFT-MS is characterized by its capability of switching between reagent ions, less than 10 ms, offers a substantial benefit in increased selectivity for the analysis of mixtures containing multiple analytes. The reagent ions such as H_3O^+, NH_4^+, NO^+ and O_2^+ in SIFT-MS offer flexibility in the measurement of isobars and isomers [8]. It is worth noting that the same ion-molecule chemistry can be applied for PTR-MS/SIFT-MS measurements at thermal energy conditions. However at higher temperature, the PTR-MS working conditions are quite different due to the applied electric field. The applied electric field makes ion-molecule collisions far more energetic than thermal conditions. We have studied proton transfer and charge transfer reactions under collision based models and calculated rate coefficients of IMRs. The rate coefficients are vital in the quantification of VOCs in PTR-MS/SIFT-MS measurements as the rate coefficients omit the calibration requirement, since calibration procedures are generally laborious, time consuming and source of errors [9].

The IMRs are among the fastest chemical reactions and proceed without the activation energy [10]. The rate coefficients of such IMRs can be obtained from capture collision cross-section generally called collision rate coefficients. The magnitude of collision rate coefficients is obtained by physical properties such as dipole moment and polarizability of the reactants as suggested in average dipole orientation theory [11]. The basic long-range interactions between ion and polarizable neutral molecule involved are ion-induced and ion-permanent dipole interactions. Alternatively, ion-molecule rate coefficients can be obtained from classical trajectory calculations [12, 13]. We studied ion-molecule collisions through proton transfer and charge transfer reactions frequently occur in PTR-MS and SIFT-MS instruments. Also, we obtained physical and chemical parameters that influence

the ion-molecule chemistry occurring in the PTR-MS and SIFT-MS flow (drift) tubes.

Structure of the thesis is organized as follows: Chapters under part (I) present introduction and technical information about wine, wine analytic methods, chemistry of IMRs and theoretical procedures. Chapter (1) provides detailed review of wine and wine components present before and during the course of production. Various flavourant and aroma compounds responsible for wine flavor have been listed. Other than this, off-flavor and wine taint producing components and their cause of production has been been discussed thoroughly. The factors affecting quality and our perception to the wine flavor and aroma are also discussed. The experimental methods commonly used in the analysis of wine and food including their working principle, their working conditions and applications in various fields have been reviewed in Chapter (2). The ion-molecule chemistry under PTR-MS and SIFT-MS conditions has also been discussed in Chapter (2). Chapter (3) describes the theoretical view points of IMRs occurring in PTR-MS/SIFT-MS flow (drift) tubes. Various reaction modes including proton transfer and charge transfer have been discussed. We also investigate various models based on the collision to find the rate coefficients of barrierless reactions. Last chapter under part (I), Chapter (4), is the review of electronic structure methods for the calculation of molecular properties and the methods implemented in this project. We provide detailed information of the DFT methods computationally put into practice in this thesis.

Part (II) of the thesis provides comprehensive data of results and in-depth review of the results obtained. Chapter (5) lists the dipole moment and polarizability values obtained from two different methods and a comparison of the results is made. Experimentally important parameters to interpret IMRs in the drift-tube such as proton affinity and ionization energies of 74 off-flavor and cork-taint VOCs are obtained. In Chapter (6), we compute rate coefficients of the reactions of H_3O^+, NH_4^+, NO^+ and O_2^+ reagent ions to off-flavor and cork-taint VOCs commonly occur in PTR-MS/SIFT-MS instruments. Also, we report rate coefficients under various modes of reactions such as proton transfer and charge transfer at different experimental conditions of temperature and energy. Chapter (7) comprises the results of thermodynamic and chemical reactivity parameters which are the descriptors of probability of occurrence and reaction products in IMRs. Finally, conclusion is given in Chapter (8).

Bibliography

[1] R. S. Jackson. 12 - Wine, Health, and Food. In R. S. Jackson, editor, *Wine Science*, Food Science and Technology, pages 591–607. Academic Press, San Diego, 2 edition, 2000.

[2] R. S. Jackson. 6 - Chemical Constituents of Grapes and Wine. In R. S. Jackson, editor,

Wine Science, Food Science and Technology, pages 232–280. Academic Press, San Diego, 2 edition, 2000.

[3] L. Nykänen and H. Suomalainen. *Aroma of Beer, Wine and Distilled Alcoholic Beverages*. Springer Netherlands, 1983.

[4] C. Roullier-Gall, M. Witting, R. Gougeon, and P. Schmitt-Kopplin. High precision mass measurements for wine metabolomics. *Frontiers in Chemistry*, 11 2014.

[5] M. Sefton and R. Simpson. Compounds causing cork taint and the factors affecting their transfer from natural cork closures to wine–A review. *Australian Journal of Grape and Wine Research*, 11:226–240, 07 2005.

[6] A. L. Waterhouse, G. L. Sacks, and D. W. Jeffery. *Understanding Wine Chemistry*. Society of Chemical Industry. Wiley, 2016.

[7] L. Cappellin, T. Karl, M. Probst, O. Ismailova, P. M. Winkler, C. Soukoulis, E. Aprea, T. D. Märk, F. Gasperi, and F. Biasioli. On Quantitative Determination of Volatile Organic Compound Concentrations Using Proton Transfer Reaction Time-of-Flight Mass Spectrometry. *Environmental Science & Technology*, 46(4):2283–2290, 2012.

[8] K. Wyche, R. Blake, K. Willis, P. Monks, and A. Ellis. Differentiation of isobaric compounds using chemical ionization reaction mass spectrometry. *Rapid communications in mass spectrometry*, 19:3356–62, 11 2005.

[9] R. Taipale, T. Ruuskanen, J. Rinne, M. Kajos, H. Hakola, T Pohja, and M Kulmala. Technical Note: Quantitative long-term measurements of VOC concentrations by PTR-MS measurement, calibration, and volume mixing ratio calculation methods. *Atmospheric Chemistry and Physics*, 8, 05 2008.

[10] D. K. Böhme. Ion-Molecule Reactions in Mass Spectrometry. In J. C. Lindon, G. E. Tranter, and D. W. Koppenaal, editors, *Encyclopedia of Spectroscopy and Spectrometry*, pages 338–346. Academic Press, Oxford, 3 edition, 2017.

[11] T. Su and M. T. Bowers. Theory of ion-polar molecule collisions. comparison with experimental charge transfer reactions of rare gas ions to geometric isomers of difluorobenzene and dichloroethylene. *Journal of Chemical Physics*, 58(7):3027–3037, 1973.

[12] T. Su and W. J. Chesnavich. Parametrization of the ion-polar molecule collision rate constant by trajectory calculations. *The Journal of Chemical Physics*, 76(10):5183–5185, 1982.

[13] T. Su. Parametrization of kinetic energy dependences of ion-polar molecule collision rate constants by trajectory calculations. *The Journal of Chemical Physics*, 100(6):4703–4703, 1994.

Contents

List of Acronym

ADO Average Dipole Orientation

CI Chemical Ionization

CIMS Chemical Ionization Mass Spectrometry

DFT Density Functional Theory

EI Electron Ionization

HOMO-LUMO Highest occupied-Lowest Unoccupied Molecular Orbitals

IE Ionization Energy

IMR Ion-Molecule Reaction

MHP Maximum Hardness Principle

MPP Minimum Polarizability Principle

PA Proton Affinity

PTR Proton Tranfer Reaction

PTR-MS Proton Tranfer Reaction Mass Spectrometry

SIFT-MS Selected Ion Flow Tube Mass Spectrometry

VOCs Volatile Organic Compounds

Part I

VOCs: A Wine Perspective

1

Wine Components and Occurrence of Wine Faults

1.1 Introduction

The knowledge of the volatile composition of a wine is of great interest since these compounds are essential to the quality of the wine being produced [1, 2]. Wine is a complex mixture housing many aroma and flavor compounds proffer wine a unique texture and bouquet [3, 4]. Thousands of chemical compounds have been identified in grapes and wines that directly or indirectly control the key quality aspects of the wine. These compounds determine the organoleptic properties (aroma, flavor, appearance), safety, and stability in the wine [5]. The perception of wine flavor and aroma is the result of a multitude of in-

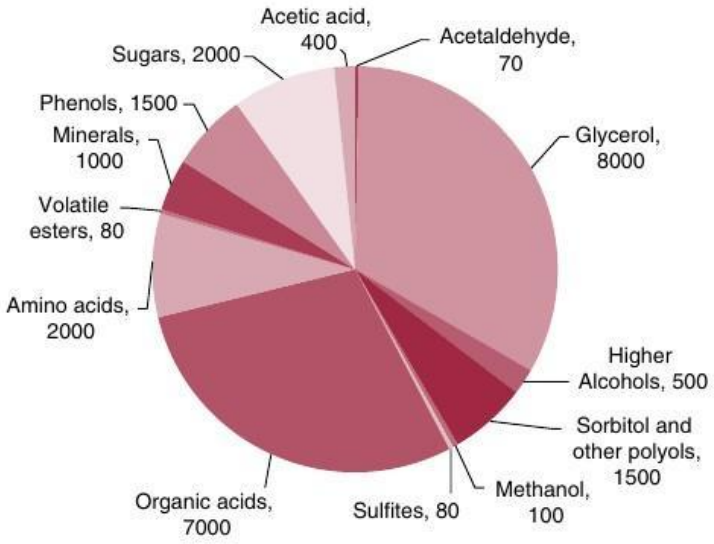

Figure 1.1: Typical wine components breakdown concentration in mg/L. The major components water, ethanol, and the trace components (0.1 ng/L to 10 mg/L) that are not visible, are not included. (*Source: Andrew et al., Understanding Wine Quality.*)

teractions between a large number of chemical compounds, see Figure 1.1, and sensory receptors. The wine components such as higher alcohols, acids, and esters are quantitatively dominant in wine aroma and are important for the sensory properties and quality of the wine. The distinguishing factor of wine from other alcoholic beverages and products is the relative concentration of the compounds rather than the presence of unique components. In perticular, a small amount of higher alcohols contribute positively to wine quality while excessive amounts may detract from the quality [6, 7]. Similarly, esters contribute to wine odor and relative concentrations of fatty acids give an appreciable strong odor [8]. Many other compounds related to off-flavor[1] are usually present at trace level in part per trillion by volume (pptv) range. On the other hand, taints are generally regarded as unpleasant odors or tastes resulting from contamination of food by some foreign chemical with which it accidentally comes into contact. Even at very small concentrations they can spoil the wine to a greater extent. These volatile compounds appear during the production process and continue until the bottling process or even many years after bottling. The most prominent wine faults, their occurrence, and how their occurrence deteriorates the wine quality have been discussed in the present chapter.

[1] An unpleasant odor or taste resulting from the biochemical or non-enzymatic changes to the compounds of food.

1.2 Most Common Wine Faults

1.2.1 Oxidation

Oxygen plays a vital role in the winemaking process. The oxidized wine is the wine that has been spoiled after having too much exposure to oxygen. The initial wine oxidation starts in the vineyard when grape skin is ruptured and fruit and juice are exposed to air. Oxygen can come into contact with wine at any stage during the production process. The wine may get oxidized, if the wine bottle is kept open for a long time and in the barrel while aging, or oxygen that enters through the cork after bottling.

A controlled oxygen interaction with wine imparts a positive impact on the color, changes in mouthfeel, and reducing in reductive aromas [9, 10]. While excessive oxidation flattens the wine flavor and aroma or even turns it up unpleasantly vinegary and discolored. In other words, oxidative wine is more likely suited to palates rather than oxidized wine. The molecular oxygen (O_2) does not directly react with most wine components, but oxidation occurs in the presence of some transition metal catalysts and prominent in Fe(II) and O-diphenols (excessive hydrogen donor) molecules [11]. The hydroperoxyl radicals[1] reacts with phenolics to produce phenolate anions, that can be oxidized to semi-quinone radicals, which further oxidized to form quinone [12, 13]. Hydrogen peroxide is the source of production of acetaldehyde on reacting with ethanol [14]. Oxidation of ethanol to acetaldehyde by direct chemical reaction with air occurs at an appreciable rate in wine only by a coupled autoxidation of certain phenolic substances occurring in the wine [15]. In a wine must and during wine oxidation, phenolic compounds serve as the primary substrates [16].

The oxidation can be enzymic or nonenzymic which is also called auto-oxidation. In the case of enzymic oxidation, enzymes such as polyphenol oxidase and laccase catalyze the reaction [17, 18]. This kind of oxidation mostly occurs in wine must. In wines, the oxidation usually occurs without the mediation of enzymes. This type of reaction is called

[1] O_2 is not very reactive in its triplet ground state but can be reduced to superoxide, peroxide, and hydroxyl radicals by reduced metal ions such as Fe^{2+}.

chemical oxidation. As outlined, it is recommended to limit the oxidation because high oxidation could lead to the accumulation of O_2 inside or in the headspace of the wine with subsequent microbial or oxidation spoilage.

1.2.2 Reduction

The presence of reductive characteristics in a natural wine shows the addition of various forms of sulfur (e.g. sulfate, sulfite, and sulfur-containing amino acids); however, are important for yeast biosynthesis [1]. The most common elements are hydrogen sulfide (H_2S) and mercaptans (thiols) produced during alcoholic fermentation under reducing conditions [19, 20]. The former is responsible for 'rotten eggs' like smell and latter produces an aroma of 'garlic', 'struck flint', 'cabbage', 'rubber', and 'burnt rubber' in wines. The production of the excessive hydrogen sulfide by yeast during fermentation depends on the various factors such as the presence of elemental sulfur on the grape skin, inadequate levels of free $\alpha-$amino nitrogen, unusually high levels of cysteine in juice, or a high concentration of metal ions. It is thought that ethyl mercaptan (ethanethiol) is probably formed in wine by the direct chemical reaction between H_2S and ethanol [21]. These characteristics can originate in the vineyard, the winery, or the bottle–for reasons that may have as much to do with vine biology as with winemaking technique or the microbiology of finished wines. Maintaining sufficient nitrogen level in soil[1] is also a challenge for natural wine producers. The nitrogen concentration is important because the main reductive compound H_2S develops under low nitrogen fermentation condition.

1.2.3 Microbiological Spoilage

The microbial organisms are considered as a spoilage if their presence is not desired at a particular space and time. Any organism produces off-flavor, odor, color, or precipitates, or has the potential to do so under the conditions of the present and future storage of the

[1]Linked to the challenges in organic viticulture or no-sulfur vinification. Instead of using chemical fertilizer, implementing composting and using nitrogen-fixing cover crops aren't as easy for natural-wine producers. Organic grapes may provide less nitrogen to the yeasts during fermentation which can lead to the formation of reductive compounds.

Figure 1.2: A cartoon of wine spoilage by bacteria and micro-organisms. (*Source: Wikipedia*)

wine is treated as spoilage to the wine [22]. Many unwanted organisms can be found almost anywhere, see Figure 1.2. The most common places include wineries and out in the vineyards. These microbial organisms can develop at any stage of wine production. The yeasts such as Brettanomyces spp. popularly known for "Brett character" and Lactobacillus spp. are responsible for 'mousiness' in wines [23]. The presence of yeast can be on the grapes themselves, it can be hanging out in a winery, and it can hide in barrels. Generally, 'mousiness' occurs at a lowered concentration of sugar and an increased pH level; an ideal situation which interns encourages the growth of various yeast and bacteria [21, 24]. Since the winemaking process is all about fermentation and yeasts and converting one thing to another, there are plenty of opportunities for Brett to occur. For some winemakers, a bit of Brett is considered as their house style, but not for others. Once Brett takes residence in a cellar it can be difficult to get rid of. It causes wines to have an 'earthy', 'muddy' taste which in small quantities is not particularly unpleasant. Indeed, wineries often encourage a little bit of Brett in their wines to establish a signature style. The bacterial spoilage (lactic acid and diacetyl) during malo-lactic fermentation produces 'sauerkraut'[1] off-flavor [25]. Also, an increased level of volatile acidity by acetic acid and ethyl acetate imparts a vinegary, solvent aroma, and taste to the wine flavor. An increased bitterness and butyric off-flavor can also be attributed to the bacterial spoilage. It is not possible to remove them completely but can prevent their occurrence by proper use of sulfur dioxide and sorbic acid.

[1] Distinctive sour flavor.

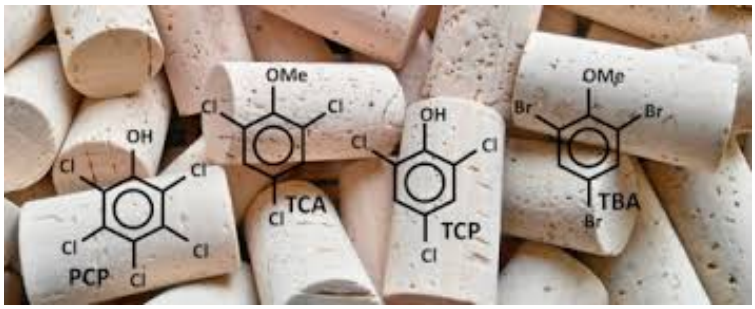

Figure 1.3: A picture showing cork-taint compounds from cork stoppers of wine bottle. (*Source: Wikipedia*)

1.2.4 Cork-Taint

The wine taint, in principle when flavor compounds originate from external environment contamination such as packaging, winery equipment, additives, and processing aids, air (or other gases), or microbial activity external to the product [5]. One of the most common taint molecule that comes from the cork stopper of the bottled wine is 2,4,6-trichloroanisole known as cork-taint[1]; a compound so powerful that even in infinitesimal amounts it can cause 'musty' aromas and flavors in wines [26–28]. 2,4,6-trichloroanisole forms through the interaction of plant phenols, chlorine, and mold. It occurs most frequently in the natural corks and transferred to the wine bottle through the cork stopper of bottled wine, and the wines that produce 'musty' off-aromas are often called 'corky'. However, cork is not the only source of trichloroanisole (TCA) contamination. Other sources of TCA contamination include oak barrels, filters, winery equipment and bottling plants [5]. TCA is a highly volatile compound and migrates easily. Generally, anisoles (di-, tri-, and tetra-anisoles) are believed to be produced by the microbial methylation of highly toxic chlorophenols and bromophenols as a result of normal detoxification reaction conciliated by different microbial species. A pictorial representation of a fewer compounds is given in Figure 1.3. Mostly, the taint is caused by other environmental problems at wineries such as moldy cellars, anti-fungal treatments, and flame-retardant paints. Although, TCA taint poses no immediate health concerns for wine drinkers, but more importantly it has potential to ruin a wine. At higher concentration level, it makes a wine smell like 'moldy' or 'musty',

[1] Cork is the bark of the cork oak used for making stoppers for wine bottles, especially expensive ones. Whose main component is suberin, a complex aromatic biopolymer structurally related to lignin and accordingly highly resistant to degradation.

'cardboard', 'damp cement', or 'wet newspapers'. At its worst, the wine is undrinkable. At lower levels, TCA taint merely strips a wine of it's flavor making normally rich fruity wines taste dull or muted without imparting a noticeable defect. This can leave wine drinkers disappointed in a bottle of wine without being able to pinpoint why? TCA can be recognized instantly by the nose even without tasting. Usually, it smells like a 'damp cellar', a 'heavy mustiness', a smell of a 'wet sack', perhaps with tones of 'mushrooms' or 'dry rot' [27]. Upon tasting it introduces 'dirty', 'fusty', and 'earthy' character at the back of the tongue.

1.2.5 Wine Off-Flavors

Off-flavor compounds arise from chemical or microbiological transformations of wine components, and thus can often be identified even in sound wines, but at sufficiently low concentrations and even hard to detect in some wines. Their presence may not be considered an off-flavor in certain wine styles or by particular groups of consumers or wine experts [29, 30].

Usually, off-flavor is caused due to acetic acid and ethyl acetate associated with volatile acidity, sulfur compounds (H_2S) related to reductive characters, nitrogenous compounds imparting 'vegetal' or 'mousy' flavors, carbonyl compounds from oxidation, and ethyl phenols indicative of the spoilage by Brettanomyces (Dekkera) yeast [28]. Typically, inappropriate handling and ill-storage conditions (such as light, temperature, oxidation, microbial load, and processing operations) may also lead to an off-flavor in wines [1, 31]. All these conditions promote consumers to carefully monitor wines when wine aroma and flavor exceed a certain threshold. One of the major causes of the origin of off-flavor in wines is due to the chlorinated phenols. The chlorophenols have been used industrially as fungicides, biocides, and herbicide intermediates most commonly in the treatment of wooden storage pallets [32–34]. When phenols present in wood/board, from the decomposition of the lignin, react with a source of bromine or chlorine halophenols are usually formed. Similarly, tribromophenol can be formed by the reaction of certain biocides with phenols.

1.3 Wine Taint and off flavor Causal Compounds

1.3.1 Chlorinated and Brominated Anisoles

The cork of the wine bottle is believed to have significant impact on the wine flavour and consumer's acceptance of wine. Around 3 to 5% of all the sealed wines under cork suffer a taint called cork-taint and 2,4,6-trichloroanisole (2,4,6-TCA) being the major contributor which transfers 'earthy', 'musty', 'moldy' odor to the wine [28, 35]. 2,4,6-TCA is a chemical so powerful that even in infinitesimal amounts it can cause 'musty' aromas and flavors in wines. TCA is characterized by high volatility and dramatically low perception threshold in wines starting from 1.5 to 2 ng/L [28, 36]. Above this limit TCA can spoil the wine quality. If TCA goes undiscovered, it can spread and eventually taint the aroma and flavor of the wine.

TCA forms mainly through the interaction of plant phenols, chlorine, and mold. However, it can originate anywhere in wineries where damp surfaces and chlorine-based cleaning products are commonplace; barrels, wooden pallets, wood beams, and cardboard cases are all sources of phenols. The potential cause of chloroanisoles in cork can be due to the microbial degradation of chlorophenols commonly used in insecticides and herbicides or chemical solutions used to bleach the cork. In wines, TCA comes from the microbiological methylation of chlorophenols and the primitive source of chlorophenols is the hypochlorite. Treating cork-raw materials in the presence of hypochlorite chemicals result in the introduction of TCA into wine when barrels or tanks are emptied and refilled.

Similarly, tribromoanisole is also responsible for wine taint and known to contaminate other materials such as corks, barrel, and winemaking equipment via atmosphere. More than 50% of the wine defected by fungal taints is believed to be contaminated by TCA above 2 ng/L concentration [37]. While the rest of the spoilage comes from other 'musty' smelling compounds. In addition to TCA other anisole compounds include 2,3,4-trichloroanisole, 2,3,6-trichloroanisole, 2,3,4,5-tetrachloroanisole, 2,3,4,6-tetrachloroanisole, 2,3,5,6-tetrachloroanisole and pentachloroanisole are also constitute 'musty' and 'earthy'

flavor to the wines [27, 28, 38]. The source of the production of the above anisoles is their corresponding chloro- and bromophenol impurities which then can be methylated by microorganisms.

1.3.2 Phenolics and Flavonoids

The phenolic compounds composition in the wine is responsible for wine style, type, and the color of the wine [39, 40]. Generally, red wines have higher phenolic concentration than white wines. Phenols are the major contributors to the wine stability and organoleptic properties (astringency and bitterness). Simple phenols have a single aromatic ring with one or more hydroxy groups, but two distinctive groups of phenols flavonoid and non-flavonoid phenols also occur in grapes and wines [5, 41]. The grape phenols are mainly found in the skin and seed of the berry. The grape berry is the source of vast majority of the phenols present in the wine. The aromatic ring of phenols is highly susceptible to electrophile aromatic substitution such as chlorine and bromine that can be added to the ring so as to form halophenols.

Several types of chlorophenols and bromophenols namely mono, di-, tetra-, pentachloro- and pentabromophenols, are considered as environmental contaminants, can be produced and transferred to the wine by many possible sources during wine production or post-processing[1] (transportation, packaging, and handling). Polyphenols are the main phenolic compounds extracted from grapes during the winemaking process, initially obtained by the crushing of the fruit, and intensified by the maceration and pumping-over processes during fermentation. Fermenting and storage in oak provide additional sources of phenolic compounds in wine. Volatile phenols such as 4-ethylphenol, 4-ethylguaicol, and 4-ethylcatechol are associated with the growth of yeast (Brettanomyces) in the wine usually impart 'clove', 'spicy', 'smoky', 'leather', 'horsey' aroma in wine [42].

Generally, the volatile phenols are present in the range of μg/L to mg/L supra-threshold concentrations. The reported concentration of 4-ethylphenol up to 425 μg/L is considered

[1] Chlorine based sterilizing agents such as hypochlorite solutions can react with traces of phenols present in materials of everyday use: plastic, fiberglass or lining, phenolic based resins, paints, and fittings. Sometimes wooden pallets are stored near disinfectants containing chlorine or bromine.

objectionable in many wines [1]. And, 4-ethylguaiacol having sensory threshold with 10 μg/L found as high as 150 μg/L in some Australian wines [28]. 4-ethylcatechol with 'horsey' aroma can be found above detection threshold of 774 μg/L. Few di-chlorophenols such as 2,4-dichlorophenol and 2,6-dichlorophenol are considered more potent and sensory pertinent [27]. Their detection threshold is found to be 32 ng/L and reported up to 236 ng/L in many wines. Recently, 2-chloro-6-methylphenol has been reported in dry white wines at 70 ng/L concentration [43]. 2-chloro-6-methylphenol has been commonly observed in other food products like meat, biscuits, and soft drinks.

1.3.3 Alcoholic Compounds

Transforming grape juice (wine must) into wine is a highly complex chemical process. Alcoholic fermentation, the primary fermentation, is a fundamental process for the production of the wine. The fermentation process can be considered as a chain reaction of the chemical phenomena. During this process, the sugar contained in the grape juice is converted by yeast's enzymes into ethyl alcohol and carbon dioxide[1] [5, 44]. Depending upon the type of yeast, from this conversion of sugar one can obtain about 50% of alcohol, 45% of carbon dioxide, 3% of glycerol, and 2% of other byproducts. These byproducts are responsible for most of the aromatic and gustatory qualities of wine.

Ethanol, the far most important compound in the wine known for its stimulating properties and its concentration can vary from 8-15% by volume. Methanol, although present at low concentrations (0.1 to 0.2 g/L) commonly found in red wines. Methanol is formed due to the pectin degradation and as the pectin level in grapes is low the amount of methanol is also low. At this low-level concentration, methanol does not pose any toxicity risk. Likewise, about 39 alcohols have been identified in various wine types. Higher alcohols, having more than two carbon atoms are also produced as a byproduct of yeast amino acid metabolism and are common to all products of alcoholic fermentation. They often constitute more than 50% of the volatile aroma excluding ethanol, however, their concentration

[1] Since there is no ethyl alcohol content found in the fresh grapes or must its content depends on the amount of sugar from which it is derived during fermentation. The basic reaction is : $C_6H_{12}O_6 \longrightarrow 2\ C_2H_5OH + 2\ CO_2 + 27$ Kcal.

can be increased with the spoilage by yeast and bacteria. Some of the investigated higher alcohols in this thesis include cis-1,5-octadiene-3-ol, 1-octen-3-ol and trans-2-octen-1-ol belong to the organic compounds known as fatty alcohols [45–47]. These are the aliphatic alcohols comprise a chain of a least six carbon atoms, hydrophobic in general and relatively neutral. The compound 1-octen-3-ol is a secondary alcohol derived from 1-octene. It is also a wine fault (cork taint) composed of bunch rot[1] contaminated grapes.

1.3.4 Amines and Pyrazines

Many organic compounds characterized by the presence of a nitrogen atom with lone pair of electrons termed amines are found in grapes and wines. These are the class of compounds derived by ammonia (NH_3) by the loss of one or more hydrogen to yield primary, secondary, and tertiary amines respectively [5, 48, 49]. Some of the compounds are also present in inorganic forms such as ammonia and nitrates and diverse organic forms such as amines and amides. The majority of the soluble nitrogen that exists in ammonia along with free amino acids usually present in the wine must. Many complex organic nitrogenous compounds such as proteins, pyriamides, and nucleic acid are of utmost importance for the growth and metabolism of grapes and yeast cells. The free amino acids serve as the primary nitrogen source during alcoholic fermentation.

In grapes and wines, the primarily α-amino acids are the main amino acids [50]. Indole, an odorous compound present in its volatile form at wine pH [51]. It appears to be formed as a result of the microbial metabolism of an amino acid called tryptophon. Indole is detected at 1-10 μg/L and appears as off-flavor above 30 μg/L. Some reports claim its presence up to 350 μg/L primarily as a result of sluggish fermentation. Most of the contribution to the off-flavor of the wine comes from the pyrazines especially "methoxy pyrazines" possess odor generally similar to 'vegetal' or 'earthy' even at lower as $\sim$ 1 ng/L. Pyrazines contribute significantly to the flavor of many natural and baked foods. The common compounds reported in grapes are 3-isobutyl-2-methoxypyrazine, 2-isopropyl-3-methoxypyrazine, 2-sec-butyl-3-methozypyrazine and 2-methoxy-3,5-dimethylpyrazine

[1] A kind to fungi generated infection in grapes. In viticulture, it is commonly known as 'Botrytis bunch rot'; in horticulture, it is usually called 'grey mould' or "gray mold".

produce 'bell pepper', 'peas' like flavor in the wine [52–56]. Notably, 2-methoxy-3,5-dimethylpyrazine reported in grapes and wines below its sensory threshold originates from different sources. Oftenly, 2-methoxy-3,5-dimethylpyrazine derived from the contamination of ferments by insects like Asian ladybeetal or 7-spot ladubeetal largely known for producing 'musty' and 'fungal' taint in many wines.

1.3.5 Sulphur Related Compounds

The volatile sulfur compounds exhibit unpleasant odors generally ascribed to 'rotten eggs', 'skunk aroma', 'garlic', and 'onion' [57]. These compounds present at trace level mostly produced during fermentation by yeast due to the presence of elemental sulfur in the grape skin and their sensory impact is apparently damaging to the wine quality [58]. The important sulfur compound H_2S can be used as an universal antimicrobial agent and antioxidant. It's careful use inhibits the production of acetic acid and Brettanomyces but excessive use could lead to unwanted texture and aroma in wine. Many reports claim its presence in the range of 1 to 5 mg/L or even much higher depending on the wine production, storage, and handling.

Other sources of H_2S production include higher metallic ion concentrations and nitrogen deficiency which block the amino acid bio-system and make a passage to H_2S production. From a chemical point of view, sulfur exhibits similar electronic configuration and form analogous to oxygen but shows different properties due to its d-orbital and ability to form multiple bonds. Sulfur is more polarizable and less electronegative than oxygen, thus easily available for bond formation. Excessive H_2S in wine can be detected directly on the nose. Occasionally, a prickly sensation is experienced at the back of the nose or in the throat. The volatile sulfur compounds especially those with oxidation state -1 or -2 are considered aroma compounds. Many thiols and sulfur compounds such as dimethyl sulfide, dimethyl-disulfide, ethyl thioacetate, 3-mercaptohaxan-1-ol and 4-mercapto-4-methylpentan-2-one are essential to wine aroma and considered off-flavor at higher concentrations give 'cabbage', 'grape fruit', 'passion fruit', 'onion', 'box-tree', 'guava' character to the wine [5, 49, 59]. Although, most of the compounds are not de-

tectable in grapes, but they may be classified based on their origin in the winemaking process.

1.3.6 Terpenes and Terpenoids

Terpenes are a group of aromatic compounds characterized by their aromatic qualities and play a major role in the traditional herbal remedies. Terpenes are often found as herb-flavored and aroma to several grapes varieties [5, 60]. Chemically, terpenes are hydrocarbons with a basic five-carbon isoprene unit (2-methyl-1,3-butadiene) constitutes terpenes [42]. Their distinctive carbon skeleton-like structure may contain more than two isoprene units. Terpenes are occasionally called "terpenoids" with the additional functional group usually oxygen-containing. Monoterpenes or isoterpenoids (containing two isoprene units) are typically associated with white wines where their concentration may exceeds threshold limit by 100-fold in some cases [1]. Monoterpenoids are derived mainly from grapes and impart substantial contribution to the wine aroma. Other conditions such as cultivar and growing conditions of grapes may contribute to a wide variety of wine flavor.

Apart from this, their concentration in wine is greatly influenced by the extraction from grapes and transportation of precursors or free volatile during fermentation and storage. The most potent terpenoids are linalool, geraniol, eucalyptol (1,8-cineole), rotundone, hotrineol and α-terpenol produce distinctive off-flavor [47, 61]. Rotundone is the most notable compound found in higher concentrations in red wines gives rise to distinctive ‘spicy’, ‘black pepper’ character in red grapes and wine (increases up to 6-fold with the inclusion of grape leaves and roots). It’s presence in the other sources such as black and white pepper is reported up to 145 ng/L. Apart from grape varieties, rotundone concentration increases with grape maturation. The VOCs like geraniol, rotundone, hotrineol and α-terpenol contribute to the wine flavor resembling ’floral’ and ’citrus’ [62, 63]. Of these, 1,8-cineole produces ‘eucalyptus’ aroma in red wines generally described as being ‘spicy’ and ‘mint-like’.

1.3.7 Aldehydes and Ketones

The most frequently occurring and important carbonyl compounds in the wines are aldehydes and ketones [5]. Aldehydes and ketones originate as fermentation metabolites and oxidation products. Acetaldehyde is one of the major sensory profile carbonyl compound found in wine approximates 90% of the total aldehyde content in the wine [64]. It is a volatile compound present at various levels in different wines. The average value of acetaldehyde in red wines can vary up to 30 mg/L while white wines contain 80 mg/L. At moderate concentration it can transmit a pleasant fruity aroma to wine, however, above a threshold value (100-125 mg/L) it is considered as a defect and off-flavor resembling with 'rotten' apples. Acetaldehyde is often deemed as an early metabolic-by-product of fermentation and can be formed by yeast and acetic acid bacteria.

Generally, acetic acid bacteria forms acetaldehyde by oxidizing ethanol [65]. It's concentration decreases with the fermentation, as long as the fermentation finished acetaldehyde transported back into yeast cells and reduced to ethanol. The amount of acetaldehyde formed by yeast varies with the species and is considered to be the leakage product of alcoholic fermentation. Many medium-chain aldehydes (C_8-C_{10}) such as octanal are found in many food products including wines and impart 'fruity' type aroma in wines. Octanal, if present at higher concentrations it is regraded as an odorous element reminiscent to 'citrus'. Other aldehydes that may impart sensory properties to the wine are furfural and 5-(hydroxymethyl)-2-furaldehyde [49].

Most of the ketones are produced during fermentation and not many volatile ketones are found in wine, but those that are present in grapes usually survive through fermentation. Cis-1,5-octadien-3-one and 1-octen-3-one are the organic compounds known as enones which commonly contribute to the wine aroma (buttery, lactic off-odor) above their sensory threshold. 1-octen-3-one (fungal ketone) found in fruits, specifically infected grapes, may provide a 'mushroomy' note in the wine.

1.4 Factors Influencing Wine Aroma & Flavor

Other than water and alcohol, many VOCs are present at smaller concentrations and can strongly influence the wine flavor. The taste and mouthfeel sensation of wine is due to the compounds that are present at concentrations above 0.1 g/L. A number of aromatic compounds by and large at 0.8 to 1.2 g/L constitute 1% of the wine's ethanol content. The most common are fusel alcohols, volatile acids, and fatty acid esters. A much smaller contribution comes from carbonyl, phenols, lactones, terpenes, acetals, hydrocarbons, sulfur, and nitrogen compounds. Although, present at very low concentrations but are most important to the varietal and unique sensory features of wine fragrance.

The acidity in wine is a feature important for regulating the freshness desired in sparkling wines [66]. Wine is a combination of volatile (acetic) and non-volatile (malic and tartaric) acids. Volatile acid is composed of acetic acid and other acids such as carbonic acid (from CO_2), sulphuric acid, and to a lesser extent, butyric, folic, lactic, and tartaric acids. Each wine contains some sort of acidity content in it. If the acidic content present is low, the wine complexity will be increased. On the other hand, higher acidic content may make wine smell similar to 'vinegar' or of nail varnish remover type. The volatile acids can be detected by the nose while other acids sensed on the palates. On the palates, wine may lose its 'fruity' character and can give a burning sensation on the back of the mouth.

Yeast exhibits an important property that distinguishes wine from grape juice and converts the sugars of wine grapes into alcohol [1, 5, 67]. Grape sugar content is critical to the yeast growth and metabolism. Saccharomyces cerevisiae, the primary wine yeast, derives most of its metabolic energy from glucose and fructose. Grapes skin (contains coloring matter, flavor constituents, and tannins) have two types of yeasts named wild and wine yeast. Wild yeast converts sugars to alcohol at up to 4% alcohols once in contact with the grape sugars until they die. While wine yeast of the type Saccheormyces starts from where wild yeast had left and continue to work until there is no more sugar left. In the course of the conversion, it converts up to 15% grape sugar to alcohol. Brettanomyces spp. can produce a smell of 'cheese' or 'wet horse' caused by poor hygiene. SO_2 production is

highly sensitive to the yeast and can be controlled by its careful use. Brett may be soaked by barrels and can be a potential source of contamination during the maturation process.

Ageing in wines play an important role and depends on the amount of oxygen entered into the wine, however, oxygen can enter at any point in a wine's life-time. If so much oxygen is absorbed, it can damage structure of the wine [49, 68]. This can happen due to not sensibly handling processing or bottled wine is not stored properly. Every bottled wine has some lifespan and should be consumed before it gets too old. Similarly, reducing exhibit H_2S and mercaptans. H_2S is known to produce a pronounced smell similar to 'rotten eggs' or 'drains'. On a similar note, mercaptan produces a much more intense odor resembling 'sweet rotten cabbage' or 'garlic'. Reducing defects are commonly originate due to careless handling. The common cause of excessive H_2S is the use of sulfur in the vineyard treatment which then reduced to H_2S during winemaking by the action of the yeast. To counter this reduction problem in wines, proper level of N_2 and O_2 should be maintained.

H_2S in wine is best known for giving wine's antiseptic and antioxidants properties [49]. It is detected by the nose and may smell like a 'struck match' or 'burning coke' and may wipe out much of the 'fruity' character of the wine. Occasionally, a prickly sensation is felt at the back of the nose or in the throat. Of course, wine can be tainted at any stage of production many factors may influence the aroma and flavor of the wine. The common factors that are prominent in controlling the aroma and flavor of wine from winemaking to the final product are washing oak barrels, transportation, storage, and handling [1, 42].

1.5 Identification & Quality control

The smell and taste of wine is the collective effect of a large number of chemical compounds with different properties like volatility and polarity which occur at different concentrations from mg/L to ng/L. Often these compounds interact in complicated ways through many different reaction channels and influence the sensory stimulation. To fully understand the variables affecting wine chemical composition, sensory properties, production practices, and to the greater extent the consumer preferences, it would be ideal to target

all known major compounds and measure them in every experiment [69]. The quality of many alcoholic beverages (wine, beer, and spirits) directly depends on their composition and amount of taint and off-flavor compounds they contain [1]. Wine is a highly complex mixture of several hundreds of compounds known to significantly contribute the sensory properties, impact stability, and affect product safety. The aroma compounds present in wine are considered vital to the wine industry as they influence the product quality and hence the consumer's acceptance.

Winemaking is the time-honored technique where grapes are crushed and allow the naturally-occurring yeast present on the grape skins (and/or in the winery) to ferment the juice into wine. In the beginning, a large number of organisms present during fermentation, by the end of fermentation, very few can survive at low wine pH (3-4). Many factors from pre-processing to post-processing can affect the nature, texture, and sensory perception of wine and pose a significant threat to the quality of the final product. Understanding threats to wine quality, having strategies to control those threats, and maintaining systems to verify that threats are under control, are the key factors to any winery's success. Most common key threats to the wine are:

- **Raw materials**: Water usage in wine remains ubiquitous throughout the production process. Water is used as an ingredient in the production process or either for rinsing and cleaning production vessels. It is well observed that conventional water treatment procedures are not always sufficient to get rid of off-flavor. Water is the source of the two most problematic taints, geosmin and 2-methylisoborneol responsible for 'earthy' and 'musty' smell. Water quality must be included as a part to maintain product quality [70]. Other materials such as sugars level, selection of yeast variety are to be equally scrutinized during wine production.

- **Excessive Oxygen**: A small amount of oxygen could play important role in the development of flavor, aroma, and phenolic composition especially in red wines [71]. As limited oxygen exposure is a necessary part of wine development, though, too much oxygen exposure damage the structure and limits shelf life [72]. Closures, including various types of corks and screw caps, all offer benefits and downsides in

maintaining seals on bottles, which impact oxygen exposure.

- **Microbiol spoilage**: Major microorganisms that play important role in winemaking include species and strains of yeasts, lactic acid bacteria, and acetic acid bacteria [49]. They can cause numerous unwelcome wine spoilage defects such as bitterness, off-flavors, and sensory visual faults like film formation, turbidity, viscosity, and sediments. The management of wine spoilage bacteria can be as simple as manipulating wine acidity or adding sulfur dioxide. During winemaking optimizing the alcoholic and malolactic fermentation can be another way to prevent spoilage [73].

- **Temperature & pH**: The temperature and pH control are critical to wine production. The temperature must be controlled so as not to inhibit enzymatic actions. During wine storage, the optimum temperature is generally 40 degrees to 60 degrees Fahrenheit [74]. Wine is known to develop with age. At lower temperatures, it develops more slowly. At higher but moderate temperatures, it ages more quickly. At very high temperatures, 90 degrees to 100 degrees Fahrenheit-plus, wine can cook quickly. The yeast activity is greatly influenced by the pH of the mash during fermentation [75]. Each yeast strain operates in its optimal pH range.

- **Exposure to light**: Exposure to the light can trigger undesirable chemical reactions in some wines. UV rays can produce harmful effects on the wine [76]. Studies have shown that too much exposure to light causes imbalance and may break down the chemicals and molecules that allow the wine to age so delicately. The aging process can be accelerated and cause the wine quality tastings poor.

1.6 Summary

The wine aroma is collectively comes from hundreds of volatile compounds that produce an effect on sensory senses. The volatile compounds serve an important factor to consider wine's sensorial quality. A good wine is characterized by its appearance, color, taste, mouthfeel, and wine bouquet. For a wine to earn its reputation and merit price, it must fulfill certain quality standards. More importantly, the products must be free from impurities

commonly known as taint and off-flavor. The most important aspect of making good quality wines is to identify and quantify volatile compounds that are responsible for off-flavor. There can be many sources of contamination and different level of concentrations. For example, cork-taint, one of the problems in the wine industry, originates from cork, although other sources such as oak barrels, filters, winery equipment could be the potential sources and can not be overlooked. Therefore, it is difficult to predict how the chemical composition will affect sensory perception. The ability to characterize these compounds would influence the winemaking operations and help them to be better managed, also improve the consistency and quality of the final product. Besides, wine analysis is important in terms of meeting regulatory requirements, detecting adulteration, discovering new compounds, and detecting authenticity.

Bibliography

[1] A. Reynolds, editor. *Managing wine quality: Oenology and wine quality*. Woodhead Publishing Limited, Reading, Massachusetts, 2 edition, 2010.

[2] B. Zoecklein, K. C. Fugelsang, B. Gump, and F. S. Nury. *Wine Analysis and Production*. Springer US, Reading, Massachusetts, 1 edition, 1999.

[3] J. Piggott, editor. *Alcoholic Beverages: Sensory Evaluation and Consumer Research*. Woodhead Publishing, Reading, Massachusetts, 1 edition, 2011.

[4] S. Lubbers, C. Charpentier, M. Feuillat, and A. Voilley. Influence of yeast walls on the behavior of aroma compounds in a model wine. *American Journal of Enology and Viticulture*, 45(1):29–33, 1994.

[5] *Taints, Off-flavors, and Mycotoxins*, chapter 18, pages 149–157. John Wiley & Sons, Ltd, 2016.

[6] J. D. Dougherty, R. D. Campbell, and R. L. Morris. Actinomycete: Isolation and identification of agent responsible for musty odors. *Science*, 152(3727):1372–1373, 1966.

[7] M. Ugliano, E. J. Bartowsky, J. McCarthy, L. Moio, and P. A. Henschke. Hydrolysis and transformation of grape glycosidically bound volatile compounds during fermentation with three saccharomyces yeast strains. *Journal of Agricultural and Food Chemistry*, 54(17):6322–6331, 2006.

[8] R. B. Boulton, V. L. Singleton, L. F. Bisson, and R. E. Kunkee. *Principles and Practices of Wine making*. Springer US, Reading, Massachusetts, 1 edition, 1999.

[9] V. Atanasova, H. Fulcrand, V. Cheynier, and M. Moutounet. Effect of oxygenation on polyphenol changes occurring in the course of wine-making. *Analytica Chimica Acta*, 458(1):15–27, 2002.

[10] V. Cheynier, V. Atanasova, H. Fulcrand, Jean-Paul Mazauric, and M. Moutounet. Oxygen in wine and its role in phenolic reactions during ageing. *Uses of Gases in Winemaking.*, pages 23–27, 2002.

[11] J. C. Danilewicz. Review of reaction mechanisms of oxygen and proposed intermediate reduction products in wine: Central role of iron and copper. *American Journal of Enology and Viticulture*, 54(2):73–85, 2003.

[12] J. E. LuValle. The reaction of Quinone and Sulfite. I. Intermediates. *Journal of the American Chemical Society*, 74(12):2970–2977, 1952.

[13] M. Nikolantonaki and A. Waterhouse. A method to quantify quinone reaction rates with wine relevant nucleophiles: A key to the understanding of oxidative loss of varietal thiols. *Journal of agricultural and food chemistry*, 60, 08 2012.

[14] J. V. McArdle and M. R. Hoffmann. Kinetics and mechanism of the oxidation of aquated sulfur dioxide by hydrogen peroxide at low pH. *The Journal of Physical Chemistry*, 87(26):5425–5429, 1983.

[15] H. L. Wildenradt and V. L. Singleton. The Production of Aldehydes as a Result of Oxidation of Polyphenolic Compounds and its Relation to Wine Aging. *American Journal of Enology and Viticulture*, 25(2):119–126, 1974.

[16] N. Es-Safi, C. Le Guernevé, V. Cheynier, and M. Moutounet. New phenolic compounds formed by evolution of (+)-Catechin and Glyoxylic Acid in Hydroalcoholic Solution and Their Implication in Color Changes of Grape-Derived Foods. *Journal of Agricultural and Food Chemistry*, 48(9):4233–4240, 2000.

[17] V. L. Singleton, M. Salgues, J. Zaya, and E. Trousdale. Caftaric Acid Disappearance and Conversion to Products of Enzymic Oxidation in Grape Must and Wine. *American Journal of Enology and Viticulture*, 36(1):50–56, 1985.

[18] V. L. Singleton, J. Zaya, E. K. Trousdale, and M. Salgues. Caftaric acid in grapes and conversion to a reaction product during processing. *Vitis: Journal of Grapevine Research*, 23:113–113, 2016.

[19] Vinifera. Can you explain reductive wine making and reduced notes ? https://www.winespectator.com/, April 2012.

[20] B. Campbell MW. Reduction in wine explained. https://www.therealreview.com/2016/09/12/reduction-in-wine-explained/, September 2016.

[21] J. Robinson. *Oxford Companion to Wine*. Oxford University Press, Reading, Massachusetts, 4 edition, 1994.

[22] E. Bartowsky and I. Pretorius. *Microbial Formation and Modification of Flavor and Off-Flavor Compounds in Wine*, pages 209–231. 01 2009.

[23] E. Bartowsky. Bacterial spoilage of wine and approaches to minimize it. *Letters in applied microbiology*, 48:149–56, 02 2009.

[24] M. Du Toit and I. S. Pretorius. Microbial spoilage and preservation of wine: using weapons for nature's own arsenal. 2000.

[25] G. E. Bousbouras and R. E. Kunkee. Effect of pH on Malo-Lactic Fermentation in Wine. *American Journal of Enology and Viticulture*, 22(3):121–126, 1971.

[26] P. Chatonnet, S. Bonnet, S. Boutou, and M. D. Labadie. Identification and responsibility of 2,4,6-tribromoanisole in musty, corked odors in wine. *Journal of Agricultural and Food Chemistry*, 52(5):1255–1262, 2004.

[27] A. P. Pollnitz, K. H. Pardon, D. Liacopoulos, G. K. Skouroumounis, and M. A. Sefton. The analysis of 2,4,6-trichloroanisole and other chloroanisoles in tainted wines and corks. *Australian Journal of Grape and Wine Research*, 2(3):184–190, 1996.

[28] D. A. Barker, D. L. Capone, A. P. Pollnttz, H. J. Mclean, I. L. Francis, H. Oakey, and M. A. Sefton. Absorption of 2,4,6-trichloroanisole by wine corks via the vapour phase in an enclosed environment. *Australian Journal of Grape and Wine Research*, 7(1):40–46, 2001.

[29] J. Goode. *The Science of Wine: From Vine to Glass*. University of California Press, 2005.

[30] R.S. Jackson. *Wine Tasting: A Professional Handbook*. ISSN. Elsevier Science, 2002.

[31] J. Jager, J. Diekmann, D. Lorenz, and L. Jakob. Cork-borne bacteria and yeasts as potential producers of off-flavours in wine. *Australian Journal of Grape and Wine Research*, 2:1–7, 03 2008.

[32] Sally-Jean Bell and P. A. Henschke. Implications of nitrogen nutrition for grapes, fermentation and wine. *Australian Journal of Grape and Wine Research*, 11(3):242–295, 2005.

[33] A. Barba, J. Oliva, and P. Pay. *Influence of Fungicide Residues in Wine Quality*. 12 2010.

[34] K. Ridgway, S. P. D. Lalljie, and R. M. Smith. Analysis of food taints and off-flavours: a review. *Food Additives & Contaminants: Part A*, 27(2):146–168, 2010.

[35] 2,4,6-trichloroanisole. https://en.wikipedia.org/wiki/, April 2020.

[36] D. Özhan, R. E. Anli, N. Vural, and M. Bayram. Determination of chloroanisoles and chlorophenols in cork and wine by using HS-SPME and GC-ECD detection. *Journal of the Institute of Brewing*, 115(1):71–77, 2009.

[37] S. Jonsson, T. Uusitalo, B. van Bavel, I. B. Gustafsson, and G. Lindstrom. Determination of 2,4,6-trichloroanisole and 2,4,6-tribromoanisole on ng/L to pg/L levels in wine by solid-phase microextraction and gas chromatography-high-resolution mass spectrometry. *Journal of Chromatography A*, 1111(1):71–75, 2006.

[38] M. L. Rodríguez, L. López-OCaña, J. López-Coronado, E. Rodriguez, M. J. Martinez, G. Larriba, and Juan-José Coque. Cork Taint of Wines: Role of the Filamentous Fungi Isolated from Cork in the Formation of 2,4,6-Trichloroanisole by O Methylation of 2,4,6-Trichlorophenol. *Applied and environmental microbiology*, 68:5860–5869, 01 2003.

[39] J. Harbertson and S. Spayd. Measuring phenolics in the winery. *American Journal of Enology and Viticulture*, 57:280–288, 01 2006.

[40] L. Casassa and J. Harbertson. Extraction, Evolution, and Sensory Impact of Phenolic Compounds During Red Wine Maceration. *Annual review of food science and technology*, 5, 01 2014.

[41] V. L. Singleton and P. Esau. Phenolic substances in grapes and wine, and their significance. *Advances in food research. Supplement*, 1:1–261, 1969.

[42] M. Victoria, M. Arribas, and C. Polo, editors. *Wine Chemistry and Biochemistry*. ISSN. Springer-Verlag New York, 1 edition, 2009.

[43] D. L. Capone, K. A. Van Leeuwen, K. H. Pardon, M. A. Daniel, G. M. Elsey, A. D. Coulter, and M. A. Sefton. Identification and analysis of 2-chloro-6-methylphenol, 2,6-dichlorophenol and indole: causes of taints and off-flavours in wines. *Australian Journal of Grape and Wine Research*, 16(1):210–217, 2010.

[44] W. R. Sponholz. *Alcohols Derived from Sugars and Other Sources and Fullbodiedness of Wines*. Springer, Berlin, Heidelberg, 1988.

[45] J. M. Amon, J. M. Vandepeer, and R. F Simpson. Compounds responsible for cork taint in wine. *Australian and New Zealand Wine Industry Journal*, 4:62–69, 1989.

[46] A. Peña-Neira, T. Hernández, María García-Vallejo, I. Estrella, and J. Suarez. A survey of phenolic compounds in Spanish wines of different geographical origin. *European Food Research and Technology*, 210:445–448, 04 2000.

[47] M. A. Sefton and R. F. Simpson. Compounds causing cork taint and the factors affecting their transfer from natural cork closures to wine–a review. *Australian Journal of Grape and Wine Research*, 11(2):226–240, 2005.

[48] Sally-Jean Bell and P. A. Henschke. Implications of nitrogen nutrition for grapes, fermentation and wine. *Australian Journal of Grape and Wine Research*, 11(3):242–295, 2005.

[49] R. S. Jackson. *Wine Science: Principles, Practice, Perception*. ISSN. Elsevier Science, 2000.

[50] G. Gutiérrez-Gamboa, T. Garde-Cerdán, Y. Moreno-Simunovic, and E. P. Pérez-Álvarez. Amino acid composition of grape juice and wine: Principal factors that determine its content and contribution to the human diet. In A. M. Grumezescu and A. M. Holban, editors, *Nutrients in Beverages*, pages 369–391. Academic Press, 2019.

[51] M. Arevalo-Villena, E. J. Bartowsky, D. Capone, and M. A. Sefton. Production of indole by wine-associated microorganisms under oenological conditions. *Food Microbiology*, 27(5):685–690, 2010.

[52] P. Chatonnet, A. Fleury, and S. Boutou. Origin and incidence of 2-methoxy-3,5-dimethylpyrazine, a compound with a “fungal” and “corky” aroma found in cork stoppers and oak chips in contact with wines. *Journal of Agricultural and Food Chemistry*, 58(23):12481–12490, 2010.

[53] P. A. Henschke and V. Jiranek. Yeasts-metabolism of nitrogen compounds in wine microbiology and biotechnology. *Harwood Academic Publishers*, pages 77–164, 01 1993.

[54] S. A. Harris, I. Ryona, and G. L. Sacks. Behavior of 3-Isobutyl-2-hydroxypyrazine (IBHP), a Key Intermediate in 3-Isobutyl-2-methoxypyrazine (IBMP) Metabolism, in Ripening Wine Grapes. *Journal of Agricultural and Food Chemistry*, 60(48):11901–11908, 2012.

[55] M. Allen, M. Lacey, R. Harris, and W. Brown. Contribution of Methoxypyrazines to Sauvignon blanc Wine Aroma. *American Journal of Enology and Viticulture*, 42:109–112, 01 1991.

[56] A. Fontana and R. Bottini. QuEChERS Method for the Determination of 3-Alkyl-2-Methoxypyrazines in wines by gas chromatography-mass spectrometry. *Food Analytical Methods*, 9, 05 2016.

[57] R. J. McGorrin. *The Significance of Volatile Sulfur Compounds in Food Flavors*, chapter 1, pages 3–31. 2011.

[58] M. Mestres, O. Busto, and J. Guasch. Analysis of organic sulfur compounds in wine aroma. *Journal of Chromatography A*, 881(1):569–581, 2000.

[59] D. Dubourdieu and T. Tominaga. *Polyfunctional Thiol Compounds*, pages 275–293. Springer New York, NY, 2009.

[60] F. M. Carrau, E. Boido, and E. Dellacassa. Terpenoids in Grapes and Wines: Origin and Micrometabolism during the Vinification Process. *Natural Product Communications*, 3(4):577–592, 2008.

[61] D. Slaghenaufi and M. Ugliano. Norisoprenoids, Sesquiterpenes and Terpenoids Content of Valpolicella Wines During Aging: Investigating Aroma Potential in Relationship to Evolution of Tobacco and Balsamic Aroma in Aged Wine. *Frontiers in Chemistry*, 6:66, 2018.

[62] C. A. Black, M. Parker, T. E. Siebert, D. L. Capone, and I. L. Francis. Terpenoids and their role in wine flavour: recent advances. *Australian Journal of Grape and Wine Research*, 21(S1):582–600, 2015.

[63] J. J. Mateo and M. Jiménez. Monoterpenes in grape juice and wines. *Journal of Chromatography A*, 881(1):557–567, 2000.

[64] L. Pripis-Nicolau, G. de Revel, A. Bertrand, and A. Maujean. Formation of flavor components by the reaction of amino acid and carbonyl compounds in mild conditions. *Journal of Agricultural and Food Chemistry*, 48(9):3761–3766, 2000.

[65] A. Escudero, E. Asensio, J. Cacho, and V. Ferreira. Sensory and chemical changes of young white wines stored under oxygen. An assessment of the role played by aldehydes and some other important odorants. *Food Chemistry*, 77(3):325–331, 2002.

[66] L. Pechamat, L. Zeng, M. Jourdes, R. Ghidossi, and Pierre-Louis Teissedre. Occurrence and formation kinetics of pyranomalvidin-procyanidin dimer pigment in merlot red wine: Impact of acidity and oxygen concentrations. *Journal of Agricultural and Food Chemistry*, 62(7):1701–1705, 2014.

[67] R. E. Anli and Özge A. Cavuldak. A review of microoxygenation application in wine. *Journal of the Institute of Brewing*, 118(4):368–385, 2012.

[68] R. F. Simpson. Aroma and compositional changes in wine with oxidation, storage and ageing. *VITIS–Journal of Grapevine Research*, 17(3):274, 2016.

[69] K. A. Lattey, B. R. Bramley, and I. L. Francis. Consumer acceptability, sensory properties and expert quality judgements of Australian Cabernet Sauvignon and Shiraz wines. *Australian Journal of Grape and Wine Research*, 16(1):189–202, 2010.

[70] R. Srinivasan and G. Sorial. Treatment of taste and odor causing compounds 2-methyl isoborneol and geosmin in drinking water: A critical review. *Journal of environmental sciences (China)*, 23:1–13, 01 2011.

[71] P. Ribéreau-Gayon, Y. Glories, A. Maujean, and D. Dubourdieu. Handbook of enology. *Handbook of Enology*, 2:1–441, 06 2006.

[72] L. Blanchard, P Darriet, and D. Dubourdieu. Reactivity of 3-mercaptohexanol in red wine: Impact of oxygen, phenolic fractions, and sulfur dioxide. *American Journal of Enology and Viticulture*, 55(2):115–120, 2004.

[73] S. La Guerche, B. Dauphin, M. Pons, D. Blancard, and P. Darriet. Characterization of some mushroom and earthy off-odors microbially induced by the development of rot on grapes. *Journal of Agricultural and Food Chemistry*, 54(24):9193–9200, 2006.

[74] C. De la Presa-Owens and A. C. Noble. Effect of storage at elevated temperatures on aroma of chardonnay wines. *American journal of enology and viticulture*, 48(3):310–316, 1997.

[75] P. Naouri, P. Chagnaud, A. Arnaud, P. Galzy, and J. Mathieu. Optimization of the conditions for preparing bacterial cultures for malolactic bioconversion. *Journal of Biotechnology*, 10(2):135–150, 1989.

[76] S. F. Price, P. J. Breen, M. Valladao, and B. T. Watson. Cluster sun exposure and quercetin in pinot noir grapes and wine. *American Journal of Enology and Viticulture*, 46(2):187–194, 1995.

2

Experimental Methods for VOC Concentration Measurement

2.1 Introduction

Analysis of food products, in view of food quality and safety, has been an important research area in food science and technology [1, 2]. Food analysis is an area of continuous evolution, where accurate analytical results are critical, be for exporters, importers, or government bodies to ensure safe food of the highest nutritional quality, assessment of product quality, and other attributes that influence a product's value to the consumer [3]. Food analysis, in particular, is highly complex because it integrates and applies principles of biology, chemistry, microbiology, biochemistry, nutrition, and engineering to characterize

new ingredients and food products, detect the food processing techniques used and ensure the safety and nutritional value of the food supply [2]. The primary factor of concern in the assessment of quality and safety of food and drinks is the VOCs released during their consumption. VOCs are the aroma and flavor compounds which are intimately linked to our enjoyment, palatability, and our perception of the food. They further help us to determine subtle changes in individual concentration, modification of ingredients, and contaminants responsible for food and drinks spoiled. Being a highly complex mixture of gases, hundreds of VOCs, wine analysis requires real-time and high-time resolution measurement analytical techniques capable of processing information quickly and for exploring events that happen relatively rapidly such as flavor and aroma release during wine consumption are of paramount importance.

2.2 Experimental Techniques

Analysis of the wine components poses a challenge to the researchers as they present at trace level (generally in pptv range) and highly complex mixture of many such compounds. Determining the concentration of such VOCs in wine requires detection techniques that should be able to meet the following standards: able to separate and quantify highly complex gas mixtures, should have very low detection limit (sub pptv level), and able to track changes in the concentrations that rapidly change with time [4, 5]. Direct injection mass spectrometry (DIMS) based on CI such as proton transfer reaction mass spectrometry (PTR-MS) and selected ion flow tube mass spectrometry (SIFT-MS) have been very successful due to their highly selective, high sensitivity and high time resolution modes of functioning. When coupled with other mass spectrometric techniques, these methods could yield high throughput and enhance analytic information.

2.2.1 Popular Analytical Techniques

Many well-established techniques include cyclic voltammetry, headspace solid-phase microextraction (HS-SPME) and gas chromatography coupled with electron capture detector

(GC-ECD), gas chromatography with high-resolution mass spectrometry (GC–HRMS), high-performance liquid chromatography (HPLC) and other mass spectrometry coupled techniques such as mass spectrometry-based e-noses (MS-e-noses), atmospheric pressure chemical ionization mass spectrometry (APCI-MS) [6–11]. A most common compound in wine is 2,4,6-trichloroanisole (TCA), usually detected by chromatographic techniques coupled (or not) to solid phase microextraction, lately, immunoanalytical techniques[1] were developed and applied allowing the detection of TCA, although in ranges well above the human detection threshold for wine. All of these above-mentioned techniques have their advantages and disadvantages as well. Nevertheless, the development of more simple analytical procedures to quantify TCA and other wine-related compounds is still a challenging task from both academic and industrial point of view. We will focus our discussion on PTR-MS and SIFT-MS methods because they allow real-time VOCs monitoring and at very low detection limits. Also, they provide non-invasive measurements of VOCs with very high sensitivity having applications in environmental, food science, biology, pharmaceutical, and medical science [12, 13].

2.2.2 Chemical Ionization

CI is called a soft ionization technique that was developed during 1960s [14, 15], where a reagent gas is ionized by electron impact at a high reagent gas pressure. The resulted product ions of IMRs between the reagent gas ions and reagent gas neutrals are allowed to react with the analyte molecule via proton transfer or hydride transfer reactions. The PTR will be favored if the PA of the sample analyte molecules is higher than that of the reagent gas ion and hydride transfer will be dominated if the PA of the sample analyte molecules is lower than that of the reagent gas ion. CI in particular plays a significant role in minimizing the fragmentation to a larger extent, which interns helpful in minimizing the mass spectrum complexity. CI generates stable charged molecules and the reactions under CI are low in energy as compared to EI[2] method. CI is very useful to elucidate the molecular ions of

[1] Bisensor based and immunosorbent solid phase extraction followed by enzyme-linked immunosorbent.

[2] In EI, the molecules are bombarded with electrons of ∼70 eV emitted from a (rhenium or tungsten) filament. A molecular radical ion with a sufficient amount of energy accumulated in its bonds to dissociate into typical fragment ions, radicals, and neutral species.

unknowns and is often the ionization method of choice for quantitative mass spectroscopy via ion monitoring.

2.3 Proton-Transfer Reaction Mass-Spectrometry

DIMS based techniques such as PTR-MS is an established method for the rapid and non-invasive online monitoring of VOCs [16]. PTR-MS uses CI and the concept of swarm type technique of flow tube in combination with flow drift tube for determining the concentration of trace gases. PTR-MS was first introduced by Werner Lindinger and his collaborators in 1995 as a technique for accurate quantification of the densities of neutral components by measuring the primary and product ion signals in the IMR usually with H_3O^+, a widely used ion in PTR-MS analysis [17]. The gases analyte sample containing VOCs to be analyzed (for example, ambient air) is sampled directly into the PTR mass spectrometer without any sample preparation. The analyte sample must have PAs higher than that of water for PTR to occur. This is an analytic technique that uses the kinetics of the reaction or gas calibration standards to determine the concentration of unknown compounds.

PTR-MS technique is pioneered by the group of Werner Lindinger[1]. The primary strength of PTR-MS, especially in food science, is its ability to monitor rapid changes in trace volatile concentrations (with an ultimate time resolution of 100 ms) within the complex chemical matrix of food i.e. it has the ability to investigate the dynamic release of aromas and, therefore rapid changes in composition [18, 19]. PTR-MS has been widely used in the trace gas analysis of volatile organic compounds (VOCs). PTR-MS employs soft ionization (CI) which considered to be one of the strengths of PTR-MS as it avoids fragmentation at a larger extent and H_3O^+ ions as primary reactant ions. The advantage of using H_3O^+ is that it does not react with most of the air constituents, as their proton affinities values are lower than that of H_2O (166.5 kcal/mol). Moreover, most of the the VOCs fall in the range having PAs larger than that of water except smaller alkanes and ethenes.

[1] Innsburk, Austria 1998. Originally developed for environmental studies but its potential applications in food science (flavor study, food quality assessment and monitoring technological processes) is recognized shortly after it's inception.

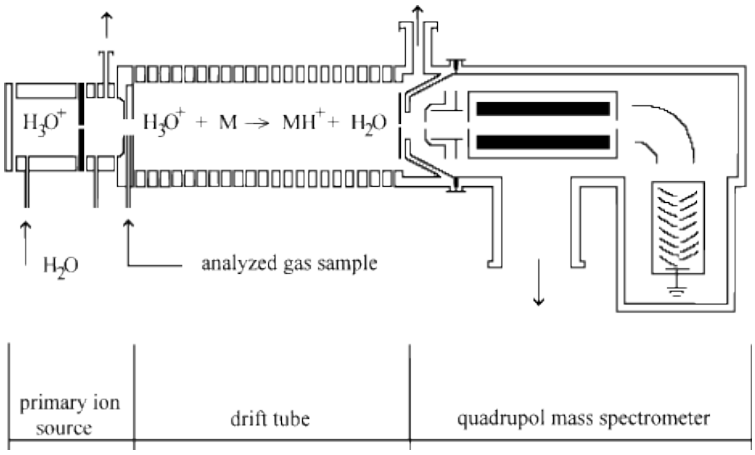

Figure 2.1: PTR-MS schematic illustration and working principle. (*Source: Wikipedia*)

2.3.1 Experimental Components

The basic operation of the PTR-MS instrument follows as: the gas sample of the analyte molecule is continuously introduced in the drift tube where it is mixed with pure (greater than 99.8%) beam of highly intense ($\sim 10^7$ counts per second) H_3O^+ ions[1] [20–23]. The VOCs with PA values higher than water (H_2O = 166.5 kcal/mol) undergo PTRs from H_3O^+ ion eventually ionized the analyte molecule, and the mass spectrum is analyzed in mass spectrometer and detected as count rate per second. A schematic diagram of a PTR-MS instrument is shown in Figure 2.1.

The PTR-MS instrument consists of five basic components.

- **Sample Inlet :** The sampling inlet draws the gas-phase analyte molecules directly into the PTR cell. The inlet designs may vary and must consider factors such as inertness of materials and flow rate. The inlet line may be heated in order to facilitate the detection of "sticky" VOCs. Unheated inlets are preferred for the analysis of VOCs that are easily degraded by temperature.

- **Ion Source :** The H_3O^+ reagent ions are generated in the hollow cathode that works on DC voltage. In hollow cathode, the H_3O^+ ions are produced from humidified

[1]The ion source in most PTR-MS instruments is a hollow cathode that operates of a DC voltage, and generates H_3O^+ from a discharge of water vapor at a typical pressure of ~ 0.75 Torr. Other fragment ions OH^+, N_2^+, O^+, H_2^+, and H_2O^+ produced in the discharge are converted into H_3O^+ so that hollow cathode can deliver H_3O^+ ions with 99.8% purity.

air. In addition to H_3O^+ ions, other spurious ions such as H_2O^+, OH^+, and O^+ are also generated owing to the dissociation of H_2O in the discharge undergo efficient reactions with water that also lead to H_3O^+ such that the equilibrium ion population is highly pure consisting of 99.8% of H_3O^+. The applied electric field accelerates the generated H_3O^+ ions from the ion source to the drift tube where the ions interact with gaseous analyte molecules exiting the sampling inlet.

- **Drift Tube :** The drift tube in a typical PTR-MS instrument consists of a series of equally spaced rings separated by insulators in order to establish a voltage gradient inside the drift tube that accelerates the ions in the direction of flow. An electric field strength of most of the commercial PTR-MS instruments is 50 V cm^{-1} for a drift tube length of ∼10 cm and voltage gradient of 500 V. Other working conditions critical for the IMRs to occur within a volume in drift tube are stable and controlled electric field, temperature, and pressure. Both tunability and stability are important to provide absolute quantification of VOCs concentration in real-time. Pressure of ∼ 1.5 Torr (2 mbar) is maintained in a typical PTR cell. An important parameter is the applied electric field that controls the collisions between the ions and the neutral gas molecules inside the drift tube. Electric field inside the chamber moves the reagent H_3O^+ ions and the product ions (protonated VOCs) along the drift axis towards the detector region. The quantity E/N is conveniently employed to describe the conditions in the reaction chamber, where E is the electric field along the drift axis and N is the gas number density. Typical value of E/N in the range of 80-150 Td[1] is commonly employed in PTR-MS.

- **Ion Focusing Region :** The Ion focusing interface must efficiently transmit ions from the PTR cell to the mass analyzer. This region is more specific as a transfer region between the drift tube and the mass spectrometer. It may be necessary to accelerate or decelerate ions with specific kinetic energies while reconciling the pressure difference between the reaction cell (e.g. 1.5 Torr) and the low-pressure mass analyzer (e.g. 7.5e-7 Torr). The pressure drop from the reaction cell to the mass ana-

[1] 1 Td = 1 Townsend = $10^{-17} cm^2 V^{-1} s^{-1}$

lyzer occurs across a succession of differentially pumped vacuum stages each having lower pressure. Ion optics is used to steer and focus the ions through these stages. Instrumentation design may vary and include both static steering and focusing elements and RF components, such as quadrupole ion guides. The efficiency with which the interface is able to transmit the ions into the mass analyzer significantly affects achieved sensitivity.

- **Mass Analyzer :** Analytic ions are detected by a mass analyzer that enables identification of VOCs based on their mass-to-charge ratio (m/Q) and the determination of their concentrations based on recorded signal intensity. Quadrupole mass analyzers were used in the initial PTR-MS instruments due to their low cost. But they suffered from limited mass range and unit mass resolution meaning they cannot resolve ions that have the same nominal m/Q. A user may monitor specific m/Q values of interest, or scans across an entire range of m/Q to produce a complete mass spectrum. Other mass analyzers such as ion trap mass analyzers have been used recently, although, with limited success for PTR-MS analysis. The major breakthrough was the use of time-of-flight (TOF) PTR-TOF-MS, which provides good mass resolution without the mass discrimination problems as exhibited by quadrupole instruments. The use of TOF mass analyzers has become common in the recent years. TOF mass analyzers separate ions based on differences in their velocities after acceleration by a fixed potential. TOF mass analyzers inherently measure all m/Q simultaneously, and therefore excel for any PTR-MS analyses that intend to measure many different VOCs species. Further, TOF mass analyzers can have much higher mass resolving power than quadrupole mass analyzers.

2.3.2 Ion-Molecule Chemistry

As already mentioned, PTR-MS is based on swarm type experiments, where the primary (reactant) ions travel through a buffer/carrier gas to which the reactant gas R is added in small amounts such that the carrier gas density higher than the density of R [24, 25]. On the way through the reaction region, the ions have many non-reactive collisions with buffer

gas atoms or molecules; however, once they collide with a reactant gas-particle they may undergo a reaction and specifically in the case of hydronium (H_3O^+) ion[1], a proton will be transferred to the analyte molecule (if energetically allowed). In the PTR-MS drift tube, H_3O^+ ions in the buffer gas (air or He) are allowed to react with the analyte molecule R and undergo PTR as follows [26]

$$H_3O^+ + R \longrightarrow RH^+ + H_2O\,. \tag{2.1}$$

The reaction is of first order (pseudo) as only trace components of [R] are to reacts with H_3O^+ ions. This means the reaction does not decrease the strength of the reactant ion significantly and $[RH^+] \ll [H_3O^+]$ will always remain effective. Hence, the density of the product ion $[RH^+]$ can be calculated as

$$[RH^+] = [H_3O^+]_o(1 - \exp^{-k[R]t}) \approx [H_3O^+]_o k[R]t, \tag{2.2}$$

where concentration [R] of the analyte compound in the above exothermic reaction can be measured from the following equation

$$[R] = \frac{1}{k\tau}\frac{[RH^+]}{[H_3O^+]_o}, \tag{2.3}$$

where $[H_3O^+]_o$ is the density of H_3O^+ ions without the reactant neutrals in buffer gas. k is the rate coefficient of the reaction and τ is the reaction time[2] for the reagent ions traversing the drift tube usually $\sim 100\ \mu$s. From equations (2.2) and (2.3) the density of a neutral R can be obtained by measuring the primary $[H_3O^+]_o$ and product ion $[RH^+]$ signals if the rate coefficient k and reaction time τ are already known. The reaction time, however, does not change since the pressure and electric field strength in the drift tube are kept constant at all times. The reaction time can be calculated either by pulsing the entrance and the exit slits of the drift tube and monitoring the arrival time spectrum, or by from ($v_d = \mu E$)

[1]The choice of this ion is highly significant. Proton donation from H_3O^+ to many organic molecules is exothermic and the PAs of these molecules must exceed those of water molecule.

[2]The reaction time τ is the time it takes for the reagent ion to travel from the point where it is first mixed with the analyte to the end of the drift tube (beyond which reaction essentially stops).

ion mobility values in air, where E is the electric field strength and is kept high enough to ensure that it is large compared to the flow velocity of the air through the drift tube[1].

In a typical PTR-MS instrument, the fixed length of the drift tube $\sim$ 10 cm provides fixed reaction time for the H_3O^+ ions for a given value of the reduced electric field, E/N (where E is the applied electric field and N is the gas number density[2]). The electric field strength is often given by E/N which delivers energy to the ion-molecule collisions to prevent excessive clustering of neutral molecules onto ions. In particular, some VOCs show excessive clustering formation of $H_3O^+(H_2O)_n$, n=1,2.. with H_3O^+ reaction leads to the different reaction chemistry which is always averted. Usually, throughout the measurements, E/N is kept in between 120–140 Td. The applied electric field supplies additional energy to the H_3O^+ ions traveling along the drift tube. The following equation provides a good approximation to the mean kinetic energy of the ion-molecule collisions inside the drift tube.

$$\mathrm{KE_{ion}} = \frac{3}{2}k_\mathrm{B}T + \frac{1}{2}\mathrm{m_{ion}v_d^2} + \frac{1}{2}\mathrm{m_b v_d^2}. \tag{2.4}$$

Here $\mathrm{m_{ion}}$ is the mass of the ion, T is the drift-tube temperature. At the right-hand side of equation (2.4), the first term is the thermal energy, second term is the kinetic energy contribution of the ions drift and the third contribution comes from the collision between ions and buffer-gas molecules having mass $\mathrm{m_b}$. The drift velocity, v_d, in the tube resulting from the applied electric field E/N and the collisions with the buffer gas. Equation (2.4) represents the ion kinetic energy in the laboratory frame of reference as derived by Wannier from basic principles and later by McFarland [27–29]. The kinetic energy in equation (2.4) evaluates to 0.25 eV for a typical PTR-MS working conditions (E/N = 120 Td, $T = 300$ K and mean ion drift velocity, $v_\mathrm{d} = 906\ \mathrm{m\,s^{-1}}$). This kinetic energy is much higher than the typical thermal energy $\simeq 0.03$ eV. In ion-molecule collisions the mean relative center-of-mass kinetic energy ($\mathrm{KE_{com}}$) is of greater relevance than $\mathrm{KE_{ion}}$ between ions and the neutral reactants, embedded in the buffer gas. The $\mathrm{KE_{com}}$ for the ion-neutral molecule

[1]Drift tube consists of a series of equally spaced electrodes separated by insulating spacer in order to maintain voltage on each electrode. The primary role of drift tube is to generate a uniform electric field that draws ions along the drift tube and delivers an increased migration velocity for the ions.

[2]The gas number density is defined as the number of gas particles per unit volume and can be derived from the ideal gas equation.

collision in PTR-MS drift tube can be expressed as

$$\mathrm{KE_{com}} = \frac{3}{2}k_{\mathrm{B}}T + \frac{\mathrm{m_n}}{\mathrm{m_{ion}} + \mathrm{m_n}}\left(\mathrm{KE_{ion}} - \frac{3}{2}k_{\mathrm{B}}T\right), \tag{2.5}$$

where $\mathrm{m_n}$ is the mass of the neutral molecule. The collision energy is the key parameter to understand the effect of the ion kinetic energy on the ion-molecule collision. The effective temperature occurring inside the PTR-MS drift tube for PTRs is an uncertain quantity. Since ions within the drift tube are provided with additional energy by the applied electric field, the translational temperature is not the same as the laboratory temperature of the drift tube. The ion-molecule collision reactions as a result in the PTR-MS drift tube is far more energetic than thermal temperature collisions as mentioned above. An effective ion temperature, T_{eff}, can be defined by equating an effective ion thermal energy with the mean center-of-mass collision energy between the ion and the buffer gas. Assuming a temperature of 298 K for the drift tube the calculated effective ion temperature (e.g. Hydrogen sulfide, T_{eff} = 1316 K) is clearly well above 1000 K as evaluated by equation (2.6). Following expression should be used for a fair estimation of the effective ion translational temperature inside the drift tube

$$T_{\mathrm{eff}} = T + \frac{v_{\mathrm{d}}^2}{3k_{\mathrm{B}}}\frac{\mathrm{m_n}(\mathrm{m_{ion}} + \mathrm{m_b})}{\mathrm{m_{ion}} + \mathrm{m_n}}. \tag{2.6}$$

Here $\mathrm{m_b}$ is the mass of a buffer-gas[1] molecule and T is the drift-tube temperature, and v_{d} the speed of the ions.

2.3.3 Applications of PTR-MS

- **Environmental Science :** Environmental VOCs are generated by natural and anthropogenic processes. Natural source of VOCs include biogenic emission and emission from plants and oceans while anthropogenic contains man-made sources of VOCs commonly used household products such as paints, varnishes, wax, disinfecting,

[1] If the buffer gas used is air, the molecular mass of the buffer gas is a weighted average of those of N_2 and O_2 (28.8 a.m.u.).

cosmetic, degreasing, and hobby products. Natural emission produces more severe effects than anthropogenic sources in the atmosphere. Given their importance in the atmosphere, accurate atmospheric measurements of VOCs, in terms of their identification, concentrations, and evolution, covering a wide range of environments and altitudes are important for a quantitative understanding of atmospheric chemical processing. PTR-MS as a tool in monitoring the atmospheric VOCs has been an established method of analysis due to the following reasons: high sensitivity, fast response, and non-reactivity of H_3O^+ with various air constituents. The applications exhibited using PTR-MS cover a wide range of volatiles arising from widely different sources and processes. These include monitoring normal atmospheric volatile variations, anthropogenic VOCs, biogenic VOCs, and pollution monitoring analysis for a real-time appraisal of atmospheric VOCs [30–34]. General atmospheric performance studied by measuring nitrogen-containing compounds including other trace level species is important for the range of oxidation processes in the atmosphere and oxygenated VOCs (alcohols, aldehydes, ketones, and carboxylic acids) ambiguous in the troposphere has been studied using PTR-MS [35, 36]. Other applications include analysis of biogenic VOCs, anthropogenic VOCs, biomass burning, plant studies, and soil emissions [37, 38].

- **Food Science :** Monitoring the emission of VOCs has many potential applications in the food industry, since biological materials that are aged, cooked, treated, etc. often release characteristic VOCs that serve as the indicator of the extent of changes in the food product which interns linked to the quality, stability, and degradation with the age. PTR-MS is widely used for monitoring rapid changes in trace VOCs concentrations because it has the ability to investigate dynamic changes in aroma and composition in foodstuffs [18, 39, 40]. Most of the studies have been performed on food and alcoholic beverages are related to the flavor released during consumption. The volatiles in coffee aroma were studied by using PTR-MS and the effect of the VOCs emitted from coffee beans roasting has been studied using PTR-TOF-MS [41]. Cappellin et al. have reviewed PTR-MS applications in agri-food and health sciences

[42]. A comprehensive study using PTR-MS has been done on cheese, strawberry fruits, and other related foodstuffs [43–45]. Quality control in daily usage products such as cheese, meat, fruit, and vegetable (ripening, storage, and monitoring) is an another intensely investigated work area using PTR-MS instrument. Boscaini et al. [46] have used PTR-MS for the characterization of wine using direct headspace analysis and mass spectral fingerprints. Another study by H. Campbell-Sills et al. [47] advances using PTR-TOF-MS in wine analysis is thoroughly investigated [48]. However, it is worthwhile to note that higher concentration of ethanol in wine limits the use of PTR-MS in its conventional way for VOCs identification and quantification [49]. The large concentration of ethanol content in wine greatly influences the PTR-MS ionization processes. Because high ethanol content in the head space of the wine sample leads to the depletion of H_3O^+ ions and complicates the mass spectra by promoting the generation of peaks that contain ethanol dimer $C_2H_5OHH^+$ (C_2H_5OH), trimers $C_2H_5OHH^+$ $(C_2H_5OH)_2$, mixed ethanol cluster $C_2H_5^+$ (C_2H_5OH) and $C_2H_5^+$ $(C_2H_5OH)_2$, and fragments associated with combined ethanol and VOCs [50]. Although, the problem is addressed by many researchers by proposing either dilution of sample gas to reduce the concentration of ethanol [50] or by coupling of PTR-ToF-MS to a rapid step of chromatographic separation (FastGC) [51] and instead of using hydronium ions H_3O^+ protonated ethanol clusters $C_2H_5OHH^+$ $(C_2H_5OH)_n$, n = 1,2... [46] are used as chemical ionization reagent ions. However, a detailed theory of protonated ethanol-VOCs ion-chemistry would be required for a useful implementation of the latter method in PTR-MS measurements. Owing to the constant improvement in the PTR technology, fast and non-invasive analysis of VOCs provided by PTR-MS head-space analysis has huge potential in wine analysis and quality control.

- **Medical Science :** The use of PTR-MS in diagnosis and monitoring disease provides an option to overcome invasive medical procedures which can be stressful for many patients. Another reason is that such procedures are usually time-consuming as well as expensive since they include the collection of biological materials and laboratory

investigations. PTR-MS is widely used in medical science for a number of potential medical applications including breath analysis, urine analysis, in vivo human skin studies, and occupational health exposure in medical environments [52–54]. Taking the most common example of exhaled air which contains endogenous VOCs components[1], the concentration lies in the ppmv or ppbv range. Many VOCs are produced within the human body in metabolic processes. These processes are influenced by the intake of unusual amounts of specific kinds of food or chemicals, also by illness, VOCs in the body (through breath) can show concentrations deviating significantly from the normal values. PTR-TOF-MS has been used for the analysis of liver cirrhosis and the severity of the disease assessed by the exhaled breath [55]. Other applications include finding acetone, isoprene in breath, lung study, kidney, and liver disease [56, 57]. A comprehensive list of PTR-MS applications in medical science can be obtained in many reports [57, 58].

2.4 Seleted Ion Flow Tube Mass Spectrometry

SIFT-MS is a method for the real-time quantification of the trace gases developed by Spanel and Smith in 1996 [59]. SIFT-MS is used as a direct mass spectrometry technique suitable for the analysis of VOCs with a typical detection limit as low as pptv. In this technique, real-time and quantitative analysis is achieved by applying precisely controlled soft CI and eliminating the requirement of sample preparation, pre-concentration, and chromatography. SIFT-MS was a follow-up technique of SIFT developed by Adams and Smith in the mid-seventies [60]. SIFT in turn was an extension of the early work of adapting flow tubes to investigate IMRs begun in the late 1960s by Ferguson and collaborators [61]. The chemistry of SIFT-MS and SIFT thought to be opposite to each other, although core methodology remains same. In SIFT, kinetic parameters of IMRs are derived from the known reactant concentration while in SIFT-MS, the concentration of the analyte molecules is determined from known kinetic parameters. Ultra-soft CI in SIFT-MS allows it to provide unparalleled selectivity among other mass spectrometric techniques. Another factor that

[1] Common VOCs present are acetone, methanol and isoprene.

makes SIFT-MS technology unique to other techniques is the reagent (or precursor) ions which are well characterized, mass-selective and undergo known IMRs with the analytes. Eight chemical ionization agents (reagent ions) including positive and negative viz H_3O^+, NO^+, O_2^+, O^-, O_2^-, OH^-, NO_2^-, and NO_3^- are commonly applied in SIFT-MS instrument. These eight reagent ions react with analyte VOCs and inorganic gases in very well controlled IMRs, but they do not react with the major components of air (N_2, O_2, and Ar). This enables SIFT-MS to analyze air at trace and ultra-trace levels without preconcentration.

2.4.1 Experimental Components

SIFT-MS can be viewed as a combination of four main components [12, 58]. The working principle of the SIFT technique is as follows: the mixture of positive and negative ions are created in a gas discharge ion source and from this plasma mixture a current of ions of a chosen m/Q is obtained using a quadrupole mass filter. Then these ions are injected into a fast-flowing inert carrier gas (helium) through a Venturi type inlet. Thus, a cold precursor ion/helium gas swarm is created possessing a Maxwellian speed distribution appropriate to the temperature[1] of the helium carrier gas. This swarm is convected along the flow tube and the ions are sampled downstream via a pinhole orifice and focused into a deferentially pumped quadrupole mass spectrometer. After m/Q analysis, they are detected and counted by an electron multiplier/pulse counting system. A full schematic of all the components of SIFT-MS is shown in Figures 2.2 and 2.3 below.

[1] Usually 300 K, but can range from 80 K to 600 K in more sophisticated instruments.

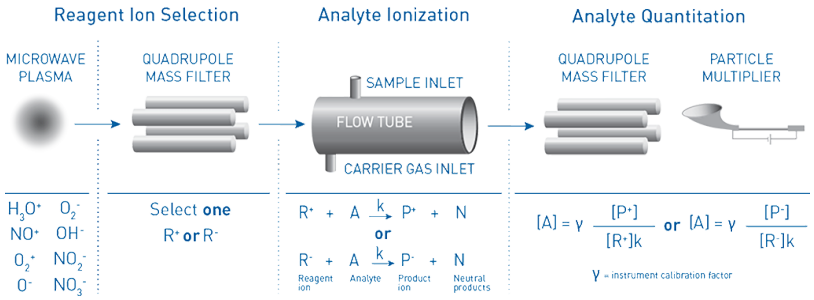

Figure 2.2: SIFT-MS representation of ion-molecule reaction. (*Source: Syft Technologies Ltd.)*

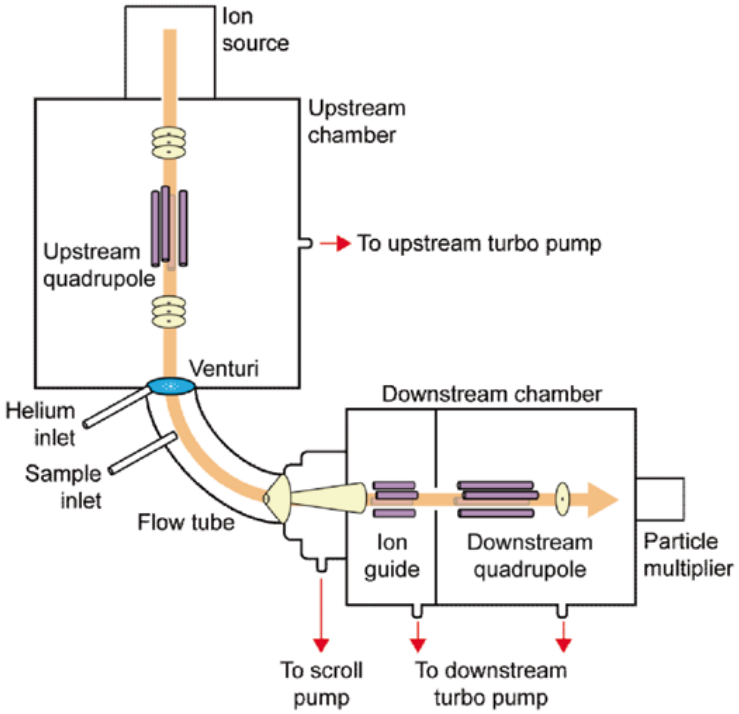

Figure 2.3: Schematic of commercial SIFT-MS instrument with various components. (*Source: Syft Technologies Ltd.)*

- **Reagent Ion Generation and Selection :** Eight SIFT-MS reagent ions are formed by microwave discharge through moist or dry air at low pressure. These ions are then transmitted to low-pressure upstream quadrupole mass filter. In this region, one reagent ion out of eight is selected at any particular time using the first quadrupole mass filter at typical pressure 10^{-4} Torr.

- **Analyte Ionization :** The selected reagent ion (H_3O^+, NO^+, O_2^+ or O^-) is injected into the flow tube and excess energy is removed through collisions with the carrier gas (usually helium, nitrogen may be used depending on the application). Typical pressure in this region is maintained at around 0.6 Torr so the ions from the upstream quadrupole enter the flow tube against a pressure gradient. The sample is then introduced at a known flow rate and the reactive compounds it contains are ionized by the reagent ion to form well-characterized product ions.

- **Analyte Detection and Quantitation :** All the ions (product ions and unreacted reagent ions) in the flow tube then sampled through a small orifice at the downstream end of the flow tube and are mass analyzed by the second quadrupole mass spectrometer. The ion number densities are then counted by the pulse counting electronics.

2.4.2 Reagent Ions in Flow (Drift) Tube

- **Reactions of H_3O^+:** PTRs are generally identified as a soft form of ionization usually one product ion is produced for each volatile present in the analyte. In the PTR-MS ion source, consists of a hollow cathode, H_3O^+ ions are produced from the discharge of water vapor. H_3O^+ is predominately considered as ion of choice because of PA values of H_2O (166.5 kcal/mol) is lower than the PA of most of the organic molecules. When the PA of the molecule is greater than that of H_2O, the exothermic reaction occurs in a non-dissociative proton transfer pathway as given by

$$H_3O^+ + R \longrightarrow RH^+ + H_2O\,. \tag{2.7}$$

Most of the PTR chemistry in PTR-MS is subjected to H_3O^+ ions for the analysis of alcohols, esters, aldehydes, amines, ketones, and thiols through non-dissociative proton transfer at 300 K [62–64]. Depending on the energetic condition in the PTR-MS drift tube, other reaction pathways could occur for e.g. reaction of water cluster ions, association reaction, and dissociative proton transfer. However, cluster ion formation is minimized and always avoided in PTR-MS experiments.

- **Reactions of NH_4^+:** Implementation of reagent ions other than H_3O^+ such as NH_4^+ has been reported in many publications [65, 66]. NH_4^+ ions are produced from H_2O vapor and N_2 gas. In contrast to H_3O^+ ions, ionization with NH_4^+ is more specific and limited to the volatile molecules having PA values greater than that of ammonia (NH_3 = 204.0 kcal/mol). Due to the large PA of ammonia, a limited number of reactions are exothermic and occur through fast proton transfer from NH_4^+ to the volatile molecule. If the analyte molecules possess higher PA than ammonia then the reaction (2.8) will be exothermic and PTR occurs at every collision.

$$NH_4^+ + R \longrightarrow RH^+ + NH_3\,. \tag{2.8}$$

NH_4^+ is specific in those cases where ionization with H_3O^+ produce fragmentation (molecules with very high PA) could produce complex spectra and decrease the sensitivity. And the cases where two molecules show the same nominal masses with H_3O^+, the use of NH_4^+ in place of H_3O^+ provides a means of distinguishing between these two compounds. NH_4^+ is suitable for the identification and quantification of amines and many nitrogen-containing molecules.

- **Reactions of NO^+:** The source of NO^+ ions is ambient air passed through a charcoal filter. NO^+ produces only one or two product ions on the reaction with an analyte molecule. Also, very useful and important reagent ion in identifying isobaric compounds in SIFT-MS analysis [64, 67, 68]. The VOCs undergo charge transfer reaction with NO^+ only when the IE of the neutral molecule is less than the IE of NO (9.26 eV). In general, NO^+ reacts with analyte molecule primarily via three reaction

modes namely: addition or adduct formation (2.9), hydride ion abstraction (2.10) and charge transfer (2.11).

$$NO^+ + M \longrightarrow [M.NO]^+, \tag{2.9}$$

$$NO^+ + M \longrightarrow [M-H]^+ + HNO, \tag{2.10}$$

$$NO^+ + M \longrightarrow M^+ + NO. \tag{2.11}$$

With many aromatic compounds, NO^+ reacts by charge transfer or by adduct ion formation. Aromatic compounds with very high IE, adduct ions are formed while compounds with lower IE charge exchange (2.11) reactions will be favored.

- **Reactions of O_2^+:** In the source region, O_2^+ ions are produced from pure air. O_2^+ is the most energetic of usual SIFT-MS reagent ions with O_2 IE $\sim$ 12.06 eV. O_2^+ reacts with many of the volatile molecules through charge exchange reaction (2.12) and dissociative reactions (2.13) producing many fragments [63, 67, 69, 70]. The charge transfer will be thermodynamically favored if VOCs have IE smaller than the IE of O_2. O_2^+ is particularly useful in monitoring analytes that are non-reactive with NO^+ and H_3O^+ reagent ions such as the small hydrocarbons.

$$O_2^+ + M \longrightarrow M^+ + O_2, \tag{2.12}$$

$$O_2^+ + M \longrightarrow [M-\text{fragment}]^+. \tag{2.13}$$

It is worthwhile to note that most of the organic molecules have first IEs between 8 to 11 eV [15]. Molecules with small IEs, charge transfer predominately occurs with one or two product ions. However, there is a strong possibility that a large amount of excess energy will be deposited on the product side ion that could lead to dissociative charge transfer and produces multiple fragment ions in a few cases. The reaction products of these fragment ions are highly complex and could be studied under fragmentation pathways of these ions.

2.4.3 Applications of SIFT-MS

- **Environmental Science :** The use of SIFT-MS in the real-time monitoring of atmospheric VOCs has made significant progress in the past decade and received enormous attention in numerous laboratories around the world [71, 72]. An immediate SIFT-MS analysis of VOCs is to appraise very low volatile concentrations. A remarkable advantage of using SIFT-MS lies in the immediacy of the results and in absolute quantification of a wide variety of low molecular weight compounds and able to detect molecules like ammonia and some small aldehydes that are not easy to analyze by other mass spectrometory techniques [73, 74]. The study of aromatic hydrocarbons along with other VOCs (notably alcohols) emitted from vehicle exhausts gases have been analyzed [75]. In a similar study, diesel engine exhaust gases such as NO, NO_2, HNO_2, aldehyde and ketones were reported. The VOCs present in the air originating from the chemistry laboratories and pollutants greatly dependent on the traffic density and the weather conditions were nicely presented by Španěl et al. [12]. A method was developed to study peroxyacetyl nitrate[1] (PAN) using SIFT-MS with a detection limit of up to 20 pptv in 10 seconds [76]. In order to study landfills, methods were developed using SIFT-MS to monitor siloxanes[2] [77]. A large number of VOCs have been examined using SIFT-MS which originate from intensive farming and are reported [12].

- **Food Science :** The first SIFT-MS study of real-time monitoring of food flavor was dated back in 1999 [78]. Since then there has been a myriad of articles reported related to SIFT-MS applications in food science [79]. SIFT-MS accomplishes the analysis and quantification of trace gases originated from food and food products through a process of chemical ionization using three precursor ions H_3O^+, NO^+, and O_2^+. These ions are mass selective and switchable during the analysis process which makes SIFT-MS distinctive from other analytic techniques and demonstrates

[1] PAN is a precursor to photochemical smog.
[2] Anthropogenic compounds found in landfill sites, posed significant problems when gas emissions from landfills are combusted.

the worth of SIFT-MS to the area of food science. The application of trace gas analysis in monitoring food freshness, food preparation, and the brewing industry has been exploited by many authors. Basil (Ocimum basilicum) belongs to the genus Ocimum comprising approximately 30 varieties have been studied for the reaction of series of terpenoids with H_3O^+, NO^+ and O_2^+ by Gianluca Amadei et al. [67]. A similar study has been carried out by Liana Iachetta et al. to analyze fluorescent esters which are common in naturally occurring foodstuffs [80]. SIFT study of the reactions of different precursor ions, H_3O^+, NO^+, and O_2^+, with a series of diols (alcohols) is reported by Patrik Španěl et al. [69]. A comprehensive list of SIFT-MS analysis for the following volatile compounds such as aliphatic aldehydes, alcohols, esters, and terpenes emitted by many food items and alcoholic beverages can be found in the respective articles [63, 64, 68, 81]. In food science, real-time SIFT-MS measurements of VOCs is crucial and it provides input for a number of food quality markers such as food flavor, ripening stages, food quality and freshness.

- **Medical Science :** SIFT-MS was originally designed to study breath analysis and over the years it has shown a great promise in the medical field. SIFT-MS has been advantageous over other analytic methods for many pilot investigations in several areas of research especially as a non-invasive breath analysis tool to investigate physiological processes in humans and animals also for clinical diagnosis and for therapeutic monitoring [82, 83]. Direct Breath analysis alone serves identification and quantification of VOCs present in exhaled breath, abnormal concentrations of common metabolites in breath and identify biomarker compounds responsible for disease and track the processes related to prophylactic effects. Spanal and Smith have conducted SIFT-MS study on the air/breath samples with different precursor ions such as H_3O^+, NO^+ and O_2^+ to measure aldehydes and other compounds in exhaust gases and breath analysis for respiratory irritants and metabolites present in breath along with their distribution in the healthy population. The VOCs present in the headspace of vapor of urine samples in the patients with gastro-esophageal cancer has been reported [84]. Dweik et al. have made significant progress in identifying the num-

ber of VOCs while monitoring breath which includes trimethylamine, acetone, and pentane[1] [85]. Breath analysis for advanced kidney disease, bowel disease, juvenile idiopathic arthritis and ethanol metabolism using SIFT-MS can be found in various articles [12, 22, 86].

2.5 Difference Between PTR-MS and SIFT-MS

DIMS oriented techniques such as PTR-MS and SIFT-MS have clear advantages over other analytic techniques as they eliminate many sample pre-treatment processes. Both technologies allow immediate quantification of an analyte in a gas mixture in real-time and employ the kinetics taking place in a flow tube to determine the concentration of one or many constituents of the gas sample. However, there are some differences in their operation and technology. PTR-MS operates under the effect of the applied electric field which makes PTR-MS to work under higher effective temperatures and kinetic behavior is mostly unknown at such high temperatures. In other words, thermal ion-analyte chemistry in the PTR-MS drift tube changes continuously. While in SIFT-MS no such field is present and the ion-analyte reactions occur at well-controlled thermal conditions [87]. Another major difference is that PTR-MS usually operates with one reagent ion i.e. H_3O^+ which is not mass selective and switching[2] to other ions is time-consuming as a clean source is always required every time. SIFT-MS on the other hand operates with a microwave discharge and mass-selected reagent ions usually H_3O^+, NO^+ and O_2^+ that can be switched within a few ms [22]. This is a clear advantage of SIFT-MS over the PTR-MS instrument. Switching between the ions in SIFT-MS has another advantage as the ion-molecule chemistry will be different as ions such as NO^+ can not supply proton to the analyte, so the NO^+ undergo charge transfer reaction with some analyte gases and this difference in chemistry sometimes useful to identify isobaric compounds [22]. The PTR-MS generally uses air as the carrier gas whereas helium is used in SIFT-MS, although nitrogen as the carrier gas is be-

[1] Patients with liver disease, increased pentane level is found and could predict diagnosis and severity of the disease (especially in case of alcoholic hepatitis patients).

[2] Switching to gases that produce NO^+ and O_2^+ ions in addition to H_3O^+ is possible in some instruments with a switching delay of 10 s.

ing used in many applications. The PTR-MS is considered more sensitive, since no mass selection is present, than SIFT-MS as the reagent ion number density in the PTR-MS drift tube is greater than in SIFT-MS. This can be true in some cases, however, the difference in the sensitivities is not as large as imagined because other important factors that need to be included.

2.6 Calibration vs Computed Rate Coefficient

The measurement of ion signals using mass spectrometry-based techniques such as in PTR-MS/SIFT-MS provide a route to determine the absolute concentration of a specific constituent of a gas mixture. The kinetic procedure used to determine the concentration of one or more constituents of a gas sample is relatively similar in PTR-MS[1] and SIFT-MS. From equation (2.3) absolute concentration of a compound of interest can be known without calibration if the rate coefficient of the reaction and reaction time τ are already known [88]. However, finding rate coefficients experimentally is a complicated process. Mostly, calibration is carried out at a calibrated gas concentration that is close to the concentration in the sample mixture to be analyzed. Lack of data on gas vapor phase physical properties such as measuring flow rates of their neat vapors into the carrier gas, as is used normally to determine rate coefficients, makes it extremely difficult. Also, gas standards of most of the compounds are not available especially for the new compounds, for example, cork-taint and off-flavor compounds. The calibration procedure for some compounds such as alcohols and aldehydes is problematic because they fragment under the collisional regime brought about by specific E/N in PTR-MS. Whenever fragmentation occurs, the uncertainty in the concentration determination follows which limits the analytic accuracy. Radial diffusion, however, small can also be a factor that limits the calibration accuracy. Cumulatively, the quoted error could arise from $\pm 15\%$ to $\pm 50\%$ in experimental rate coefficients [89, 90]. Also, calibration methods are slow and involve laborious efforts and typically not included in an automated work-flow. As a consequence, calibration is done infrequently and long-

[1] Although PTR-MS is loosely based on PTR rate coefficients, these procedures might be different from SIFT-MS because presence of electric field in the drift tube in the former while SIFT-MS works under controlled thermal conditions. Equation (2.6) is used to obtain rate coefficients at variable E/N.

term accuracy of PTR-MS measurements is often questionable. The possible alternative to calibration is the theoretical calculation of the rate coefficients for IMRs. In almost all IMRs that are fast, exothermic, and proceed at zero activation energy, the rate coefficients can be calculated from ion-molecule collision cross-section known as capture collision. The rate coefficients obtained are called capture collision rate coefficients k_c. The value of k_c can be determined theoretically by the procedures suggested by Su and Chesnavich [91, 92]. The dipole moment and polarizability are the input ingredients for these procedures that can be obtained from the DFT methods relatively with reasonable accuracy. Finding the rate coefficient using theoretical models is being discussed thoroughly in the following chapters.

2.7 Summary

DIMS based methods such as PTR-MS and SIFT-MS are extensively used for accurate and real-time analysis of trace gases in air and breath analysis. Both focus on soft CI and based on drift flow tube analysis of trace gases. Proton transfer from H_3O^+ is a soft, low energetic ionization method that lessens the fragmentation of the analyte molecule as compared to electron impact ionization. Electron ionization often used in other mass spectrometry instruments. CI, thus minimizing complex mass spectra and improving the identification capability and hence sensitivity. Another benefit of PTR-MS is that the energy level, E/N, in the PTR drift tube where the actual ionization takes place can even be adjusted by the user. This flexibility is very important since it allows to precisely control and adapts the ion-chemistry to the applications. The SIFT-MS on the other hand provides reagent ion mass selection from the frequently used ions H_3O^+, NO^+ and O_2^+, thus capable in the quantification as low as pptv. The ion switching time of a few ms is advantageous over PTR-MS in differentiating between isobaric compounds. The PTR-MS and SIFT-MS are widely used in fields as diverse as atmospheric chemistry, food science, botany, medicine, and process monitoring. The mass spectrometric analytic methods rely on a large kinetic database of IMRs for absolute quantification. A comprehensive kinetics database including molecular properties like proton affinity and ionization energy is primarily essential for

various IMRs occurring in the flow (drift) tubes.

Bibliography

[1] K. Ridgway, S. Lalljie, and R. Smith. Analysis of Food Taints and off-flavours–A review. *Food additives & contaminants. Part A, Chemistry, analysis, control, exposure & risk assessment*, 27:146–68, 02 2010.

[2] *PTR-MS in the Food Sciences*, chapter 6, pages 221–265. John Wiley & Sons, Ltd, 2013.

[3] Y. Pico, editor. *Chemical Analysis of Food: Techniques and Applications*. ISSN. Elsevier Science, 2 edition, 2020.

[4] Food taints and off-flavours. In M. J. Saxby, editor, *Taints and Off-Flavours in Foods*, Woodhead Publishing Series in Food Science, Technology and Nutrition. Springer US, 2 edition, 1996.

[5] D. Kilcast. 2 - Sensory analytical methods in detecting taints and off-flavours in food. In Brian Baigrie, editor, *Taints and Off-Flavours in Foods*, Woodhead Publishing Series in Food Science, Technology and Nutrition, pages 5–30. Woodhead Publishing, 2003.

[6] A. R. Fontana. Analytical methods for determination of cork-taint compounds in wine. *TrAC Trends in Analytical Chemistry*, 37:135–147, 2012.

[7] S. Jonsson, T. Uusitalo, B. van Bavel, I.B. Gustafsson, and G. Lindstrom. Determination of 2,4,6-trichloroanisole and 2,4,6-tribromoanisole on ng/L to pg/L levels in wine by solid-phase microextraction and gas chromatography-high-resolution mass spectrometry. *Journal of Chromatography A*, 1111(1):71–75, 2006.

[8] P. Freitas, L. G. Dias, A. M. Peres, L. M. Castro, and A. C. A. Veloso. Determination of 2,4,6-Trichloroanisole by Cyclic Voltammetry. *Procedia Engineering*, 47:1125–1128, 2012. 26th European Conference on Solid-State Transducers, Eurosensor 2012.

[9] E. Staples. Detecting 2,4,6 TCA in Corks and Wine Using the zNose^{TM}. 08 2020.

[10] D. Özhan, R. E. Anli, N. Vural, and M. Bayram. Determination of Chloroanisoles and Chlorophenols in Cork and Wine by using HS-SPME and GC-ECD Detection. *Journal of the Institute of Brewing*, 115(1):71–77, 2009.

[11] G. Bianco, G. Novario, Z. Rosalia, and T. Cataldi. Comparison of two SPME fibers for the extraction of some off-flavor cork-taint compounds in bottled wines investigated by GC-HRMS. *Analytical and bioanalytical chemistry*, 393:2019–27, 03 2009.

[12] P. Španěl, J. Žabka, I. Zymak, and D. Smith. Selected ion flow tube study of the reactions of H_3O^+ and NO^+ with a series of primary alcohols in the presence of water vapour in support of selected ion flow tube mass spectrometry. *Rapid Communications in Mass Spectrometry*, 31(5):437–446, 2017.

[13] H. Campbell-Sills, V. Capozzi, A. Romano, L. Cappellin, G. Spano, M. Breniaux, P. Lucas, and F. Biasioli. Advances in wine analysis by PTR-ToF-MS: Optimization of the method and discrimination of wines from different geographical origins and fermented with different malolactic starters. *International Journal of Mass Spectrometry*, 397-398:42–51, 2016.

[14] F. H. Field, M. S. B. Munson, and D. A. Becker. Chemical ionization mass spectrometry: paraffin hydrocarbons. ACS Publications, 1966.

[15] A. G. Harrison. *Chemical Ionization Mass Spectrometry, Second Edition*. Taylor & Francis, Canada, 2 edition, 1992.

[16] F. Biasioli, C. Yeretzian, T. D. Märk, J. Dewulf, and H. Van Langenhove. Direct-injection mass spectrometry adds the time dimension to (B)VOC analysis. *TrAC Trends in Analytical Chemistry*, 30(7):1003–1017, 2011.

[17] A. Hansel, A. Jordan, R. Holzinger, P. Prazeller, W. Vogel, and W. Lindinger. Proton transfer reaction mass spectrometry: on-line trace gas analysis at the ppb level. *International Journal of Mass Spectrometry and Ion Processes*, 149-150:609–619, 1995.

[18] F. Biasioli, F. Gasperi, C. Yeretzian, and T. D. Märk. PTR-MS monitoring of VOCs and BVOCs in food science and technology. *TrAC Trends in Analytical Chemistry*, 30(7):968–977, 2011.

[19] P. Bayón, M. Angeles, J. P. Schirlé-Keller, and G. Reineccius. Determining specific food volatiles contributing to PTR-MS ion profiles using GC-EI-MS. *Journal of agricultural and food chemistry*, 56:5278–84, 08 2008.

[20] R. S. Blake, P. S. Monks, and A. M. Ellis. Proton-Transfer Reaction Mass Spectrometry. *Chemical Reviews*, 109(3):861–896, 2009.

[21] *Experimental: Components and Principles*, chapter 3, pages 49–109. John Wiley & Sons, Ltd, 2013.

[22] T. Fujii. Ion-Molecule Attachment Reactions: Mass Spectrometry. In *Springer US*, 2015.

[23] PTR-MS trace gas analysis in real-time. https://www.ionicon.com/. Accessed June 2019.

[24] F. C. Fehsenfeld, A. L. Schmeltekopf, P. D. Goldan, H. I. Schiff, and E. E. Ferguson. Thermal Energy Ion-Neutral Reaction Rates. I. Some Reactions of Helium Ions. *The Journal of Chemical Physics*, 44(11):4087–4094, 1966.

[25] W. Lindinger, A. Hansel, and A. Jordan. On-line monitoring of volatile organic compounds at pptv levels by means of proton-transfer-reaction mass spectrometry (PTR-MS) medical applications, food control and environmental research. *International Journal of Mass Spectrometry and Ion Processes*, 173(3):191–241, 1998.

[26] *Chemical Ionization: Chemistry, Thermodynamics and Kinetics*, chapter 2, pages 25–48. John Wiley & Sons, Ltd, 2013.

[27] G. H. Wannier. On the Motion of Gaseous Ions in a Strong Electric Field. I. *Physical Review*, 83:281–289, Jul 1951.

[28] G. H. Wannier. Motion of gaseous ions in strong electric fields. *The Bell System Technical Journal*, 32(1):170–254, 1953.

[29] M. McFarland, D. L. Albritton, F. C. Fehsenfeld, E. E. Ferguson, and A. L. Schmeltekopf. Flow-drift technique for ion mobility and ion-molecule reaction rate constant measurements. II. Positive ion reactions of N^+, O^+, and H_2^+ with O_2 and O^+ with N_2 from thermal to 2 eV. *The Journal of Chemical Physics*, 59(12):6620–6628, 1973.

[30] C. N. Hewitt, S. Hayward, and A. Tani. The application of proton transfer reaction-mass spectrometry (PTR-MS) to the monitoring and analysis of volatile organic compounds in the atmosphere. *Journal of Environmental Monitoring*, 5:1–7, 2003.

[31] G. Eerdekens, L. N. Ganzeveld, J. Vilà-Guerau de Arellano, T. Klüpfel, and V. Sinha. Flux estimates of isoprene, methanol and acetone from airborne PTR-MS measurements over the tropical rainforest during the GABRIEL 2005 campaign. *Atmospheric Chemistry and Physics*, 9:4207–4227, 2009.

[32] B. Davison, R. Taipale, B. Langford, P. Misztal, S. Fares, G. Matteucci, F. Loreto, J. Cape, J. Rinne, and C. N. Hewitt. Concentrations and fluxes of biogenic volatile organic compounds above a Mediterranean macchia ecosystem in Western Italy. *Biogeosciences Discussions*, 6, 08 2009.

[33] J. A. de Gouw, P. D. Goldan, C. Warneke, W. C. Kuster, J. M. Roberts, M. Marchewka, S. B. Bertman, A. A. P. Pszenny, and W. C. Keene. Organic aerosol formation downwind from the deepwater horizon oil spill. *Science*, 331(6022):1295–1299, 2011.

[34] R. Fall, T. Karl, A. Jordan, and W. Lindinger. Biogenic C_5 VOCs: release from leaves after freeze-thaw wounding and occurrence in air at a high mountain observatory. *Atmospheric Environment*, 35(22):3905–3916, 2001.

[35] R. Holzinger, A. Jordan, A. Hansel, and W. Lindinger. Methanol measurements in

the lower troposphere near Innsbruck (047°16 ′N; 011°24 ’E), Austria. *Atmospheric Environment*, 35(14):2525–2532, 2001.

[36] D. Smith, P. Španěl, D. Dabill, J. Cocker, and B. Rajan. On-line analysis of diesel engine exhaust gases by selected ion flow tube mass spectrometry. *Rapid Communications in Mass Spectrometry*, 18(23):2830–2838, 2004.

[37] T. J. Christian, B. Kleiss, R. J. Yokelson, R. Holzinger, P. J. Crutzen, W. M. Hao, B. H. Saharjo, and D. E. Ward. Comprehensive laboratory measurements of biomass-burning emissions: 1. Emissions from Indonesian, African, and other fuels. *Journal of Geophysical Research: Atmospheres*, 108(D23), 2003.

[38] T. Ruuskanen, M. Müller, R. Schnitzhofer, T. Karl, M. Graus, I. Bamberger, L. Hörtnagl, F. Brilli, G. Wohlfahrt, and A. Hansel. Eddy covariance VOC emission and deposition fluxes above grassland using PTR-TOF. *Atmospheric chemistry and physics (Print)*, 11, 01 2011.

[39] K. Buhr, S. van Ruth, and C. Delahunty. Analysis of volatile flavour compounds by Proton Transfer Reaction-Mass Spectrometry: fragmentation patterns and discrimination between isobaric and isomeric compounds. *International Journal of Mass Spectrometry*, 221(1):1–7, 2002.

[40] A. Romano, L. Cappellin, V. Ting, E. Aprea, L. Navarini, F. Gasperi, and F. Biasioli. Nosespace analysis by PTR-ToF-MS for the characterization of food and tasters: The case study of coffee. *International Journal of Mass Spectrometry*, 365-366:20–27, 2014.

[41] M. L. Mateus, C. Lindinger, J. C. Gumy, and R. Liardon. Release kinetics of volatile organic compounds from roasted and ground coffee: online measurements by PTR-MS and mathematical modeling. *Journal of agricultural and food chemistry*, 55(25):10117–10128, 12 2007.

[42] M. Tsevdou, C. Soukoulis, L. Cappellin, F. Gasperi, P. S. Taoukis, and F. Biasioli. Monitoring the effect of high pressure and transglutaminase treatment of milk on the

evolution of flavour compounds during lactic acid fermentation using PTR-ToF-MS. *Food Chemistry*, 138(4):2159–2167, 2013.

[43] F. Gasperi, G. Gallerani, A. Boschetti, F. Biasioli, A. Monetti, E. Boscaini, A. Jordan, W. Lindinger, and S. Iannotta. The mozzarella cheese flavour profile: a comparison between judge panel analysis and proton transfer reaction mass spectrometry. *Journal of the Science of Food and Agriculture*, 81(3):357–363, 2001.

[44] E. I. Boamfa, M. M. L. Steeghs, S. M. Cristescu, and F. J. M. Harren. Trace gas detection from fermentation processes in apples; an intercomparison study between proton-transfer-reaction mass spectrometry and laser photoacoustics. *International Journal of Mass Spectrometry*, 239(2-3):193–201, 12 2004.

[45] F. Carbone, F. Mourgues, F. Biasioli, F. Gasperi, T. Märk, C. Rosati, and G. Perrotta. Development of molecular and biochemical tools to investigate fruit quality traits in strawberry élite genotypes. *Molecular Breeding*, 18:127–142, 08 2006.

[46] E. Boscaini, T. Mikoviny, A. Wisthaler, E. von Hartungen, and T. D. Märk. Characterization of wine with PTR-MS. *International Journal of Mass Spectrometry*, 239(2):215–219, 2004.

[47] H. Campbell-Sills, V. Capozzi, A. Romano, L. Cappellin, G. Spano, M. Breniaux, P. Lucas, and F. Biasioli. Advances in wine analysis by PTR-ToF-MS: Optimization of the method and discrimination of wines from different geographical origins and fermented with different malolactic starters. *International Journal of Mass Spectrometry*, 397-398:42–51, 2016.

[48] I. Déléris, A. Saint-Eve, P. Lieben, Marie-Louise Cypriani, N. Jacquet, P. Brunerie, and I. Souchon. Chapter 98–Impact of Swallowing on the Dynamics of Aroma Release and Perception During the Consumption of Alcoholic Beverages. In Vicente Ferreira and Ricardo Lopez, editors, *Flavour Science*, pages 533–537. Academic Press, San Diego, 2014.

[49] *PTR-MS in the Food Sciences*, chapter 6, pages 221–265. John Wiley & Sons, Ltd, 2014.

[50] R. Spitaler, N. Araghipour, T. Mikoviny, A. Wisthaler, J. Dalla Via, and T. Märk. PTR-MS in enology: Advances in analytics and data analysis. *International Journal of Mass Spectrometry*, 266:1–7, 10 2007.

[51] A. Romano, L. Fischer, J. Herbig, H. Campbell-Sills, J. Coulon, P. Lucas, L. Cappellin, and F. Biasioli. Wine analysis by FastGC proton-transfer reaction-time-of-flight-mass spectrometry. *International Journal of Mass Spectrometry*, 369:81–86, 2014.

[52] M. Lechner, H. P. Colvin, C. Ginzel, P. Lirk, J. Rieder, and H. Tilg. Headspace screening of fluid obtained from the gut during colonoscopy and breath analysis by proton transfer reaction-mass spectrometry: A novel approach in the diagnosis of gastro-intestinal diseases. *International Journal of Mass Spectrometry*, 243(2):151–154, 2005.

[53] G. M. Pinggera, P. Lirk, F. Bodogri, R. Herwig, G. Steckel-Berger, G. Bartsch, and J. Rieder. Urinary acetonitrile concentrations correlate with recent smoking behaviour. *British Journal of Urology International*, 95(3):306–309, 2005.

[54] M. Steeghs, B. Moeskops, K. Swam, S. M. Cristescu, P. Scheepers, and F. Harren. On-line monitoring of uv-induced lipid peroxidation products from human skin in vivo using proton-transfer reaction mass spectrometry. *International Journal of Mass Spectrometry*, 253:58–64, 06 2006.

[55] F. Morisco, E. Aprea, V. Lembo, V. Fogliano, P. Vitaglione, G. Mazzone, L. Cappellin, F. Gasperi, S. Masone, G. De Palma, R. Marmo, N. Caporaso, and F. Biasioli. Rapid "Breath-Print" of Liver Cirrhosis by Proton Transfer Reaction Time-of-Flight Mass Spectrometry. A Pilot Study. *Public Library of Science One*, 8:e59658, 04 2013.

[56] M. Righettoni, A. Schmid, A. Amann, and S. Pratsinis. Correlations between Blood Glucose and Breath Components from Portable Gas Sensors and PTR-TOF-MS. *Journal of breath research*, 7:037110, 08 2013.

[57] *PTR-MS in the Medical Sciences*, chapter 7, pages 267–309. John Wiley & Sons, Ltd, 2013.

[58] M. J. McEwan. *Direct Analysis Mass Spectrometry*, pages 263–317. Springer US, Boston, MA, 2015.

[59] P. Španěl and D. Smith. Selected ion flow tube: a technique for quantitative trace gas analysis of air and breath. *Medical and Biological Engineering and Computing*, 34:409–419, 11 1996.

[60] N. G. Adams and D. Smith. The selected ion flow tube (SIFT); A technique for studying ion-neutral reactions. *International Journal of Mass Spectrometry and Ion Physics*, 21(3):349–359, 1976.

[61] E. E. Ferguson, F. C. Fehsenfeld, and A. L. Schmeltekopf. Flowing afterglow measurements of ion-neutral reactions. volume 5 of *Advances in Atomic and Molecular Physics*, pages 1–56. Academic Press, 1969.

[62] P. Španěl and D. Smith. Selected ion flow tube studies of the reactions of H_3O^+, NO^+ and O_2^+ with several amines and some other nitrogen-containing molecules. *International Journal of Mass Spectrometry*, 176(3):203–211, 1998.

[63] K. Sovová, K. Dryahina, and P. Spanel. Selected ion flow tube (SIFT) studies of the reactions of H_3O^+, NO^+ and O_2^+ with six volatile phytogenic esters. *International Journal of Mass Spectrometry*, 300:31–38, 01 2011.

[64] D. Smith, T. W. E. Chippendale, and P. Španěl. Selected ion flow tube, SIFT, studies of the reactions of H_3O^+, NO^+ and O_2^+ with some biologically active isobaric compounds in preparation for SIFT-MS analyses. *International Journal of Mass Spectrometry*, 303(2):81–89, 2011.

[65] W. Lindinger, A. Hansel, and A. Jordan. On-line monitoring of volatile organic compounds at pptv levels by means of proton-transfer-reaction mass spectrometry (PTR-MS) medical applications, food control and environmental research. *International Journal of Mass Spectrometry and Ion Processes*, 173(3):191–241, 1998.

[66] N. G. Adams, L. M. Babcock, T. M. Mostefaoui, and M. S. Kerns. Selected ion flow tube study of NH_4^+ association and of product switching reactions with a series of organic molecules. *International Journal of Mass Spectrometry*, 223-224:459–471, 2003.

[67] G. Amadei and B. M. Ross. The reactions of a series of terpenoids with H_3O^+, NO^+ and O_2^+ studied using selected ion flow tube mass spectrometry. *Rapid Communications in Mass Spectrometry*, 25(1):162–168, 2011.

[68] T. Wang, P. Spanel, and D. Smith. Selected Ion Flow Tube, SIFT, studies of the reactions of H_3O^+, NO^+ and O_2^+ with eleven $C_{10}H_{16}$ monoterpenes. *International Journal of Mass Spectrometry*, 228:117–126, 08 2003.

[69] P. Španěl, T. Wang, and D. Smith. A selected ion flow tube, SIFT, study of the reactions of H_3O^+, NO^+ and O_2^+ ions with a series of diols. *International Journal of Mass Spectrometry*, 218(3):227–236, 2002.

[70] M. Norman, A. Hansel, and A. Wisthaler. O_2^+ as reagent ion in the PTR-MS instrument: Detection of gas-phase ammonia. *International Journal of Mass Spectrometry*, 265:382–387, 09 2007.

[71] B. J. Prince, D. B. Milligan, and M. J. McEwan. Application of selected ion flow tube mass spectrometry to real-time atmospheric monitoring. *Rapid Communications in Mass Spectrometry*, 24(12):1763–1769, 2010.

[72] G. J. Francis, V. S. Langford, D. B. Milligan, and M. J. McEwan. Real-time monitoring of hazardous air pollutants. *Analytical Chemistry*, 81(4):1595–1599, 2009.

[73] G. J. Francis, P. F. Wilson, D. B. Milligan, V. S. Langford, and M. J. McEwan. GeoVOC: A SIFT-MS method for the analysis of small linear hydrocarbons of relevance to oil exploration. *International Journal of Mass Spectrometry*, 268(1):38–46, 2007.

[74] D. Smith, P. Cheng, and P. Spanel. Analysis of petrol and diesel vapour and vehicle engine exhaust gases using selected ion flow tube mass spectrometry. *Rapid communications in mass spectrometry*, 16:1124–34, 02 2002.

[75] D. Smith, P. Španěl, D. Dabill, J. Cocker, and B. Rajan. On-line analysis of diesel engine exhaust gases by selected ion flow tube mass spectrometry. *Rapid Communications in Mass Spectrometry*, 18(23):2830–2838, 2004.

[76] D. R. Hastie, J. Gray, V. S. Langford, R. G. A. R. Maclagan, D. B. Milligan, and M. J. McEwan. Real-time measurement of peroxyacetyl nitrate using selected ion flow tube mass spectrometry. *Rapid Communications in Mass Spectrometry*, 24(3):343–348, 2010.

[77] V. Langford, J. Gray, R. Maclagan, and M. Mcewan. Detection of Siloxanes in Landfill Gas and Biogas Using SIFT-MS. *Current Analytical Chemistry*, 9, 07 2013.

[78] P. Španěl and D. Smith. Selected ion flow tube-mass spectrometry: detection and real-time monitoring of flavours released by food products. *Rapid Communications in Mass Spectrometry*, 13(7):585–596, 1999.

[79] N. Sumonsiri and S. Barringer. Application of SIFT-MS in monitoring volatile compounds in fruits and vegetables. *Current Analytical Chemistry*, 9, 07 2013.

[80] L. Iachetta, L. Malek, and B. M. Ross. The reactions of H_3O^+, NO^+ and O_2^+ with several flavourant esters studied using selected ion flow tube mass spectrometry. *Rapid Communications in Mass Spectrometry*, 24(6):815–822, 2010.

[81] G. Francis, P. Wilson, D. Milligan, V. Langford, and M. Mcewan. GeoVOC: A SIFT-MS method for the analysis of small linear hydrocarbons of relevance to oil exploration. *International Journal of Mass Spectrometry*, 268:38–46, 11 2007.

[82] P. Španěl, P. Rolfe, B. Rajan, and D. Smith. The selected ion flow tube (SIFT)–A novel technique for biological monitoring. *The Annals of Occupational Hygiene*, 40(6):615–626, 1996.

[83] A. M. Diskin, P. Spanel, and D. Smith. Time variation of ammonia, acetone, isoprene and ethanol in breath: a quantitative SIFT-MS study over 30 days. *Physiological Measurement*, 24(1):107–119, 01 2003.

[84] S. Kumar, J. Huang, N. Abbassi-Ghadi, P. Španěl, D. Smith, and G. B. Hanna. Selected Ion Flow Tube Mass Spectrometry Analysis of Exhaled Breath for Volatile Organic Compound Profiling of Esophago-Gastric Cancer. *Analytical Chemistry*, 85(12):6121–6128, 2013.

[85] I. A. Hanouneh, N. N. Zein, F. Cikach, L. Dababneh, D. Grove, N. Alkhouri, R. Lopez, and R. A. Dweik. The breath-prints in patients with liver disease identify novel breath bio-markers in alcoholic hepatitis. *Clinical gastroenterology and hepatology : The official clinical practice journal of the American Gastroenterological Association*, 12(3):516–523, 03 2014.

[86] S. J. Davies, P. Španěl, and D. Smith. Breath analysis of ammonia, volatile organic compounds and deuterated water vapor in chronic kidney disease and during dialysis. *Bioanalysis*, 6(6):843–857, 03 2014.

[87] *Background*, chapter 1, pages 1–23. John Wiley & Sons, Ltd, 2013.

[88] N. G. Adams and L. M. Babcock. *Advances in Gas Phase Ion Chemistry*, volume 1 of *Advances in Gas Phase Ion Chemistry*. JAI Press, 1992.

[89] *Quantitative Analysis*, chapter 4, pages 111–127. John Wiley & Sons, Ltd, 2013.

[90] J. A. de Gouw, P. D. Goldan, C. Warneke, W. C. Kuster, J. M. Roberts, M. Marchewka, S. B. Bertman, A. A. P. Pszenny, and W. C. Keene. Validation of proton transfer reaction-mass spectrometry (PTR-MS) measurements of gas-phase organic compounds in the atmosphere during the New England Air Quality Study (NEAQS) in 2002. *Journal of Geophysical Research: Atmospheres*, 108(D21), 2003.

[91] T. Su and M. T. Bowers. Ion-polar molecule collisions. Proton transfer reactions of H_3^+ and CH_5^+ to the geometric isomers of difluoroethylene, dichloroethylene, and difluorobenzene. *Journal of the American Chemical Society*, 95(5):1370–1373, 1973.

[92] T. Su and M. T. Bowers. Theory of ion-polar molecule collisions. comparison with experimental charge transfer reactions of rare gas ions to geometric isomers of difluorobenzene and dichloroethylene. *The Journal of Chemical Physics*, 58(7):3027–3037, 1973.

3

Theory of Ion-Molecule Collision in PTR-MS and SIFT-MS

3.1 Introduction

Ion-molecule collision reactions have received considerable interest in the last few decades. Various mass spectrometric techniques have been in use to study IMRs over a large range of pressure and temperature conditions. The ion-molecule collisions result in a number of products depending on the chemical and physical properties of the reactants, their relative velocities, and the impact parameter of their trajectories [1–3]. The possible reaction outcome may include charge transfer (dissociative or non-dissociative charge transfer), atom abstraction, complex formation, and dissociation of the colliding ions [1]. All these re-

actions can be classified on the basis of their rate coefficients, their reaction cross-section and other reaction kinetics. Most of the efforts have been concentrated on the prediction of the capture limiting rate coefficients, cross-section, and its dependence on the dipole moment of the neutral colliding molecule participating in the collision. During the course of time, many capture collision theories such as zero dipole and pure polarization limit to the capture rates were derived and considered as limiting bracket to capture rate coefficients of ion-molecular collisions for many years. The first in-depth treatment of ion-molecule collision reaction rate coefficients was given by Su and Bowers in their theory of average dipole orientation (ADO) in 1973 [4, 5]. The main essence of the ADO theory was to use statistical methods and predict rate coefficients on the basis of average orientation of the polar molecule in the ion field followed from an earlier explanation based on pure polarization theory by Langevin [6]. Alternatively, the parameterized classical trajectory method derived by Su and Chesnavich has predicted rate coefficients quite accurately at thermal temperature limit as well as kinetic energy-dependent rates over elevated temperatures above 1000 K.

3.2 Ion-Molecule Collision Theory

The systems where CI dominates, IMRs are particularly useful in identifying the reaction products and reaction rates. The rate coefficients are important because only such reactions that are rapid can be expected to show adequate product yields upon reaction. IMRs are among the fastest chemical reactions known and proceed very rapidly at room temperature generally at collision (or capture) rates. These reactions are exothermic and occur differently from molecule-molecule reactions as IMRs are characterized by a double minimum rather than the single minimum with finite potential barrier that can be seen in Figure 3.1 [1]. Typical reactions of two different energy profiles are given in equations (3.1) and (3.2). The nature of interaction in IMRs is determined by the electrostatic long-range interaction between charged ion and the polarizable molecule. As a result interaction energy at a short-range is often sufficiently large to overcome the intrinsic energy barriers to chemical change and hence reactions occur without activation energy barrier. The bonding of

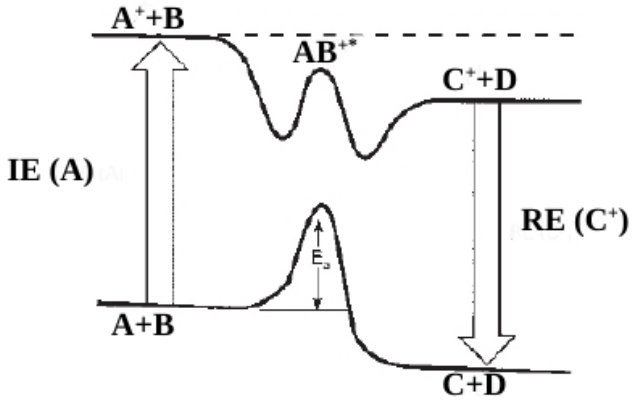

Figure 3.1: Pictorial representation of reactant energy vs reaction coordinates of Ion-molecule and molecule-molecule reaction profile. Here, IR and RE represent ionization and recombination energies respectively. (*Source: D. K. Bohme, Encyclopedia of MS, 1999*)

ion and molecule is generally found to be very weak as compared to the normal chemical bonds.

$$A^+ + B = (AB)^{+*} \tag{3.1}$$

$$(AB)^{+*} = C^+ + D \tag{3.2}$$

Ion-molecule collision theory is based on the assumption that the reactants (ion and molecule) always react whenever they are brought together. It is well known that the IMR complexes stick together by the following two interactions: ion-dipole and ion-induced dipole resulted from the classical electrostatic forces between the ion-molecule complexes [7]. The stability of the complex depends on the dipole moment and polarizability of the neutral molecule and altered with its size and the presence of functional group. As already stated that the IMRs occur at very small or zero activation energy, their rate coefficients are given by the capture rate coefficients, k_c, of the order of $\sim 10^{-9}$ $cm^3\,molecule^{-1}s^{-1}(10^{-15}$ $m^3\,molecule^{-1}\,s^{-1})$ which is about one to two order larger in magnitude than for exothermic molecule-molecule reaction occurring without activation energy [8–10]. The importance of capture approximation rather than usual and worthwhile in ion-molecule chemistry where the dominated interactions are determined by

strong long-range forces. The capture collision rate, k_c, of the IMRs can be obtained by the physical properties of the reactants.

3.3 IMRs in PTR-MS/SIFT-MS flow (drift) Tube

The IMRs are of particular interest and can provide a great deal of information on the nature of ion chemistry occurring in PTR-MS/SIFT-MS flow (drift) tubes. In CI, reaction between ion and molecule can lead to a variety of consequences such as simple electron transfer, proton transfer, collision association, condensation, clustering, and fragment accompanied by extensive chemical bond re-disposition in both the molecule and the ion [1, 11].

3.3.1 Types of IMRs

The PTRs are the most efficient exothermic reactions occurring at almost every collision. Proton is transferred either from a protonated molecule to a neutral molecule or from a neutral molecule to the negative ion. In the present context, PTRs from gaseous Brønsted acids to neutral molecules, reaction (3.3) follows. Hydride transfer reaction (3.4) is also quite common under CI. When proton transfer is exceedingly exothermic, the internal energy appearing in the protonated product will be sufficient to cause dissociative proton transfer (AH^{+*}). This is normally seen in dissociative electron-transfer reactions, although, the product ions again offer a signature of the reactant molecule so that these types of reactions also present a handful of information for the analysis of gases by CIMS.

$$AH^+ + B \longrightarrow BH^+ + A\,, \qquad \text{Proton transfer}\,, \tag{3.3}$$

$$A^+ + BH \longrightarrow B^+ + AH\,, \qquad \text{Hydride tranfer}\,. \tag{3.4}$$

Electron transfer (charge transfer) from ion to the neutral molecule takes place only when the molecule B possesses IE less than the IE of the A in the reaction (3.5) given below [12].

However, the dissociative electron transfer is quite possible at higher IEs.

$$A^{\pm} + B \longrightarrow B^{\pm} + A, \qquad \text{Electron tranfer} \tag{3.5}$$

$$A^{+} + B + Z \longrightarrow BA^{+} + Z, \qquad \text{Adduct formation} \tag{3.6}$$

$$A^{+} + B + Z \rightarrow [AB^{+}]^{*} \longrightarrow AB^{+} \rightarrow C^{+} + D, \qquad \text{Condensation reaction} \tag{3.7}$$

The reaction (3.6) proceeds through a third body Z to prevent dissociation of adduct BA^{+} by removing some amount of energy. The condensation reaction (3.7) involving two reactants collisionally stabilized and relatively a long-lived collision complex is formed. In the absence of such stabilization it decomposes, at least in part, to products different from the reactants and yields C^{+} and D as shown in reaction (3.7). The bimolecular IMRs ranging from reaction (3.3) to (3.6) are often very fast, exothermic, and occur at every collision. Which makes them useful for an efficient ionization of targeted molecules in mass spectrometry.

3.3.2 Collision Rate Coefficients in IMRs

Thermodynamics helps in determining whether the reaction is going to occur or not while information of rate coefficient governs the outcome of the reaction as a product. IMRs have been studied extensively by Bohme and co-workers using the afterglow technique in early 60s [3]. Their research showed that bimolecular IMRs especially those involve transfer of protons are fast and exothermic. A typical two-step association reaction is represented below,

$$A^{+} + B \rightleftharpoons (A+B)^{+*}, \qquad (\text{Association, } k_1 \text{ / Dissociation, } k_2) \tag{3.8}$$

$$(A+B)^{+*} + N \rightleftharpoons (A+B)^{+} + N^{*}, \qquad (\text{Stablization, } k_3 \text{ / Reverse, } k_4) \tag{3.9}$$

where A is positively charged ion, B is neutral species and N is neutral gas (the energy thus accumulated in the reaction complex could then be liberated by collision with a third body), a buffer gas whose function is to supply stabilization to ion-molecule complexes. Also, k_1,

k_2, k_3, and k_4 are the respective rates of the reaction. In the case of high-pressure region, the stabilization is much faster than the dissociation of the activated intermediate complex ($k_3[N] \gg k_2$) and the overall second-order reaction rate is equal to the ion–molecule association reaction rate, k_1 , independent of buffer gas pressure.

$$k(2)_{overall} = k_1 \,. \tag{3.10}$$

It is expected that k_1 has no activation barrier. On the similar note, low pressure region fulfills the condition ($k_3[N] \ll k_2$) and rate determining step is represented by the collisional energy transfer to the buffer gas.

$$k(2)_{overall} = \frac{k_1 k_3 [N]}{k_2} \,. \tag{3.11}$$

Here k_1 and k_3 can be determined by the Langevin theory [13, 14] (as discussed in the subsequent sections) while for dissociation rate k_2, Rice–Ramsperger–Kassel–Marcus (RRKM) theory can be used [15, 16]. In the present context, proton transfer and electron transfer reactions have been studied based on the CI generally considered as soft ionization with one product ion for every IMR without activation energy occurring in the drift tube. Therefore, the capture collision cross-section rate coefficient calculations have been performed.

3.4 Rate Coefficient Calculation

3.4.1 Ion-Molecule Interactions

The ion-molecule complexes are mainly formed due to the following interactions: ion-dipole, ion-induced dipole and ion-π interactions. When an ion interacts with a molecule (non-polar) it induces a dipole in the neutral resulting ion-induced interaction at moderately long-range [14, 17]. In IMRs, only the long-range ion-induced interactions are of particular relevance. The ion-dipole interaction, where polar molecule orient itself to the nearby ion such that partial opposite charge causes interaction between ion and dipole while in the ion-induced case the induced dipole interacts with a nearby ion that induced it. The

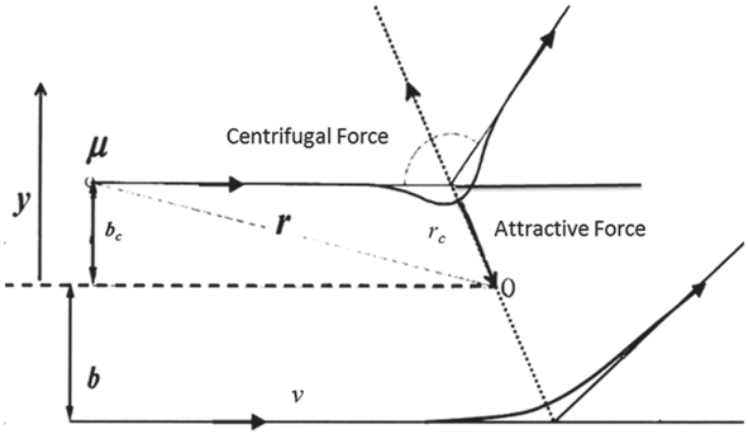

Figure 3.2: Ion-molecule collisional behavior is shown for critical impact parameter b_c. The particles orbit the scattering center with r_c. For the impact parameter b greater than b_c, the particles are simply scattered at large values of the relative inter molecular distance r.

strength of ion-dipole interaction mainly due to the magnitude of the dipole moment of the neutral molecule and the charge density[1] of the ion. On the other hand, larger the ion more readily the electron cloud will be distorted by the external field as the case of ion-induced interactions contrary to ion-dipole interactions. Clearly, a small to a significant amount of ion-induced interaction present in ion-dipole interaction. It is worthwhile to note that the ion-dipole and ion-induced dipole interactions contribute differently to the rate coefficients.

3.4.2 Langevin Collision Model

Many theoretical descriptions are available for the calculation of rate coefficients of exothermic IMRs. A general form of the capture collision cross-section was derived by Gioumousis and Stevenson based on the concepts developed by Langevin and applied to a reaction between a point ion and a spherical (non-polar) molecule [6, 14, 18]. Whenever an ion approaches a neutral molecule with no permanent dipole, it's Coulomb field induces a dipole within the neutral due to the long-range attractive force.

The schematic of the collision of ion (with a relative velocity v and impact parameter b) and the molecule is shown in Figure 3.2. The classical electrostatic potential for this ion-molecule system is given by

$$\mathrm{V(r)} = \frac{-\alpha q^2}{2\mathrm{r}^4}, \tag{3.12}$$

[1] It is the charge to volume ratio and ion-dipole interaction decreases as the ion size grows.

where α represents the polarizability of the neutral molecule, q is the charge of the ion, and r is the distance between the centers of ion and the molecule. The relative energy of the system at $r < \infty$, E_{rel}, is the sum of electric and potential energy terms

$$E_{rel} = E_{kinetic}(r) + V(r)\,, \tag{3.13}$$

Kinetic energy part of equation (3.13) further depends upon the energy along the line of center of the collision, E_{trans}, and energy corresponding to the rotation of the particles. The rotation energy (due to the centrifugal force which acts in the outward direction) is expressed as

$$E_{rot}(r) = \frac{L^2}{2\mu r^2}\,, \tag{3.14}$$

where L represents the classical angular momentum ($L = \mu v b$), and μ represents the reduced mass of the reactants. According to Langevin theory, describing the molecular interaction potential, the effective interaction potential at an ion-molecule separation r is given by

$$V_{eff}(r) = \frac{-\alpha q^2}{2r^4} + \frac{L^2}{2\mu r^2}\,. \tag{3.15}$$

And, the total relative energy becomes

$$E_{rel} = E_{trans} + V_{eff}(r)\,. \tag{3.16}$$

The variation of $V_{eff}(r)$ with r, depends on the value of the impact parameter b. Three cases can be considered (1) at $b = b_c$, where the centrifugal term namely $V_{eff}(r)$ equals to E_{rel} and $E_{trans} = 0$, the particles will orbit the scattering center with a constant ion-molecule separation r_c. (2) for $b \leq b_c$, the capture collision probability is $p = 1$ and (3) for $b > b_c$, the capture reaction does not occur and $p = 0$. The capture collision cross section at a given velocity v is indicated as

$$\sigma(v) = \pi b_c^2, \quad k_c = v\sigma_c(v)\,. \tag{3.17}$$

To obtain expression for maximum cross section at a given relative velocity v, the critical impact parameter b_c is the impact parameter such that $V_{eff} = E_r$ at $\partial V_{eff}(r)/\partial(r) = 0$ and

$V_{eff} = E_r$ at $r = r_c$:

$$\frac{\partial V_{eff}(r)}{\partial r} = 0 = \frac{-L^2}{\mu r^3} + \frac{2\alpha q^2}{r^5} \tag{3.18}$$

$$V_{eff}(r) = \frac{L^2}{2\mu r^2} - \frac{\alpha q^2}{2r^4} = E_r = \frac{1}{2}\mu v^2 . \tag{3.19}$$

The restrictions in equations (3.18) and (3.19) give rise to

$$r_c = \left(\frac{2q}{b_c v}\right)\left(\frac{\alpha}{\mu}\right)^{\frac{1}{2}}, \tag{3.20}$$

$$b_c = \left(\frac{4\alpha q^2}{\mu v^2}\right)^{\frac{1}{4}} . \tag{3.21}$$

Provided, distance of closest approach $r_c = \sqrt{b_c/2}$. Hence, the capture collision cross section and rate constant for the formation of ion-molecule complexes is given by

$$\sigma_c(v) = \pi b_c^2 = \left(\frac{2\pi q}{v}\right)\left(\frac{\alpha}{\mu}\right)^{\frac{1}{2}}, \tag{3.22}$$

$$k_{Lang} = \sqrt{\frac{\pi\alpha q^2}{\mu\varepsilon_0}} . \tag{3.23}$$

Equation (3.23) is called Langevin rate coefficient and the rate coefficient is independent of the velocity as well as temperature. Equation (3.23) predicts maximum rate coefficients reasonably well for IMRs involving non-polar molecules at low energy collisions. This indicates that reaction occurs at every collision for many ion-molecule pairs; consequently, there can be no activation energy for the reaction. However, Langevin theory fails to explain many ion-polar molecular reactions and seriously underestimates the rate coefficients.

3.4.3 Average Dipole Orientation (ADO) Theory

Langevin's theory agrees fairly well with some simple low energy IMRs and predicted rate coefficients by equation (3.23) were satisfactory for non-polar molecules but underesti-

mated the rates for most ion-polar molecule collisions. For polar molecules,[1] Moran and Hamill [19] suggested that ion-dipole forces are also important and can not be ignored. The ion-molecule collision within ion-dipole and ion-induced dipole forces, the potential V_{eff} becomes

$$V_{eff}(r) = \frac{L^2}{2\mu r^2} + \frac{-\alpha q^2}{2r^4} - \frac{\mu_D \cos\theta}{r^2}, \tag{3.24}$$

where μ_D is the dipole moment of the neutral molecule and θ is the angle that dipole makes with the line of centers of the collision. Hamill and coworkers in their theory [19] made a simplifying assumption that the dipole "locks in" on the ion by assuming $\theta = 0$. However, the assumption seriously overestimates the ion-dipole effect on IMR rate coefficients, since θ can not be a fixed quantity. In real-world colliding systems, the molecule can rotate and some valid expression must follow that can justify its variation in ion-molecule collisions. Su and Bowers [4, 5] showed up a realistic expression for thermal energy rate coefficients known as average dipole orientation theory (ADO) expression as

$$k_{ADO} = \sqrt{\frac{\pi\alpha q^2}{\mu\varepsilon_0}} + \frac{C\mu_D q}{\varepsilon_0}\sqrt{\frac{1}{2\pi\mu k_B T}}, \tag{3.25}$$

here k_B is the Boltzmann constant and T is the absolute temperature. The first-term in the right-hand side of equation (3.25) is the Langevin rate coefficient while ion-dipole term in addition to the ion-induced dipole interaction term included in the second part. The parameter C is included as a dipole locking parameter which reflects the extent to which the dipole of the molecule orients itself with the incoming charge and may have values from 0 (no alignment) to 1 (locking-in). However, for the real systems the value of C lies well below 1 and its value is further dependent on the dipole moment and polarizability of the neutral molecule ($C = \mu_D/\sqrt{\alpha}$). The temperature dependence can be obtained as suggested by Su and Bowers [20]. The limiting value of C is ~ 0.26 for large values of the dipole moment and polarizability. The procedure to obtain C is discussed in appendix A. ADO correctly predicts maximum rate coefficients for ion-polar molecule reactions with much smaller dependence of the temperature as compared to locked dipole theory ($\theta = 0$)

[1] The molecules with a permanent dipole moment.

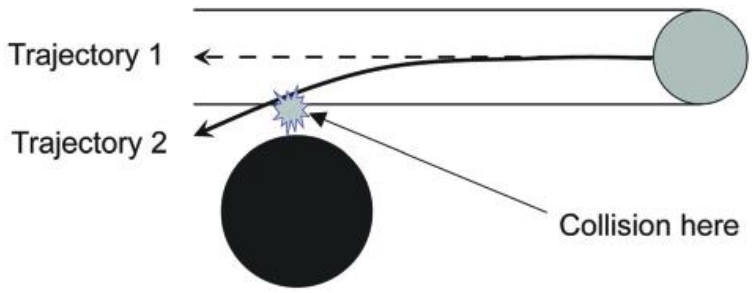

Figure 3.3: Trajectories of two hypothetical molecules represented by solid spheres and their trajectories are shown by arrows. In the absence of intermolecular force two molecules remain far from each other shown by dotted trajectory (Trajectory 1). In this scenario, two molecules miss an effective collision. In trajectory 2 (solid line), the presence of a long range attractive force modifies the trajectory which creates an effective collision cross-section that is larger than the hard-sphere limit and leads to an effective collision.

which has been confirmed experimentally [21, 22].

3.4.4 Classical Trajectory Method

The ion-molecule collision rates calculated by ADO show much better agreement with the experimental rates in comparison with Langevin rates [23]. However, the observed rate coefficients as predicted from the ADO procedure tend to underestimate the experimental rate coefficients, typically by 10–20% [24, 25]. The reason for this contrariety may attribute to the negligence of the dipole moment of the charged reagent, which considered as a point charge in the standard ADO procedure. An alternative approach is to model the reaction process through a series of classical trajectory calculations is given by Su and Chesnavich (see Figure 3.3) [26].

They studied series of trajectories in order to model ion-molecules reaction process and obtained a parametrized expressions:

$$\mathrm{k_{cap}}(T,\mathrm{CT}) = \mathrm{k_{Lang}} \times K_{\mathrm{cap}}(T_R, I^\star)\,. \tag{3.26}$$

The parameterized quantity $K_{\mathrm{cap}}(T_R, I^\star)$ in equation (3.26) is a function of two reduced parameters: the dimensionless reduced temperature, T_{R}, and the moment of inertia, $I^\star$, of the neutral molecule. Reduced temperature is given as

$$T_R = 4\pi\varepsilon_0 \frac{2\alpha k_B T}{\mu_{\mathrm{D}}^2}\,, \tag{3.27}$$

and the dimensionless parameter

$$I^\star = \frac{\mu_{\mathrm{D}} I}{\alpha q \mu}\,. \tag{3.28}$$

I is the moment of inertia of the neutral molecule and other symbols are same as defined earlier. The results from various trajectories obtained by Su and Chesnavich suggested that the value of K_{cap} is insensitive to $I^\star$ when

$$I^\star < \frac{0.7 + x^2}{2 + 0.6x}\,, \tag{3.29}$$

where

$$x = T_R^{-1/2}\,. \tag{3.30}$$

For majority of the molecular species studied in PTR-MS, the values of α, μ_D and I are such that K_{cap} lies in the insensitive region as inequality (3.29) applies. Under such cir-

cumstances, K_{cap} depends only on T_R, i.e. on x, and its value is parameterized as follows:

$$K_{\text{cap}} = \begin{cases} (x+0.5090)^2/10.526+0.9754, & x \leq 2 \\ 0.4767\,x+0.6200, & 2 < x \leq 3 \\ 0.5781\,x+0.3165, & 3 < x \leq 35 \\ 0.6201\,x-1.153, & 35 < x \leq 60 \\ 0.6347\,x-2.029, & x < 60\,. \end{cases} \tag{3.31}$$

The results obtained by the classical trajectory method provide rates higher than the ADO rate coefficients. However, the experimental rates lie in between ADO and trajectory rates, more closer to the rates by trajectory method. In particular, rate coefficients obtained from the classical trajectory method yield better agreement with the experiments (within 3% error) [27].

3.4.5 Quantum Dynamics Methods

In the last decades, a quantum mechanical theory of scattering has been implemented for ion-molecule collisions. Based on such theories, advanced methods address successfully ion-molecule capture collision rate coefficients [28–30].

Recently, quantum scattering theory approaches that have been developed to solve the Schrödinger equation on a potential energy surface (PES) have been promising in reproducing experimental results for small atom-diatom reactions such as F + H_2 , I + HI, and H + O_2 [31]. A number of improvements in quantum dynamics have been made to understand the fundamentals of the reactive collisions including the nature of PESs, nonadiabatic effects, direct collision dynamics, energy partitioning, product state and angular distributions, quantum tunneling, resonances, and other interference effects. For example, the rate coefficients obtained using the centrifugal sudden approximation by D. C. Clary [32] for IMR of H_3^+ and HCN were in good agreement with classical trajectory calculations above 10 K. Presently, quantum dynamic theories have been limited to mostly atom-diatomic and atom-triatomic systems [33] because for polyatomic molecules the large number of cou-

pled vibrational and rotational states of the molecules involved in the inelastic collisions makes the solution of the nuclear Schrödinger equation computationally unfeasible. Therefore, the list of reactions for which this level of theory exists is not very long, and serious challenges still remain in developing a theory applicable to more complicated polyatomic molecules. However, there are important applications related to low-energy unimolecular processes such as reactions involving ions, reaction dynamics in clusters, gas-surface processes that benefit of quantum scattering theory and closely related methods.

Given the current theoretical framework, in the present thesis we stick to classical collision and trajectory methods for the evaluation of reaction rates.

3.5 Energy and Temperature Dependence

The trajectory method has provided reasonably accurate ion-molecule collision rate coefficients very close to the experimental values. The method is based on the dipole moment and polarizability of the neutral molecule which considers ion-dipole and ion-induced interactions. In this method, the ion is treated as a point charge and the polar molecule as a two-dimensional rigid rotor [26, 34]. Trajectory calculations provide good numbers especially at thermal energy and various temperatures ranging from 80 K to 600 K for typical SIFT-MS instrument [35]. However, the temperature inside PTR-MS drift tube could be well above 1000 K as discussed in section (2.3.2) of the chapter (2). The impact of the applied electric field on IMRs outcome can be studies by considering the collision energy of the reaction. This is the Kinetic energy relative to the center-of-mass of the colliding system, KE_{com} [36]. With the increasing interest in experimental measurements of the rate coefficients dependent on kinetic energy, efforts have been made by Su et al. [37–39] to calculate rate coefficients on the basis of parameterized trajectory calculation at relative kinetic energy dependence at higher effective temperatures. Su stated that the ratio of capture rate coefficient k_{cap} at the center-of-mass kinetic energy, KE_{com} and a given rotational temperature T to the Langevin rate constant, k_{Lang} depends on two reduced parameters τ

and ε given by the following expressions:

$$\frac{\mathrm{k_{cap}}}{\mathrm{k_{Lang}}} = K_c(\tau,\varepsilon)\,, \tag{3.32}$$

where

$$\tau = \frac{\mu_{\mathrm{D}}}{\sqrt{\alpha T}}\,, \tag{3.33}$$

and

$$\varepsilon = \frac{\mu_{\mathrm{D}}}{\sqrt{\alpha K E_{\mathrm{com}}}}\,. \tag{3.34}$$

Su and colleagues performed calculations on more than 100 systems and thereby six-thousands trajectories were studied. The following equation was derived to fit the obtained data:

$$\begin{aligned} K_c(\tau,\varepsilon) = 1 + c_1\tau^{0.4}\varepsilon^2 S + c_2(1-S) \\ \times \sin[c_3c_4 + \ln(\tau)]\tau^{0.6}\sqrt{(\varepsilon - 0.5)}\,, \end{aligned} \tag{3.35}$$

where $\mathrm{c_1} = 0.727143$, $\mathrm{c_2} = 3.71823$, $\mathrm{c_3} = 0.586920$ and $\mathrm{c_4} = 4.97894$.

$$S = \begin{cases} \exp[-2(\varepsilon - 1.5)]; & \varepsilon > 1.5 \\ 1; & \varepsilon \leq 1.5\,. \end{cases} \tag{3.36}$$

The results obtained from (3.35) were in excellent agreement (5% error) for ion-molecule collisions with center-of-mass energies ranging from thermal to several eV and temperature in the range of 50 K to 1000 K [39]. This shows that the parametrized trajectory calculations can be useful in the interpretation of kinetic energy and higher effective temperature dependence of rate coefficients.

3.6 Summary

It has been observed that majority of the investigations for ion-molecule collisions reactions involved quasi-thermal collisions of relatively low mass ions and neutrals. Where ion is

considered as point charge interacting with polarizable neutral molecule at low energy. These low energy collisions are dominated by long-range attractive forces (ion-dipole and ion-induced dipole). These exothermic reactions are invariably fast, and in most cases agree very closely with experimental rate coefficient predictions based on barrier less ion-molecule capture processes. The rate coefficients for proton transfer and charge transfer to many different classes of organic molecules can be obtained by using models based on dipole moment and polarizability. Since experimental determination of dipole moment and polarizability is not as that easy, the density functional theory based results for molecular properties have been consistent and quite accurate if proper functional and basis sets are chosen.

An extensive database listing these properties such as proton affinities, ionization energies, dipole moment, and polarizability is required for efficient implementation of collision models. Dipole moment and polarizability based ion-molecule collision theories ADO and trajectory calculations have been promising in predicting rate coefficients accurately for dipole dependence charge transfer as well as proton transfer and quite successful in momentum transfer collisions and estimating rate coefficients for PTRs analogous to experimental rate coefficients. Consequently, the lack of experimental data for the rate coefficient of a particular IMR of importance in a PTR-MS study is not necessarily an impediment since a theoretical value can be derived that is likely to have a margin of error comparable to that in any experimental determination.

However, more experimental results at higher effective temperature and the center-of-mass kinetic energy dependent collision rate coefficients must be obtained to complement theoretical results. Alongside this, a comprehensive chemical kinetic database for ion-molecule collision reaction rate coefficients especially in food science is also needed to perform many PTR-MS/SIFT-MS experiments.

Bibliography

[1] D. K. Böhme. Ion–molecule reactions in mass spectrometry. In J. C. Lindon, G. E. Tranter, and D. W. Koppenaal, editors, *Encyclopedia of Spectroscopy and Spectrom-*

etry, pages 338–346. Academic Press, Oxford, 3 edition, 2017.

[2] D. Smith and P. Spanel. Selected ion flow tube mass spectrometry (SIFT-MS) for on-line trace gas analysis. *Mass spectrometry reviews*, 24:661–700, 09 2005.

[3] H. I. Schiff and D. K. Bohme. Flowing afterglow studies at York University. *International Journal of Mass Spectrometry and Ion Physics*, 16(1):167–189, 1975.

[4] T. Su and M. T. Bowers. Ion-polar molecule collisions. Proton transfer reactions of H_3^+ and CH_5^+ to the geometric isomers of difluoroethylene, dichloroethylene, and difluorobenzene. *Journal of the American Chemical Society*, 95(5):1370–1373, 1973.

[5] T. Su and M. T. Bowers. Theory of ion-polar molecule collisions. comparison with experimental charge transfer reactions of rare gas ions to geometric isomers of difluorobenzene and dichloroethylene. *The Journal of Chemical Physics*, 58(7):3027–3037, 1973.

[6] P. Langevin. A fundamental formula for kinetic theory. *Annales de chimie et de physique*, 5(245), 1905.

[7] A. Good. Third-order ion-molecule clustering reactions. *Chemical Reviews*, 75(5):561–583, 1975.

[8] J. Meyer and R. Wester. Ion-molecule reaction dynamics. *Annual Review of Physical Chemistry*, 68(1):333–353, 2017.

[9] L. Bass and M. T. Bowers. *Ion-Molecule Association Reactions*, volume 31 of *Ion Cyclotron Resonance Spectrometry II*. Springer, Berlin, Heidelberg, 1982.

[10] K. N. Swamy and W. L. Hase. Dynamics of ion-molecule recombination. III. Trends in the recombination efficiency. *Journal of the American Chemical Society*, 106(15):4071–4077, 1984.

[11] T. Fujii. *Ion-Molecule Attachment Reactions: Mass Spectrometry*. Springer US, 2015.

[12] P. Spanel and D. Smith. An investigation of the reactions of H_3O^+ and O_2^+ with NO, NO_2, N_2O and HNO_2 in support of Selected Ion Flow Tube Mass Spectrometry. *Rapid Communications in Mass Spectrometry*, 14, 04 2000.

[13] E. Vogt and G. H. Wannier. Scattering of ions by polarization forces. *Physical Review*, 95:1190–1198, 09 1954.

[14] G. Gioumousis and D. P. Stevenson. Reactions of Gaseous Molecule Ions with Gaseous Molecules. V. Theory. *The Journal of Chemical Physics*, 29(2):294–299, 1958.

[15] G. M. Wieder and R. A. Marcus. Dissociation and Isomerization of Vibrationally Excited Species. II. Unimolecular Reaction Rate Theory and Its Application. *The Journal of Chemical Physics*, 37(8):1835–1852, 1962.

[16] L. Bass, W. J. Chesnavich, and M. T. Bowers. Gas-phase ion-molecule association reactions. A statistical phase space theory approach. *Journal of the American Chemical Society*, 101(19):5493–5502, 1979.

[17] G. C. Maitland. *Intermolecular forces : their origin and determination*. International series of monographs on chemistry. Clarendon Press, 1987.

[18] E. Vogt and G. H. Wannier. Scattering of ions by polarization forces. *Physical Review*, 95:1190–1198, 09 1954.

[19] T. F. Moran and W. H. Hamill. Cross sections of ion-permanent-dipole reactions by mass spectrometry. *The Journal of Chemical Physics*, 39(6):1413–1422, 1963.

[20] T. Su and M. T. Bowers. Parameterization of the average dipole orientation theory: temperature dependence. *International Journal of Mass Spectrometry and Ion Processes*, 17(2):211–212, 06 1975.

[21] J. V. Dugan. A useful approximation and simple scaling laws for predicting ion-dipole capture cross sections and rate coefficients. *Chemical Physics Letters*, 21(3):476–482, 1973.

[22] J. V. Dugan and J. L. Magee. Capture collisions between ions and polar molecules. *The Journal of Chemical Physics*, 47(9):3103–3112, 1967.

[23] T. Su and M. T. Bowers. Theory of ion-polar molecule collisions. comparison with experimental charge transfer reactions of rare gas ions to geometric isomers of difluorobenzene and dichloroethylene. *The Journal of Chemical Physics*, 58(7):3027–3037, 1973.

[24] T. Su and M. T. Bowers. Ion-polar molecule collisions: the effect of ion size on ion-polar molecule rate constants; the parameterization of the average-dipole-orientation theory. *International Journal of Mass Spectrometry and Ion Physics*, 12(4):347–356, 1973.

[25] G. I. Mackay, K. Tanaka, and D. K. Bohme. Rate constants at 297 K for proton-transfer reactions with C_2H_2: An assessment of the average quadrupole orientation theory. *International Journal of Mass Spectrometry and Ion Physics*, 24(2):125–136, 1977.

[26] T. Su and W. J. Chesnavich. Parametrization of the ion-polar molecule collision rate constant by trajectory calculations. *The Journal of Chemical Physics*, 76(10):5183–5185, 1982.

[27] T. Su. Erratum: Trajectory calculations of ion-polar molecule capture rate constants at low temperatures [j. chem. phys. 88, 4102 (1988)]. *The Journal of Chemical Physics*, 89(8):5355–5355, 1988.

[28] D. C. Clary. Quantum theory of chemical reaction dynamics. *Science*, 279(5358):1879–1882, 1998.

[29] C. D. Lin and F. Martín. Chapter 2.6.2-Fast and Slow Collisions of Ions, Atoms and Molecules. In Roy Pike and Pierre Sabatier, editors, *Scattering*, pages 1025–1042. Academic Press, London, 2002.

[30] D. H. Zhang and H. Guo. Recent Advances in Quantum Dynamics of Bimolecular Reactions. *Annual Review of Physical Chemistry*, 67(1):135–158, 2016.

[31] G. C. Schatz. Scattering Theory and Dynamics: Time-Dependent and Time-Independent Methods. *The Journal of Physical Chemistry*, 100(31):12839–12847, 1996.

[32] D. C. Clary. Calculations of rate constants for ion-molecule reactions using a combined capture and centrifugal sudden approximation. *Molecular Physics*, 54(3):605–618, 1985.

[33] W. Hu and G. C. Schatz. Theories of reactive scattering. *The Journal of Chemical Physics*, 125(13):132301–1323015, 2006.

[34] W. J. Chesnavich, T. Su, and M. T. Bowers. Collisions in a noncentral field: A variational and trajectory investigation of ion-dipole capture. *The Journal of Chemical Physics*, 72(4):2641–2655, 1980.

[35] D. Smith and P. Španěl. SIFT-MS and FA-MS methods for ambient gas phase analysis: developments and applications in the UK. *Analyst*, 140:2573–2591, 2015.

[36] *Experimental: Components and Principles*, chapter 3, pages 49–109. John Wiley & Sons, Ltd, 2013.

[37] M. T. Bowers, T. Su, and V. G. Anicich. Theory of ion-polar molecule collisions. kinetic energy dependence of ion-polar molecule reactions: $CH_3OH^+ + CH_3OH \longrightarrow CH_3OH_2^+ + CH_3O$. *The Journal of Chemical Physics*, 58(11):5175–5176, 1973.

[38] T. Su. Kinetic energy dependence of ion-polar molecule collision rate constants by trajectory calculations. *The Journal of Chemical Physics*, 82(4):2164–2166, 1985.

[39] T. Su. Parametrization of kinetic energy dependences of ion-polar molecule collision rate constants by trajectory calculations. *The Journal of Chemical Physics*, 100(6):4703–4703, 1994.

4

Electronic Structure Methods

4.1 Introduction

There are many electronic structure methods available based on the approximations made to the solution of Schrödinger equation. Some methods rely solely on the laws of quantum mechanics and values of the fundamental constants such as the speed of light, masses, and charges of electrons and nuclei. While other methods combine data derived from the experimental approaches to find simplifying solutions theoretically. The real trade-off between these techniques is the computational cost and the level of accuracy [1, 2]. Depending on their approach (approximation) to solve the Schrödinger equation each have their own strengths and limitations. These methods are often called the level of theory and higher-level theories are regarded to be the most accurate ones.

Some of the most popular methods are ab initio or Hartree Fock (HF) and density functional theory (DFT) methods. In HF, the wave function is written as a product of one-electron functions called orbitals more precisely spatial orbitals, functions of space coordinates (x, y, z). A wave function which includes spatial orbitals as well as spin function can be represented in terms of Slater determinant. Ab initio methods work on the approximate solution of the Schrodinger equation directly from theoretical principles without any experimental data. While density functional methods calculate the electronic energy from electron density rather than the wave function [3–6]. In this formalism, electronic density is expressed as a linear combination of basis functions. This chapter mainly focuses on the DFT calculations and methods implementing DFT procedures.

4.2 Common Methods for Computing Properties

4.2.1 Molecular Geometry

Molecular geometry allows us to calculate molecular size, bond lengths, and angles between the binding atoms. These properties are easily accessible from quantum mechanical calculations. Many descriptors for quantitative structure-activity or property relationship calculations can be computed from the geometry only. In general, a small deviation in the molecular structure could affect molecular properties. In order to perform molecular calculations, optimization (finding the equilibrium structure) of the molecular geometry is required. Geometry optimization is nothing but to locate a point on the potential energy surface where the forces on the nucleus are essentially zero. Geometry optimization must be followed by other molecular calculations. We obtained initial molecular structures from standard databases such as PubChem and NIST molecular structure databases. Molecular structures are then geometrically relaxed to obtain the equilibrium geometry of the adopted DFT models.

4.2.2 Adiabatic Potential Energy

Many molecular properties are governed by the total electronic energy of the molecular system. Most of the information about chemistry is analogous to the energy or relative energetics associated with various species or processes. Energy is an integral part of the majority of the computational techniques. The analysis of energetics is often used to predict the likelihood of molecular processes to occur, or able to occur. All computational chemistry techniques are based on finding the lowest energy of the system which corresponds to the stability of that molecular structure. Thus, finding energy is equivalent to finding the shape of the molecule. However, some energies are easier to compute than others. For example, the energy difference between two conformers is much easier than finding the energy of the reaction barrier.

4.2.3 Wave Function

The electronic wave function of a molecule depends on the coordinates of its nuclei and electrons as well as time. The approximate solution of the Schrodinger equation let us know the wave function[1] and hence many molecular properties that are linked directly to the wave function or total electron density. Knowing the electron distribution properties such as dipole moments, polarizability, the electrostatic potential, and charges on atoms can be calculated. From electron distribution, one can know things like which part of the molecule is most likely to be attached by nucleophile or electrophile.

4.3 DFT Methods

DFT calculates the electronic energy of the molecule directly (electron distribution) from electron density rather than solving the complicated wave function. The original theory was developed by Kohn and sham used in the determination of ground state energy of a molecular system [3–5]. In DFT, the electron density is expressed as a linear combination

[1] Wave function is mathematical function that can be used to describe the electron distribution and hence, in theory, everything about the molecule.

of basis functions mathematically equivalent to the HF orbitals. A determinant is formed from these functions generally called Kohn-Sham orbitals. It is the electron density from this determinant of orbitals that are used to compute the energy. DFT is often called an ab initio method (although, in practice, the correlation exchange functional requires some fitting to give good results) faster than ab initio (HF) but slower than semi-empirical methods although subjected to the system and properties being calculated. One of the advantages of DFT over the ab initio (HF) method is that integrals for coulomb repulsion need to be solved over the electron density, a three-dimensional function bypassing the complicated wave function. Usually, DFT scales as N^3 and some electron correlation (tends to give better results) can be included in the calculation than HF which scales as N^4. In recent years, B_3LYP [7] has been widely used DFT functional[1] for molecular calculations, especially for organic molecules. There are many DFT methods available for calculation of ground state properties. Some of them are discussed here.

4.3.1 QuantumEspresso

QuantumEspresso is an integrated suite of computer codes for electronic-structure calculations and materials modeling based on the DFT, plane waves basis sets, and pseudopotentials to represent electron-ion interactions [8]. QuantumEspresso code is free, open-source, software that addresses electronic-structure calculations and various materials simulation techniques based on them. To make the treatment of infinite crystalline systems straightforward, QuantumEspresso codes are constructed around periodic boundary conditions and efficient convergence criteria. QuantumEspresso can be used for any crystal structure or supercell, and for metals as well as for insulators. The framework also includes many different exchange-correlation functionals such as LDA, GGA, advanced functionals like Hubbard U corrections and a few meta-GGA and other hybrid functionals.

- **Plane Wave Basis Set :** Plane wave basis sets provide a broad and efficient method for the calculation of electron density functional in DFT [9]. The scheme attributes to the representation of the electronic orbitals in terms of plane wave basis sets. In

[1] A functional is just a function that depends on a function.

this approach, a fast Fourier transform (FFT) algorithm is used to obtain total energy and forces. Periodic boundary conditions are taken into account when dealing with solids, crystals, and molecules. It must be noted that periodic plane wave basis sets can also be used for molecular simulations whenever the unit cell is sufficiently large to avoid image interaction between cells. Plane waves require simulating the molecular system in a supercell with periodic boundary conditions. Especially local charge imbalances, as occur in polar molecules, may lead to spurious interactions between periodic repeated copies of the molecule in nearby super cells. Our present simulations, in order to remove the spurious electrostatic interactions induced by the periodic boundary conditions and to guarantee a fair convergence of the total energy so that it is independent of the supercell size, we add standard correction terms to the energy [10]. The advantages of the plane wave approach include: simplicity in usage, orthonormality by construction and unbiased by atomic positions unlike atom-like (localized) basis sets.

- **Pseudopotential Approximation :** In pseudopotential (PP) approximation, fast varying core region of the atomic potentials and core electrons are removed and replaced by a fictitious electron-ion interaction potential acting on the valence electrons only [9]. PPs are constructed in such a way that maintains the scattering properties of the resulting PPs and the original atoms. The main idea behind the PPs approach is the assumption that changes in the electron wave function during bond formation only happen in the valance region and proper removal of the core from the problem should not affect the binding nature and properties of the system. Readers must be reminded that large oscillations of the wave function near the core region than the interstitial regions require large number of plane wave basis sets. The PP approach minimizes this requirement and considers only valance electrons for the prediction of molecular behavior. We use ultra-soft pseudopotentials of the type pbe-n-rrkjus.UHF [11] for H, C, O, N, Cl, and Br atoms to treat ions and core electrons interactions.

- **Optimization Algorithm :** The main optimization algorithm applied in QuantumEspresso is Broyden Fletcher Goldfarb Shanno (BFGS) algorithm [12]. It is a class of

quasi-newton methods which estimates the Hessian matrix in a different way. It is a hill-climbing optimization method which seeks a stationary point (preferably twice continuously differentiable) of a function. In order to solve such problems, the necessary condition for optimality is that the gradient should be zero. For the efficient convergence of Newton and BFGS methods, the function must have a quadratic Taylor expansion near optimum. BFGS has been very popular method for optimization in which the Hessian approximation is based on the full history of the gradients. BFGS has shown acceptable performance for non-smooth optimization instances as well. In our calculations, we use plane wave basis sets with 40 Ry kinetic energy cutoff for the expansion of the electronic wave functions. For all the considered structures, atomic positions were optimized using the BFGS algorithm until the total energy difference between consecutive structural optimization steps is less than 10^{-4} Ry and the force acting on the atoms is less than 10^{-3} Ry/Bohr. The adopted BLYP (Becke, Lee, Yang and Parr) [13, 14] exchange and correlation functional provides a fair account of electron-electron exchange-correlation (close to the hybrid functional B_3LYP (Becke 3-Parameter, Lee, Yang and Parr currently implemented in QuantumEspresso) [15] and accurate dipole moments and polarizabilities.

4.3.2 Gaussian Software

Gaussian (Latest version Gaussian 16) is a suite of computational chemistry software packages which offers a variety of theoretical methods that can treat systems at varying level of accuracy and in various molecular states and chemical environment [16]. Gaussian was originally released in 1970 by John Pople and co-workers at Carnegie Mellon University and has been updated regularly since then. Gaussian offers a wide variety of methods such as semiempirical, HF, coupled-cluster methods, DFT, Møller–Plesset perturbation theory, and many more. However, every method has its own limitation, and the accuracy and performance of the method depend on the type of problem and the range of elements to which type they are applicable. In Gaussian calculations, some important components worth mentioning here.

- **Basis Set :** Most of the methods mentioned in Gaussian require an appropriate basis set specification. The basis set is a collection of mathematical functions used to build the quantum mechanical wave functions of a molecular system. Broadly speaking, a basis set can be regarded as restricting each electron to a particular region of space. Larger basis sets means fewer constraints on the electrons and more accurately the exact molecular wave function gets approximated. However, large basis sets require more computational resources, so appropriate basis sets should be selected for the calculation under consideration.

- **Types of Basis Sets :** Gaussian offers a wide variety of predefined basis sets which can be classified by the number and type of basis functions that they comprise. The collection of basis functions on an atom mathematically approximates its orbitals. Some of the basis functions include: split valence, polarized, and diffuse functions. Polarized basis sets are important where orbitals change shape as well as size. Polarized basis sets add orbitals with angular momentum beyond what is required for the description of the ground state of each atom. For example, polarized basis sets introduce d functions to the carbon atom. Similarly, diffuse functions are vital for the systems where electrons are relatively far from the nucleus. They are large size s- and p-type functions allow orbitals to occupy a large region of space. Another usage of diffuse functions includes molecule with lone pairs, anions, and systems with a large negative charge, excited states and systems with low ionization potentials. In general DFT method with a large and appropriate basis set can give reliable thermodynamic properties for molecular systems including hydrogen bonding. For our calculations using Gaussian software, molecular geometry optimization is performed with B_3LYP [14] hybrid functional as a DFT method using 6-31+(d,p) or AUG-cc-pVTZ, where appropriate, basis sets which involves polarization and diffuse functions for both hydrogen and heavy atoms. All the thermodynamic properties have been calculated on fully optimized structures. Atomic polar tensor (APT) [17] charge analysis is used to determine the equivalent charges on the individual atoms from free bases and their protonated counterparts. In the calculations of cork-taint VOCs involving

sulfur molecule, we use correlated consistent basis sets for example, the AUG-cc-pVTZ basis, which places one s, one d, and one p-diffuse functions on hydrogen atoms, and one d, one p, one d, and one f-diffuse functions on B through Ne and Al through Ar. They include successively larger shells of polarization (correlating) functions (d, f, g, etc.), way to quickly converge density functional theory calculations to the complete basis set limit and give dipole moment and polarizability results close to experimental values.

- **Structural Optimization Algorithm :** Most of the optimization algorithms target in finding the set of coordinates that correspond to the minimum energy. In other words, locating the minimum on the potential energy surface is the key to predict the equilibrium geometry of the molecular systems. At both minima and saddle point[1], the first derivative of the energy (called gradient) and the forces on the nuclei are zero (since the gradient is the negative of the forces). A point on the potential energy surface is called a stationary point where the forces acting on the nuclei are zero. All the calculations of successful geometry optimization aim at locating the stationary point. There are many different algorithms available where energy and gradient of energy is required. The quasi-Newton algorithm is widely used which approximate the Hessian based on the differences of gradients over several iterations by imposing a secant quasi-Newton condition. The geometry will be adjusted until a stationary point to the potential surface is found. In Gaussian, the default optimization method for minimization (optimization to a local minimum) and optimization to transition states and higher-order saddle points is the Berny algorithm which internally builds up a second derivative Hessian matrix [18]. Berny algorithm uses forces acting on the atoms of a given structure along with the second derivative matrix (Hessian matrix) to predict energetically more favorable structures and thus optimize the molecular structure towards the next local minimum on the potential energy surface.

[1] A stable point on the PES which has a local maximum in one direction, but a local minimum in another direction. In chemical terms, the saddle point on a PES corresponds to a transition structure connecting the two equilibrium structures.

4.4 Summary

An approximate solution of the Schrödinger equation provides a means to calculate the electronic structure of atoms and molecules. We present some of the computational techniques that are used to solve the Schrödinger equation for electrons in a molecule and discuss some of the approximations that make the computations feasible. Presently, DFT is one of the most dominant computational methods for molecular electronic structure calculations among other techniques. Each method serves a different purpose rely on computational resources, level of accuracy, and available experimental data. There are several advantages in using DFT for the determination of the electronic structure of the atoms and molecules. One is that the energy of an electronic system can be written in terms of the electron probability density, ρ, one simple three-dimensional function for an N-electron molecule whereas the wave function approaches rely on the properties of a $3N$-dimensional function with a large number of constraints to ensure that it is fully anti-symmetric.

We discuss QuantumEspresso and Gaussian codes implementing DFT procedure and components on which these computational codes work. The final objective of these codes is to find the minimum energy solution but employing different optimization strategies based on an iterative procedure. These are the optimization strategies that used to move from one iterative step to the next distinguishes one algorithm from another.

Bibliography

[1] J. Foresman and A. Frisch. *Exploring Chemistry With Electronic Structure Methods*. 3 edition, 01 2015.

[2] E. G. Lewars. *Computational Chemistry: Introduction to the Theory and Applications of Molecular and Quantum Mechanics*, pages 1–664. 01 2011.

[3] P. Hohenberg and W. Kohn. Inhomogeneous electron gas. *Physical Review B*, 136:864–871, 11 1964.

[4] R. G. Parr, S. R. Gadre, and L. J. Bartolotti. Local density functional theory of atoms and molecules. *Proceedings of the National Academy of Sciences*, 76(6):2522–2526, 1979.

[5] W. Kohn, A. D. Becke, and R. G. Parr. Density functional theory of electronic structure. *The Journal of Physical Chemistry*, 100(31):12974–12980, 1996.

[6] R. M. Martin. *Electronic Structure: Basic Theory and Practical Methods*. Cambridge University Press, 2004.

[7] C. Lee, W. Yang, and R. G. Parr. Development of the Colle-Salvetti correlation-energy formula into a functional of the electron density. *Physical Review B*, 37(2):211–212, 06 1988.

[8] P. Giannozzi, S. Baroni, N. Bonini, M. Calandra, R. Car, C. Cavazzoni, D. Ceresoli, G. Chiarotti, M. Cococcioni, I. Dabo, A. Corso, S. de Gironcoli, S. Fabris, G. Fratesi, R. Gebauer, U. Gerstmann, C. Gougoussis, A. Kokalj, M. Lazzeri, and R. Wentzcovitch. QUANTUM ESPRESSO: a modular and open-source software project for quantum simulations of materials. 01 2009.

[9] E. Bylaska, K. Tsemekhman, N. Govind, and M. Valiev. *Large-Scale Plane-Wave-Based Density Functional Theory: Formalism, Parallelization, and Applications*, chapter 3, pages 77–116. John Wiley & Sons, Ltd, 2011.

[10] G. Makov and M. C. Payne. Periodic boundary conditions in ab initio calculations. *Physical Review B*, 51:4014–4022, 02 1995.

[11] A. Dal Corso. Pseudopotentials periodic table: From H to Pu. *Computational Materials Science*, 95:337–350, 2014.

[12] J. Nocedal and S. Wright. *Numerical Optimization*. Springer Series in Operations Research and Financial Engineering. Springer New York, 2006.

[13] A. D. Becke. Density-functional exchange-energy approximation with correct asymptotic behavior. *Physical Review A*, 38:3098–3100, 09 1988.

[14] C. Lee, W. Yang, and R. G. Parr. Development of the colle-salvetti correlation-energy formula into a functional of the electron density. *Physical Review B*, 37:785–789, 01 1988.

[15] A. D. Becke. Density-functional thermochemistry. III. the role of exact exchange. *The Journal of Chemical Physics*, 98(7):5648–5652, 1993.

[16] M. J. Frisch, G. W. Trucks, H. B. Schlegel, G. E. Scuseria, M. A. Robb, J. R. Cheeseman, G. Scalmani, V. Barone, G. A. Petersson, H. Nakatsuji, X. Li, M. Caricato, A. V. Marenich, J. Bloino, B. G. Janesko, R. Gomperts, B. Mennucci, H. P. Hratchian, J. V. Ortiz, A. F. Izmaylov, J. L. Sonnenberg, D. Williams-Young, F. Ding, F. Lipparini, F. Egidi, J. Goings, B. Peng, A. Petrone, T. Henderson, D. Ranasinghe, V. G. Zakrzewski, J. Gao, N. Rega, G. Zheng, W. Liang, M. Hada, M. Ehara, K. Toyota, R. Fukuda, J. Hasegawa, M. Ishida, T. Nakajima, Y. Honda, O. Kitao, H. Nakai, T. Vreven, K. Throssell, J. A. Montgomery, Jr., J. E. Peralta, F. Ogliaro, M. J. Bearpark, J. J. Heyd, E. N. Brothers, K. N. Kudin, V. N. Staroverov, T. A. Keith, R. Kobayashi, J. Normand, K. Raghavachari, A. P. Rendell, J. C. Burant, S. S. Iyengar, J. Tomasi, M. Cossi, J. M. Millam, M. Klene, C. Adamo, R. Cammi, J. W. Ochterski, R. L. Martin, K. Morokuma, O. Farkas, J. B. Foresman, and D. J. Fox. Gaussian~16 Revision C.01, 2016. Gaussian Inc. Wallingford CT.

[17] J. Cioslowski. A new population analysis based on atomic polar tensors. *Journal of the American Chemical Society*, 111(22):8333–8336, 10 1989.

[18] H. B. Schlegel. Optimization of equilibrium geometries and transition structures. *Journal of Computational Chemistry*, 3(2):214–218, 1982.

Part II

Results and Discussion

5

Computed Molecular Properties of Cork-Taint Compounds

5.1 Introduction

Over the last few years, computational calculations have become very popular because they are cheap, fairly accurate, and very fast as compared to the experiments [1–3]. Additionally, DFT methods have emerged as an attractive alternative to the traditional ab initio correlated calculations due to the correctness and the swiftness of their results. The computational calculations allow us to know the molecular geometry (shapes of the molecules, bond lengths, bond angles, and dihedral), energies of molecules and transitions (tells us which isomer is favored at equilibrium and how fast a reaction should go), chemical reac-

tivity (lets us know where the electrons are concentrated and where they want to go) and many more [3, 4]. Given the set of nuclei and electrons, a number of molecular properties can be obtained. The motion of the nuclei inside an atom is generally considered stationary as compared to the motion of electrons. In the electronic structure methods, the focus remains on the electrons [5].

Using the electronic structure methods as implemented in QuantumEspresso and Gaussian codes, physical and chemical properties of the molecules have been obtained. These methods differ in the trade-off made between the DFT functional used. QuantumEspresso results were obtained with BLYP DFT functional because the usage of hybrid functional B_3LYP in QuantumEspresso is rather restricted to geometry optimization only. Dipole moment and polarizability values have been obtained with QuantumEspresso and Gaussian. The later sections of the chapter deal with the results of ionization energy and proton affinity values as listed in the corresponding tables. Presently, very limited or no data is available for the targeted molecules in order to establish a fair comparison. A large database of molecular properties has been established using two different DFT methods.

5.2 Predicted Molecular Properties

5.2.1 Dipole Moment and Polarizability

IMRs are an important class of reactions occur routinely in the PTR-MS/SIFT-MS flow (drift) tubes. Theoretical investigation of the rate coefficients of such IMRs depends on two parameters viz dipole moment and polarizability of the neutral molecule [6–8]. These parameters act as input ingredients for collision-based models namely Langevin, ADO, and parametrized classical trajectory method. We use quantum mechanical calculations to calculate the dipole moment and polarizability of the neutral molecules.

- **Electric Dipole Moment :** The magnitude of the dipole moment is given by the absolute value of the product of the length of the bond and the net charge on either atom. Dipole moment depends on the electronegativity difference between the atoms and groups. Larger the electronegativity difference larger will be the dipole

moment. A molecule with no net dipole moment is called a non-polar molecule. To know the dipole moment, it is necessary to have detailed information on the geometry and bond polarity of the molecule. The dipole moment of a molecule is the vector sum of the individual bond dipoles. Based on the dimensional structure of the molecule, the individual dipoles might reinforce each other, cancel each other, or something in between. The dipole moment values have been computed and listed in the corresponding tables. The values in the Table 5.1 correspond to the taint and off-flavor molecules comprise anisoles, alcohols, esters, aldehydes, and terpenes, whereas the Table 5.2 solely consists of sulfur compounds that determine wine-taint. Previously, we computed dipole moment and polarizability values using QuantumEspresso for the same class of compounds [9]. Our computed dipole moments are in close agreement with the available literature values as cited. The molecules that acquire symmetric structures, their individual bond dipoles cancel one another and do not possess any dipole moment. Therefore, cis-3,6-dimethyl-1,2,4,5-tetrathiane and trans-3,6-dimethyl-1,2,4,5-tetrathiane molecules in the Table 5.2 have zero net dipole moment. The dipole moment values substantially affect the rate coefficients of the ion-molecule reactions.

- **Electric Polarizability :** The electric polarizability measures the ease with which the distortion in the distribution of electron density about an atom or a group in response to an external electric field. When this happens, the field induces a dipole moment in the atom ($\mu = \alpha$ E, where μ is the magnitude of the induced dipole moment, α is a constant called polarizability tensor, and E is the strength of electric field). The strength of the dispersion forces, the weakness of intermolecular forces, largely relies on the polarizability of the electrons. In other words, polarizability determines how tightly electrons are held by the nucleus. For example, unshared electron pairs possess higher polarizability than those shared by covalent bonding. This means farther the electrons from the nucleus, less tightly they are held and greater their polarizability will be and true contrariwise. The polarizability can also be represented as the measure of the volume of an atom. One can say that increased

polarizability results in the increased nucleophilic nature of a molecule. The computed values of polarizability using QuantumEspresso and Gaussian are listed in the Table 5.1. One can see that QuantumEspresso values are considerably higher than Gaussian values. The Table 5.2 lists Gaussian results with a higher basis set for sulfur molecules. The polarizability of a molecule increases as the number of electrons increases. Molecules such as Cl and Br contain an increasing number of electrons thus expected to have large polarizabilities. Polarizability also increases with the increased number of carbon atoms (see Tables 5.1 & 5.2).

- **Generalized Charges and Total Energy :** Atomic polar tensor (APT) charges have been used to represent charges on the atoms. The derivative of the dipole moment with respect to the nuclear coordinates measures the IR absorptions and the APT charges can be directly computed from vibrational frequency calculations. The APT charge on atom A is expressed as

$$Q_{\mathrm{A}} = \frac{1}{3}\left(\frac{\partial u_x}{\partial x_{\mathrm{A}}} + \frac{\partial u_y}{\partial y_{\mathrm{A}}} + \frac{\partial u_z}{\partial z_{\mathrm{A}}}\right). \tag{5.1}$$

Since dipole derivatives determine intensities of IR absorptions, the APT charges are therefore directly related to the experimentally observable quantities, however, computationally expensive. Table 5.5 shows the charges on the protonated complexes before and after protonation along with the total energy of the protonated complexes. Another notable aspect of APT charges is that these charges show modest basis set dependence and are sensitive to the electron correlation in the wave function. Whereas, Mulliken charge analysis is basis set dependent, and with increased basis size actual charges may diverge significantly. We report net APT charges on the corresponding atoms before and after protonation as in Table 5.5. Oxygen and nitrogen are the preferred proton attachment sites, except in 2-methyl-3-furanthionl which shows increased charge on O with O–H^+ complex. However, the formation of stable S–H^+ complex is confirmed on the basis of total energy of 2-methyl-3-furanthionl with corresponding decrease in negative charge from neutral

to the protonated atomic site. Higher negative charge on the atoms indicate their higher protonation tendency. A decrease in the charge after protonation on O and N has been reported. This decrease in charge on O–H^+/N–H^+ complexes indicate that the charge has been transferred from the ligand to the added proton.

5.2.2 Comparison of QuantumEspresso and Gaussian Results

We have listed our computed results of dipole moment and polarizability in the Table 5.1. Values in the square brackets represent Gaussian results with B_3LYP/6-31+G(d,p) level of theory. As already stated, the dipole moment of a molecule is a function of the charge distribution of the electrons around the atomic nuclei, and results from competing effects of the electron's kinetic energy, the Coulombic correlations, and the individual atomic electronegativities, in a complex interplay with the molecular equilibrium geometry. On the other hand, the dielectric polarizability is a linear-response property of the ground-state wave function can be obtained under an electric-dipole first-order perturbing operator acting on the molecule. This means that the calculation of the polarizability requires higher-level quantum chemical methods than is necessary to achieve the same level of accuracy in equilibrium properties such as the electric-dipole moment.

Many molecular properties can be related directly to the wave function or total electron density. Some of the examples are dipole moment, polarizability, the electrostatic potential, and charges on the atoms. Gaussian is a quantum chemistry code based on the basis sets which play a central role in determining the quality of quantum chemical calculations where accuracy in principle, increases with the basis functions. While QuantumEspresso is a pseudopotential code that includes valance orbitals which could be a limiting factor for calculating molecular properties. Although, not a very large difference in Gaussian and QuantumEspress results is seen (except for some complex molecules), with B_3LYP in Gaussian and BLYP in QuantumEspresso. One must note that the Gaussian includes inner as well as outer electrons in calculating the orbital energy as a result the energy bandgap of the molecule might get diminished. This could be the reason behind the smaller polarizability values as obtained by Gaussian in comparison with QuantumEspresso (Table 5.1).

Due to the lack of experimental data on dipole moment and polarizability of cork-taint molecules, direct correspondence with experimental results can not be made. Indeed, this data will serve as reference for further calculations both experimental as well as theoretical.

5.3 Proton Affinity

Protonation reactions are regarded as the first step towards many fundamental chemical rearrangement reactions [10–12]. PTRs play an important role in analytical chemistry and biochemistry. In CIMS, both positive and negative ions are operated. One of the most commonly used reagent ions is H_3O^+ ion. The PTR with H_3O^+ ions is effective only when the proton affinity of the acceptor molecule is higher than the H_2O molecule. If the molecule possesses higher PA than H_2O, the PTR will be exothermic and favored thermodynamically.

Proton affinity of a molecule is defined as the negative enthalpy change of the reaction [13]. Since the acceptance of a proton is an exothermic process, the PA is a positive quantity. In recent years, there has been much interest in computational calculations of PA values as it serves as a guide to the possible route of PTR processes [14–16]. One can expect that a molecule can have more than one site of protonation depending on the electronegativity of the individual atoms of a molecule. PA value at one site could be different from other site within a complex molecule. Also, protonation may occur on the sites other than the thermodynamically favorable sites. PA of the reaction (5.2)

$$A + H^+ \rightarrow AH^+ , \tag{5.2}$$

is defined as the negative of the reaction enthalpy at 298.15K, and hence (T: temperature, R: ideal gas constant)

$$PA = -\Delta H = -\Delta E + RT . \tag{5.3}$$

Where ΔE is the difference in the electronic energy of protonated and neutral molecule.

The energy of a non-linear poly-atomic molecule can be approximated as

$$\mathrm{E}(T) = \mathrm{E}_{\mathrm{rot}}(T) + \mathrm{E}_{\mathrm{trans}}(T) + \mathrm{ZPE} + \mathrm{E'}_{\mathrm{vib}}(T) + \mathrm{E}_{\mathrm{ele}}\,, \tag{5.4}$$

where ZPE stands for zero point energy of the normal modes. From statistics mechanics, $\mathrm{E}_{\mathrm{rot}}(T)$ and $\mathrm{E}_{\mathrm{trans}}(T)$ both contributes $\frac{3}{2}\mathrm{R}T$. The quantity $\mathrm{E'}_{\mathrm{vib}}(T)$ is usually less than 1 kcal/mol at room temperature, which is much less than the experimental error, and neglected as compared to ZPE. In this formalism, ground state energy of the proton contribution is zero. Hence

$$\mathrm{PA} = -\Delta\mathrm{E}_{\mathrm{ele}} - \Delta\mathrm{ZPE} + \frac{5}{2}\mathrm{R}T\,, \tag{5.5}$$

where, $\Delta\mathrm{E}_{\mathrm{ele}}$ and ΔZPE are the change in the electronic energy and change in zero point energy to the protonated and neutral molecule. The last term in (5.5) is the contribution from $\mathrm{E}_{\mathrm{rot}}(T)$, $\mathrm{E}_{\mathrm{trans}}(T)$ and $\mathrm{R}T$ to the equation (5.5).

We have computed PA values of the molecules of interest as listed in the Table 5.3 (column 2). Our targeted VOCs contain atoms: N, O, Cl, Br, and S, with varying electronegativity values: 3.04, 3.44, 3.16, 2.96, and 2.58 respectively, having multiple active sites available for protonation. Among many active sites, the site that has minimum total energy post protonation eventually stabilizes the structure will be considered. We identified such sites by calculating the total energy of different protonated sites. The Table 5.5 shows the charges on the atoms before and after protonation with corresponding total minimum energy. It is expected that a higher negative charge on the oxygen atom could lead to the higher proton affinity value than other atoms in a molecule. The corresponding APT charges on the oxygen, nitrogen and sulfur atom complexes before and after protonation are reported in the Table 5.5. Higher negative charge on the atoms indicates their higher protonation propensity. A decrease in the charge after protonation on O, N, and S has been reported. This decrease in charge on O–H^+, N–H^+ and S–H^+ complexes indicate that charge has been transferred from the ligand to the added proton.

In general, all the molecules studied can be protonated via N, O, Cl, and Br active sites as the case might be. However, protonation to other sites makes the structure un-

stable. For example: molecules such as pentachloroanisole, 2,4,6-trichloroanisole, 2,4,6-tribromophenol, 2,3,6-trichloroanisole, 2,3,4,5-tetrachloroanisole, 2,3,4,6-tetrachloroanisole, 2,3,5,6-tetrachloroanisole, 2,4-dichloroanisole and 2,6-dichloroanisole do not show protonation to Cl site. Similarly, molecules such as 2,4,6-trichloroanisole, 2,3,4-trichloroanisole were energetically unstable to Cl attachment, and 2,4,6-tribromoanisole, pentabromophenol were unstable to Br attachment (see Table 5.5 for energies). While oxygen being the most favorable protonation site in all the above cases. Figures, 5.1–5.4 also indicate the bond length change after proton transfer. Bond length increases in the protonated complexes. As seen in some cases, Figure 5.3, the water molecule gets separated from the molecule when oxygen accepts a proton and as a result, the carbon atom receives a positive charge. This is the reason why PA decreases when oxygen accepts a proton; it is so because bond breakage is an endothermic process. Due to this effect, lower PA values have been observed and clearly noticeable in some phenols such as chloro- and bromo-phenols; and 2-chloro-6-methylphenol in comparison to other compounds.

Nitrogen-containing molecules have the highest PA among other molecules. The molecules with higher PA values than NH_3 molecule are of particular interest in PTR-MS. The NH_4^+ ion as a reagent ion is vital in determining the concentration of such compounds which carry large PA values ill-suited for H_3O^+ quantification may produce fragmentation with H_3O^+ but conveniently accept a proton from NH_4^+. The molecules with PA values higher than NH_3 proceed through PTR in PTR-MS. From previously reported data of PAs [17], it is worthy to note that the oxygen-containing compounds found to have PAs in 180–205 kcal/mol range while nitrogen-containing compounds in 205–240 kcal/mol range.

5.4 Ionization Energy

Ionization energy can be computed as the difference between the total energies for the ground state of a molecule in ionic state to the neutral molecule.

$$IE = E_0(N-1) - E_0(N)\,. \tag{5.6}$$

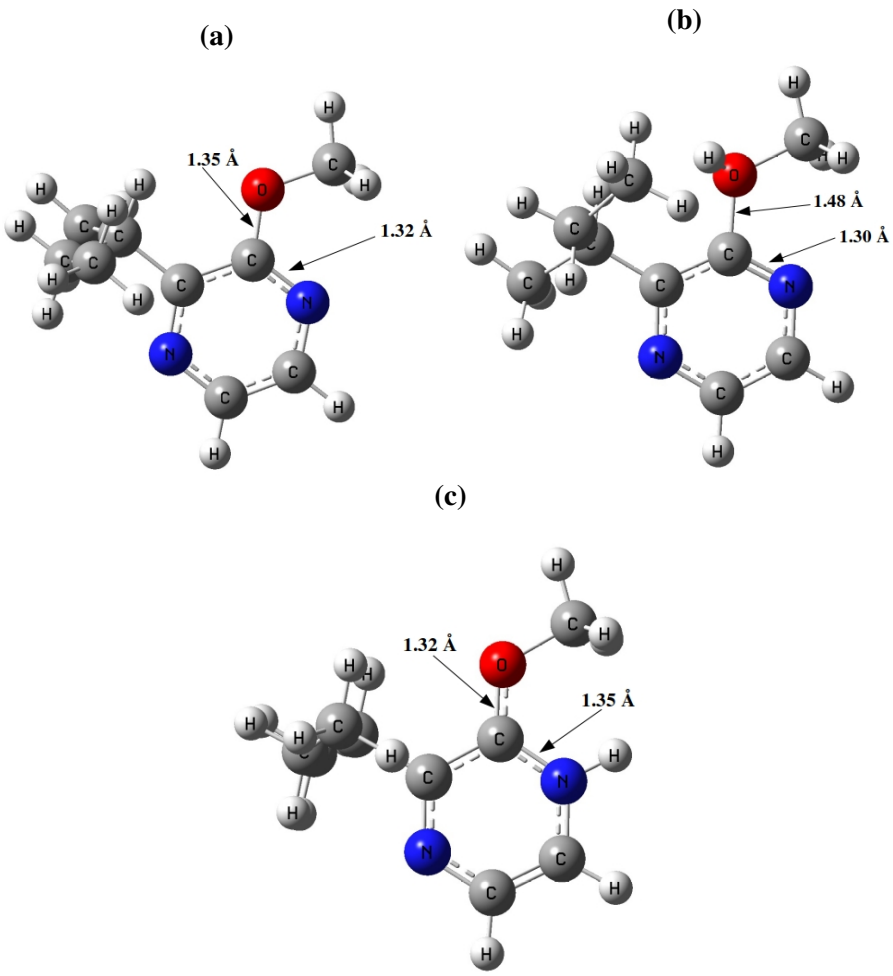

Figure 5.1: Optimized structures of 5.1a neutral, 5.1b O–site protonated, 5.1c N–site protonated 2-sec-butyl-3-methoxypyrazine molecule.

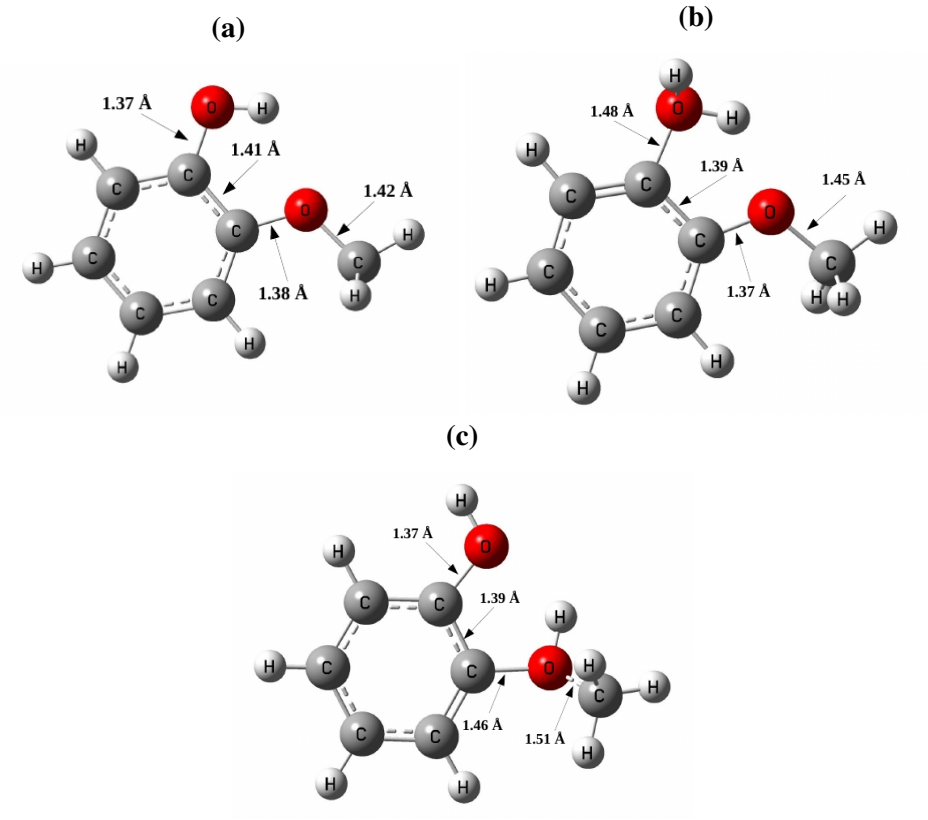

Figure 5.2: Optimized structures of 5.2a neutral, 5.2b H–O site protonated, 5.2c CH_3–O site protonated guaiacol molecule.

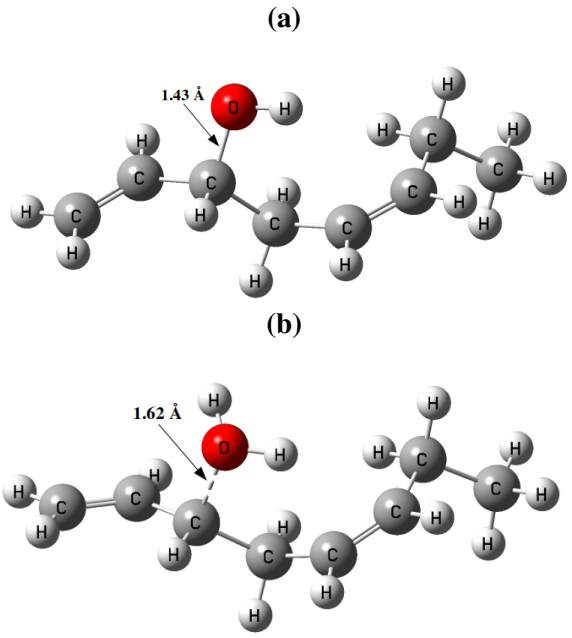

Figure 5.3: Fully optimized structures of 5.3a neutral, and 5.3b protonated cis-1,5-octadien-3-ol molecule to oxygen site.

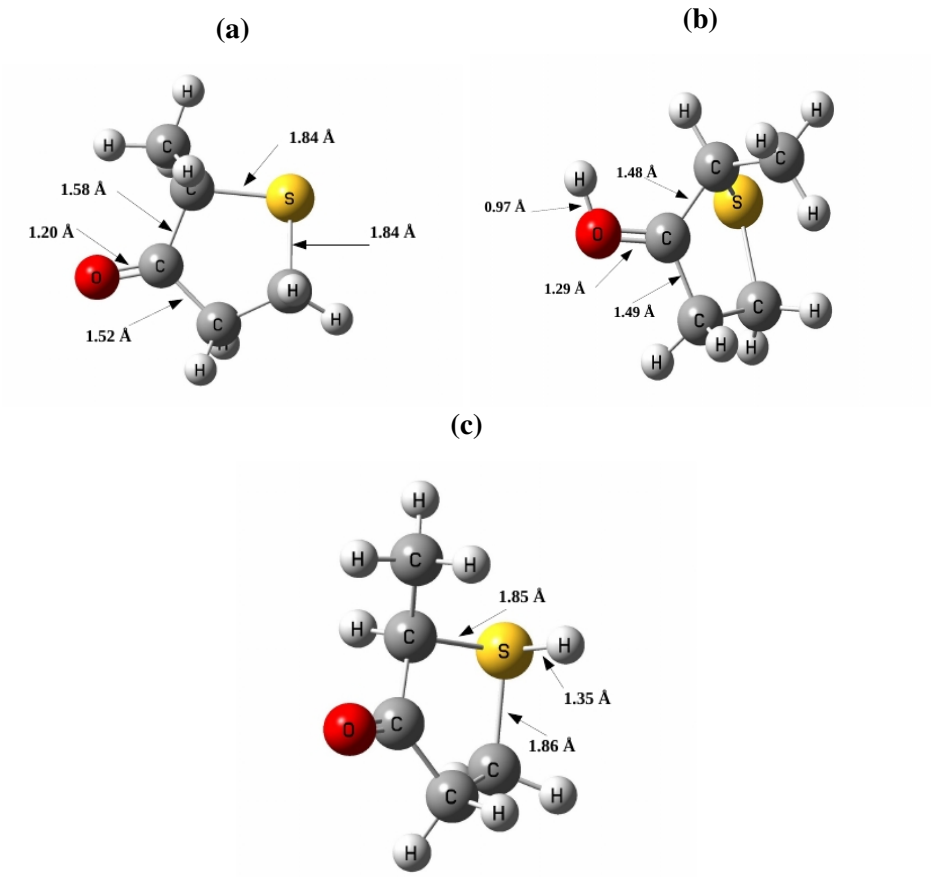

Figure 5.4: Optimized structures of 5.4a neutral, 5.4b H–O site protonated, 5.4c H–S site protonated 2-methyltetrahydrothiophen-3-one molecule.

The IE calculated by this way, equation (5.6), is often much more accurate since systematic errors cancel and the difference of energies from correlated quantum mechanical techniques give even more accurate results than that might be obtained by experimental methods [18, 19]. IE values are of great interest to the SIFT-MS experiments as these values help us to determine whether a reaction of NO^+ and O_2^+ ions to the analyte molecule occurs through charge transfer or not [20, 21]. The reactions involving charge exchange mass spectra is the net result of the energy-dependent scheme operating at fixed internal energy (over a small range of internal energies).

The exothermicity of the reaction is determined by the recombination energy of the reactant ions less than the ionization energy of the molecule. It has been observed analytically that low energy charge exchange raises the difference in the mass spectrum of most isobaric compounds. In addition to this, charge exchange spectra as a result becomes much simpler. The charge exchange reaction with NO^+ ion to volatile organic molecule is an ideal example. IE of NO is 9.3 eV, although, the effective RE of NO^+ ion under CI conditions appears to be considerably lower. Organic molecules having IE values lower than NO undergo extensive charge exchange reactions. NO^+ ion reacts with many aromatic organic compounds through charge exchange or adduct formation.

Experimental results have shown that aromatic compounds having IE higher than $\sim$ 8.7 eV promote adduct ion formation otherwise dominant charge exchange reactions will be preferred. Above verdict can be applicable to other class of compounds as well. Results have shown that under CI condition, NO^+ ions have a successful charge exchange reaction energy window with the molecules having IE $\sim$ 8.7 eV. In our calculations, Tables 5.3 and 5.4, most of the organic compounds having IE values lie conveniently well below IE of the NO molecule.

Another popular reagent ion commonly used in the SIFT-MS experiments for the application point of view is O_2^+ ion. Although, the usefulness of O_2^+ is limited due to high IE of O_2 molecule ($\sim$ 12 eV) that may deposit a large amount of energy to the product ion and promote large fragmentation upon reaction with VOCs molecules. However, most organic molecules are found to have IE values well below the IE of O_2 molecule and pro-

ceed through charge exchange reactions (see Tables 5.3 and 5.4). This suggests that all the molecules which are not quantified by NO^+ may undergo charge exchange reactions with O_2^+ ion. Hence, IE values let us know whether the reaction with reagent ions (NO^+ or O_2^+) to the VOCs proceed through charge exchange or not. To the best of our knowledge, a limited PA and IE data are available for the reported molecules.

Table 5.1: Computed values of dipole moment and polarizability of the compounds responsible for off-flavor and cork-taint in wine. Gaussian results obtained with B_3LYP on a 6-31+G(d,p) basis. In square brackets: QuantumEspresso results with BLYP level of theory on a plane-wave basis with cutoff 40 Ry.

Molecule name (Formula)	**Molecular mass** (a.m.u.)	**CAS Number**	**Dipole Moment** μ_D (Debye)	**Polarizability** α (Å^3)
2,4,6-Trichloroanisole ($C_7H_5Cl_3O$)	211.47	87-40-1	1.57[1,2] [1.41]	18.36 [21.47]
2,4,6-Tribromoanisole ($C_7H_5Br_3O$)	344.83	607-99-8	1.54 [1.44]	22.11 [25.67]
Pentachlorophenol (C_6Cl_5OH)	266.34	87-86-5	1.78 [1.90]	20.33 [25.45]
Pentabromophenol (C_6Br_5OH)	488.59	608-71-9	1.55 [2.06]	26.14 [30.11]
2,4,6-Trichlorophenol ($C_6H_2Cl_3OH$)	197-45	88-06-2	1.47[3] [1.49]	16.53 [19.67]
2,4,6-Tribromophenol ($C_6H_2Br_3OH$)	330.80	118-79-6	1.40[4] [1.46]	20.29 [23.26]
2,3,4-Trichloroanisole ($C_7H_5Cl_3O$)	211.47	54134-80-7	4.42 [4.34]	18.38 [21.21]
2,3,6-Trichloroanisole ($C_7H_5Cl_3O$)	211.47	50375-10-5	1.91 [1.57]	18.21 [21.04]
2,3,4,5-Tetrachloroanisole ($C_7H_4Cl_4O$)	245.91	938-86-3	3.75 [4.09]	20.42 [23.73]
2,3,4,6-Tetrachloroanisole ($C_7H_4Cl_4O$)	245.91	938-22-7	2.00 [1.83]	20.27 [23.58]
2,3,5,6-Tetrachloroanisole ($C_7H_4Cl_4O$)	245.91	6936-40-9	1.61 [1.57]	20.28 [23.53]
2,4-Dichloroanisole ($C_7H_6Cl_2O$)	177.03	553-82-2	3.40[5] [3.45]	16.55 [19.12]

[1] 1.42: G. Klages, J. Naturforschg 1965
[2] 1.57: M. Bowyer, Uni. of newcastle, 2002
[3] 1.42: G. Klages, J. Naturforschg 1965
[4] 1.45: G. Klages, J. Naturforschg 1965
[5] 2.77: G. Klages, J. Naturforschg 1965

Table 5.1: continued

Molecule name (Formula)	**Molecular mass** (a.m.u.)	**CAS Number**	**Dipole Moment** μ_D (Debye)	**Polarizability** α (Å^3)
2,6-Dichloroanisole ($C_7H_6Cl_2O$)	177.03	1984-65-2	2.04 [2.17]	16.21 [18.53]
Cis-1,5-octadien-3-one ($C_8H_{12}O$)	124.18	65767-22-8	3.02 [2.60]	15.20 [16.96]
Cis-1,5-octadien-3-ol ($C_8H_{14}O$)	126.20	50306-18-8	2.00 [1.66]	15.64 [17.31]
1-Octene-3-ol ($C_8H_{16}O$)	128.22	3391-86-4	1.44 [1.57]	15.39 [17.12]
1-Octene-3-one ($C_8H_{14}O$)	126.20	4312-99-6	3.16 [3.07]	14.70 [16.43]
Octanal ($C_8H_{16}O$)	128.21	124-13-0	3.33 [2.70]	14.85 [16.57]
2-Sec-butyl-3-methoxypyrazine ($C_9H_{14}N_2O$)	166.22	24168-70-5	1.33 [1.30]	18.43 [20.47]
3-Iso-butyl-2-methoxypyrazine ($C_9H_{14}N_2O$)	166.22	24683-00-9	1.41 [1.43]	18.38 [20.20]
2-Iso-propyl-3-methoxypyrazine ($C_8H_{12}N_2O$)	152.19	25773-40-4	1.38 [1.36]	16.74 [18.45]
2-Methoxy-3,5-dimethylpyrazine ($C_7H_{10}N_2O$)	138.17	92508-08-2	1.13 [1.18]	15.10 [16.88]
2-Methylisoborneol ($C_{11}H_{20}O$)	168.21	2371-42-8	1.53 [1.47]	18.71 [20.31]
Geosmin ($C_{12}H_{22}O$)	182.31	19700-21-1	1.43 [1.37]	20.28 [22.02]
Guaiacol ($C_7H_8O_2$)	124.14	90-05-1	2.87 [3.00]	13.26 [14.84]

Table 5.1: continued

Molecule name (Formula)	**Molecular mass** (a.m.u.)	**CAS Number**	**Dipole Moment** μ_D (Debye)	**Polarizability** α (Å^3)
4-Ethylguaiacol ($C_9H_{12}O_2$)	152.19	2785-89-9	1.19 [2.60]	17.19 [19.08]
4-Ethylphenol ($C_8H_{10}O$)	122.16	123-07-9	1.45 [1.62]	14.46 [15.82]
Eucalyptol ($C_8H_{10}O$)	154.25	470-82-6	1.55 [6] [1.51]	17.01[7] [18.56]
4-Ethylcatechol ($C_8H_{10}O_2$)	138.17	1124-39-6	2.38 [2.22]	15.14 [16.79]
4-Methylguaiacol ($C_8H_{10}O_2$)	138.17	93-51-6	1.21 [1.29]	15.32 [17.16]
Rotundone ($C_{15}H_{22}O$)	218.34	18374-76-0	3.97 [4.06]	26.10 [28.34]
Geraniol ($C_{10}H_{18}O$)	154.25	106-24-1	2.45 [1.55]	19.43 [21.69]
Hotrienol ($C_{10}H_{16}O$)	152.24	53834-70-1	1.74 [1.80]	19.83 [21.71]
Linalool ($C_{10}H_{18}O$)	154.25	78-70-6	1.93[8] [1.85]	18.93[9] [20.81]
Nerol ($C_{10}H_{18}O$)	154.25	106-25-2	2.64 [2.62]	18.61 [20.66]
$\alpha-$Terpineol ($C_{10}H_{18}O$)	154.25	98-55-5	1.66 [1.74]	17.98 [19.90]
Indole (C_8H_7N)	117.15	120-72-9	2.16 [2.44]	14.72 [16.00]
1-Methylindole (C_9H_9N)	131.18	603-76-9	2.48 [2.78]	16.73 [18.24]

[6] 1.57: G. Amadei,Rapid Commun. Mass Spectrom. 2011
[7] 18.1: G. Amadei,Rapid Commun. Mass Spectrom. 2011
[8] 1.58: G. Amadei,Rapid Commun. Mass Spectrom. 2011
[9] 19.6: G. Amadei,Rapid Commun. Mass Spectrom. 2011

Table 5.1: continued

Molecule name (Formula)	**Molecular mass** (a.m.u.)	**CAS Number**	**Dipole Moment** μ_D (Debye)	**Polarizability** α ($\dot{A}^3$)
2-Aminoacetophenone (C_8H_9NO)	135.16	551-93-9	1.96 [1.86]	16.08 [17.71]
2-Chloro-6-methylphenol (C_7H_7ClO)	142.58	87-64-9	0.88 [0.82]	14.37 [16.26]
3-Octanone ($C_8H_{16}O$)	128.21	106-68-3	2.74 [2.68]	14.60 [16.41]
Fenchone ($C_{10}H_{16}O$)	152.23	1195-79-5	3.10 [3.06]	16.60 [18.06]
Fenchol ($C_{10}H_{18}O$)	154.25	1632-73-1	1.46 [1.29]	17.05 [18.56]
Trans-2-octen-1-ol ($C_8H_{16}O$)	128.21	18409-17-1	1.74 [1.88]	15.59 [17.75]
Pentachloroanisole ($C_7H_3Cl_5O$)	280.35	1825-21-4	2.12 [2.18]	22.22 [26.10]

Table 5.2: Dipole moment and polarizability of sulfur compounds responsible for off-flavor and cork-taint in wine. Gaussian results are presented with B_3LYP/Aug-cc-PVTZ level of theory.

Molecule name (Formula)	**Molecular mass** (a.m.u.)	**CAS Number**	**Dipole Moment** μ_D (Debye)	**Polarizability** α ($\dot{A}^3$)
Hydrogen Sulfide (H_2S)	34.08	7783-06-4	0.99[10]	3.71
Methanethiol (CH_4S)	48.11	74-93-1	1.56[11]	5.55[12]
Ethanethiol (C_2H_6S)	62.14	75-08-1	1.68[13][14]	7.43
Dimethyl Sulfide (C_2H_6S)	62.14	75-18-3	1.60[15][16]	7.46
Diethyl Sulfide ($C_4H_{10}S$)	90.19	352-93-2	1.64[17]	11.34
Dimethyl Disulfide ($C_2H_6S_2$)	94.2	624-92-0	2.03[18]	10.79[19]
Diethyl Disulfide ($C_4H_{10}S_2$)	122.3	110-81-6	2.15	14.67
Methyl Thioacetate (C_3H_6OS)	90.15	1534-08-3	1.36	9.64
3-Mercaptohexan-1-ol ($C_6H_{14}OS$)	134.24	51755-83-0	1.68	15.43

[10] 0.97: Carl L. Yaws, Thermophysical Properties of Chemicals and Hydrocarbons.
[11] 1.52: Carl L. Yaws, Thermophysical Properties of Chemicals and Hydrocarbons.
[12] 5.55: NIST data base.
[13] 1.68: NIST data base.
[14] 1.58: Carl L. Yaws, Thermophysical Properties of Chemicals and Hydrocarbons.
[15] 1.60: NIST data base.
[16] 1.50: Carl L. Yaws, Thermophysical Properties of Chemicals and Hydrocarbons.
[17] 1.54: Carl L. Yaws, Thermophysical Properties of Chemicals and Hydrocarbons.
[18] 1.99: Carl L. Yaws, Thermophysical Properties of Chemicals and Hydrocarbons.
[19] 10.79: NIST data base.

Table 5.2: continued

Molecule name (Formula)	**Molecular mass** (a.m.u.)	**CAS Number**	**Dipole Moment** μ_D (Debye)	**Polarizability** α (Å^3)
4-Mercapto-4-methylpentan-2-one ($C_6H_{12}OS$)	132.23	19872-72-7	2.27	14.86
4-Mercapto-4-methylpentan-2-ol ($C_6H_{14}OS$)	134.24	255391-65-2	2.53	15.34
Benzothiazole (C_7H_5NS)	135.19	95-16-9	1.34	15.91
2-Furanmethanethiol (C_5H_6OS)	114.17	98-02-2	1.94	12.81
2-Mercaptoethanol (C_2H_6OS)	78.14	60-24-2	2.50	8.14
Benzenemethanethiol (C_7H_8S)	124.21	100-53-8	1.48[20]	15.74
2-Mercaptoethyl acetate ($C_4H_8O_2S$)	120.17	5862-40-8	1.83	11.91
3-mercaptopropyl acetate ($C_5H_{10}O_2S$)	134.2	26473-61-0	1.61	13.97
Cis-3,6-dimethyl-1,2,4,5-tetrathiane ($C_4H_8S_4$)	184.4	75100-46-8	0	19.83
Prenyl-mercaptan ($C_5H_{10}S$)	102.2	5287-45-6	1.78	13.35
Trans-3,6-dimethyl-1,2,4,5-tetrathiane ($C_4H_8S_4$)	184.8	75100-47-9	0	19.11

[20] 1.44 (in benzene): Carl L. Yaws, Thermophysical Properties of Chemicals and Hydrocarbons.

Table 5.2: continued

Molecule name (Formula)	**Molecular mass** (a.m.u.)	**CAS Number**	**Dipole Moment** μ_D (Debye)	**Polarizability** α ($\dot{A}^3$)
2-Methyl-3-furanthiol (C_5H_6OS)	114.17	28588-74-1	0.90	12.47
2-Methylthiolane-3-ol ($C_5H_{10}OS$)	118.2	149834-43-5	2.12	12.71
3-Mercapto-3-methylbutan-1-ol ($C_5H_{12}OS$)	120.22	34300-94-2	1.84	13.52
Ethyl-3-mercaptopropionate ($C_5H_{10}O_2S$)	134.2	5466-06-08	2.76	13.91
5-2-hydroxyethyl-4-methylthiazole (C_6H_9NOS)	143.21	137-00-8	2.79	15.29
2-Methyltetrahydro thiophen-3-one (C_5H_8OS)	116.18	13679-85-1	1.72	12.14
3-Methylsulfanyl propan-1-ol ($C_4H_{10}OS$)	106.19	0505-10-02	3.06	12.03
3-Mercaptohexylacatate ($C_8H_{16}O_2S$)	176.28	136954-20-6	1.47	19.32
Ethylthioacetate (C_4H_8OS)	104.17	625-60-5	1.41	11.57

Table 5.3: Computed values of proton affinity and ionization energy of the targeted compounds using Gaussian B_3LYP/6-31+G(d,p) level of theory.

Molecule name (Formula)	**Proton Affinity** (kcal/mol)	**Ionization Energy** (eV)
2,4,6-Trichloroanisole ($C_7H_5Cl_3O$)	183.51	8.28
2,4,6-Tribromoanisole ($C_7H_5Br_3O$)	186.17	8.19
Pentachlorophenol (C_6Cl_5OH)	167.15	8.56
Pentabromophenol (C_6Br_5OH)	174.17	8.60
2,4,6-Trichlorophenol ($C_6H_2Cl_3OH$)	174.35	8.79
2,4,6-Tribromophenol ($C_6H_2Br_3OH$)	178.56	8.62
2,3,4-Trichloroanisole ($C_7H_5Cl_3O$)	181.32	8.15
2,3,6-Trichloroanisole ($C_7H_5Cl_3O$)	183.87	8.37
2,3,4,5-Tetrachloroanisole ($C_7H_4Cl_4O$)	178.40	8.23
2,3,4,6-Tetrachloroanisole ($C_7H_4Cl_4O$)	181.96	8.35
2,3,5,6-Tetrachloroanisole ($C_7H_4Cl_4O$)	181.49	8.67
2,4-Dichloroanisole ($C_7H_6Cl_2O$)	182.77	8.04
2,6-Dichloroanisole ($C_7H_6Cl_2O$)	186.69	8.30
Cis-1,5-octadien-3-one ($C_8H_{12}O$)	211.13	8.39
Cis-1,5-octadien-3-ol ($C_8H_{14}O$)	200.87	8.28

Table 5.3: continued

Molecule name (Formula)	**Proton Affinity** (kcal/mol)	**Ionization Energy** (eV)
1-Octene-3-ol ($C_8H_{16}O$)	197.68	8.92
1-Octene-3-one ($C_8H_{14}O$)	203.94	9.01
Octanal ($C_8H_{16}O$)	192.82	9.18
2-Sec-butyl-3-methoxypyrazine ($C_9H_{14}N_2O$)	215.84	8.30
3-Iso-butyl-2-methoxypyrazine ($C_9H_{14}N_2O$)	215.77	8.28
2-Iso-propyl-3-methoxypyrazine ($C_8H_{12}N_2O$)	215.39	8.33
2-Methoxy-3,5-dimethylpyrazine ($C_7H_{10}N_2O$)	217.16	8.11
2-Methylisoborneol ($C_{11}H_{20}O$)	217.79	8.28
Geosmin ($C_{12}H_{22}O$)	205.05	8.35
Guaiacol ($C_7H_8O_2$)	191.50	7.66
4-Ethylguaiacol ($C_9H_{12}O_2$)	198.28	7.29
4-Ethylphenol ($C_8H_{10}O$)	182.32	7.86
Eucalyptol ($C_8H_{10}O$)	213.24	8.28
4-Ethylcatechol ($C_8H_{10}O_2$)	198.28	7.61
4-Methylguaiacol ($C_8H_{10}O_2$)	195.18	7.32
Rotundone ($C_{15}H_{22}O$)	219.70	8.18
Geraniol ($C_{10}H_{18}O$)	212.37	7.77
Hotrienol ($C_{10}H_{16}O$)	208.05	7.73
Linalool ($C_{10}H_{18}O$)	214.27	8.03
Nerol ($C_{10}H_{18}O$)	209.87	7.91

Table 5.3: continued

Molecule name (Formula)	**Proton Affinity** (kcal/mol)	**Ionization Energy** (eV)
$\alpha-$Terpineol ($C_{10}H_{18}O$)	200.56	7.95
Indole (C_8H_7N)	199.49	7.51
1-Methylindole (C_9H_9N)	203.64	7.30
2-Aminoacetophenone (C_8H_9NO)	214.57	7.61
2-Chloro-6-methylphenol (C_7H_7ClO)	177.47	8.20
2-Octanone ($C_8H_{16}O$)	203.37	8.92
Fenchone ($C_{10}H_{16}O$)	207.11	8.33
Fenchol ($C_{10}H_{18}O$)	198.48	8.31
Trans-2-octen-1-ol ($C_8H_{16}O$)	203.08	8.53
Pentachloroanisole ($C_7H_3Cl_5O$)	180.35	8.44

Table 5.4: Computed values of proton affinity and ionization energy of the VOCs related to sulfur using Gaussian B_3LYP/Aug-cc-PVTZ level of theory.

Molecule name (Formula)	**Proton Affinity** (kcal/mol)	**Ionization Energy** (eV)
Hydrogen Sulfide (H_2S)	169.14	10.43
Methanethiol (CH_4S)	186.08	9.37
Ethanethiol (C_2H_6S)	190.61	9.16
Dimethyl Sulfide (C_2H_6S)	199.30	8.59
Diethyl Sulfide ($C_4H_{10}S$)	206.31	8.28
Dimethyl Disulfide ($C_2H_6S_2$)	193.66	8.09
Diethyl Disulfide ($C_4H_{10}S_2$)	197.75	7.89
Methyl Thioacetate (C_3H_6OS)	198.47	9.09
3-Mercaptohexan-1-ol ($C_6H_{14}OS$)	196.58	8.62
4-Mercapto-4-methylpentan-2-one ($C_6H_{12}OS$)	198.23	8.50
4-Mercapto-4-methylpentan-2-ol ($C_6H_{14}OS$)	204.77	8.47
Benzothiazole (C_7H_5NS)	220.73	8.55
2-Furanmethanethiol (C_5H_6OS)	199.10	8.05

Table 5.4: continued

Molecule name (Formula)	**Proton Affinity** (kcal/mol)	**Ionization Energy** (eV)
2-Mercaptoethanol (C_2H_6OS)	193.42	8.98
Benzenemethanethiol (C_7H_8S)	195.26	8.26
2-Mercaptoethyl acetate ($C_4H_8O_2S$)	199.18	9.10
3-mercaptopropyl acetate ($C_5H_{10}O_2S$)	199.60	8.96
Cis-3,6-dimethyl-1,2,4,5-tetrathiane ($C_4H_8S_4$)	196.08	8.03
Prenyl-mercaptan ($C_5H_{10}S$)	198.21	8.06
Trans-3,6-dimethyl-1,2,4,5-tetrathiane ($C_4H_8S_4$)	195.31	8.25
2-Methyl-3-furanthiol (C_5H_6OS)	190.29	7.71
2-Methylthiolane-3-ol ($C_5H_{10}OS$)	207.51	8.16
3-Mercapto-3-methylbutan-1-ol ($C_5H_{12}OS$)	197.74	8.59
Ethyl-3-mercaptopropionate ($C_5H_{10}O_2S$)	196.71	8.90
5-(2-hydroxyethyl)-4-methylthiazole (C_6H_9NOS)	229.67	8.12

Table 5.4: continued

Molecule name (Formula)	**Proton Affinity** (kcal/mol)	**Ionization Energy** (eV)
2-Methyltetrahydro thiophen-3-one (C_5H_8OS)	196.14	8.57
3-Methylsulfanyl propan-1-ol ($C_4H_{10}OS$)	203.12	8.38
3-Mercaptohexylacatate ($C_8H_{16}O_2S$)	194.86	8.78
Ethylthioacetate (C_4H_8OS)	201.19	8.96

Table 5.5: Preferred sites of proton attachment for the selected molecules with net atomic charge (a. u.) on the atom before and after protonation (in square brackets) corresponding to the minimum total energy (a. u.).

Molecule name	Protonation site and net charge	Total energy
2,4,6-Trichloroanisole	O–H^+[-0.7929, -0.5878]	-1725.8685
($C_7H_5Cl_3O$)	Cl–H^+[-0.2964, 0.0701]	-1725.8161
2,4,6-Tribromoanisole	O–H^+ [-0.7859, -0.6063]	-8060.4741
($C_7H_5Br_3O$)	Br–H^+ [-0.2101, -0.1283]	-8060.4314
Pentabromophenol	O–H^+[-0.6943, -0.6846]	-13163.3932
(C_6Br_5OH)	Br–H^+[-0.1647, 0.4083]	-13163.3541
2,3,4-Trichloroanisole	O–H^+[-0.8974, -0.8248]	-1725.8617
($C_7H_5Cl_3O$)	Cl–H^+[-0.2408, -0.0479]	-1725.8282
2-Sec-butyl-3-	N–H^+[-0.3568, -0.1456]	-536.5060
methoxypyrazine	CH_3O–H^+[-0.8789, -0.7715]	-536.4563
($C_9H_{14}N_2O$)		
3-Iso-butyl-2-	N–H^+[-0.3515, -0.1428]	-536.5046
methoxypyrazine	CH_3O–H^+[-0.8736, -0.7837]	-536.4538
($C_9H_{14}N_2O$)		
2-Iso-propyl-3-	N–H^+[-0.3606, -0.1505]	-497.1885
methoxypyrazine	CH_3O–H^+[-0.8878, -0.7556]	-497.1360
($C_8H_{12}N_2O$)		
2-Methoxy-3,5-	N–H^+[-0.3462, -0.1293]	-457.8814
dimethylpyrazine	O–H^+[-0.9178, -0.6658]	-457.8298
($C_7H_{10}N_2O$)		
Guaiacol	CH_3O–H^+[-0.8829, -0.6341]	-422.3394
($C_7H_8O_2$)	HO–H^+[-0.7178, -0.5607]	-422.3297
4-Ethylguaiacol	CH_3O–H^+[-0.8697, -0.6441]	-500.9803
($C_9H_{12}O_2$)	HO–H^+[-0.7108, -0.4470]	-500.9702
4-Methylguaiacol	CH_3O–H^+[-0.8704, -0.6391]	-461.6627
($C_8H_{10}O_2$)	HO–H^+[-0.7001, -0.5711]	-461.6536

Table 5.5: continued

Molecule name	Protonation site and net charge	Total energy
2-Aminoacetophenone	O–H^+[-0.7814, -0.7688]	-440.6478
(C_8H_9NO)	H_2N–H^+[-0.7450, -0.2077]	-440.6437
Pentachloroanisole	CH_3O–H^+[-0.8200, -0.6120]	-2645.0284
($C_7H_3Cl_5O$)	Cl–H^+[0.2335, -0.0293]	-2644.9842
2-Methyl-3-furanthiol	S-H^+[-0.0703, 0.6676]	-667.9799
(C_5H_6OS)	O-H^+[-0.5003, -0.5827]	-667.9543
Ethylthioacetate	O-H^+[-0.7414, -0.5946]	-631.1290
(C_4H_8OS)	S-H^+[-0.3661, -0.1067]	-631.1127
Benzothiazole	N-H^+[-0.4725, -0.2357]	-723.2135
(C_7H_5NS)	S-H^+[-0.1253, 0.1980]	-723.1419
5-(2-hydroxyethyl)-	N-H^+[-0.4687, -0.2239]	-762.7623
4-methylthiazole	O-H^+[-0.5771, -0.6015]	-762.7010
(C_6H_9NOS)	S-H^+[-0.0965, -0.1516]	-762.6794

5.5 Summary

DFT calculations have been performed to obtain dipole moment and polarizability values using QuantumEspresso and Gaussian software. Dipole moment varies with the electronegativity difference between the atoms and the distance between the atoms while polarizability varies with the number of electrons and the distance between the electron and nuclear charge. We obtained fairly close values of the quantities from two methods based on DFT/B_3LYP (Gaussian) and DFT/BLYP (QuantumEspresso) level of theories. These two parameters, dipole moment and polarizability, can serve as essential stuff for collision-based models to study proton transfer and charge transfer reactions in mass spectrometry.

The PA values determine the proficiency of an atom or molecule to accept a proton in the gas phase and act as a deciding factor for the transfer of proton to the neutral molecule. These values are vital in PTR-MS and SIFT-MS mass spectrometry to determine whether

transfer of a proton from ion to molecule will occur or not. PA increases with the number of carbon atoms in the hydrocarbons while IE decreases with the number of carbon atoms. The molecules containing oxygen atom have higher PA than hydrocarbons. For alcohols, PA varies between 180–190 kcal/mol range.

In mass spectrometry, IE helps in determining the occurrence of charge exchange reactions. The reaction mechanism in PTR-MS and SIFT-MS flow (drift) tubes is predominately dependent on the PA and IE values. Knowing these values in advance let us predict the type of reaction and nature of the products and in short ion-molecule chemistry in mass spectrometry experiments.

Bibliography

[1] J. R. Reimers. *Computational Methods for Large Systems: Electronic Structure Approaches for Biotechnology and Nanotechnology*. Wiley, 2011.

[2] *Density Functional Theory*, chapter 5, pages 42–48. John Wiley & Sons, Ltd, 2002.

[3] P. W. Atkins and R. S. Friedman. *Molecular Quantum Mechanics*. Oxford University Press Oxford, 2011.

[4] E. G. Lewars. *Computational Chemistry: Introduction to the Theory and Applications of Molecular and Quantum Mechanics*, pages 1–664. 01 2011.

[5] J. Foresman and A. Frisch. *Exploring Chemistry With Electronic Structure Methods*. 3 edition, 01 2015.

[6] P. Langevin. A fundamental formula for kinetic theory. *Annales de chimie et de physique*, 5(245), 1905.

[7] E. Vogt and G. H. Wannier. Scattering of ions by polarization forces. *Physical Review*, 95:1190–1198, Sep 1954.

[8] T. F. Moran and W. H. Hamill. Cross Sections of Ion-Permanent-Dipole Reactions by Mass Spectrometry. *The Journal of Chemical Physics*, 39(6):1413–1422, 1963.

[9] M. Bhatia, F. Biasioli, L. Cappellin, P. Piseri, and N. Manini. Ab initio calculation of the proton transfer reaction rate coefficients to volatile organic compounds related to cork taint in wine. *Journal of Mass Spectrometry*, 55(11):e4592, 2020.

[10] A. Moser, K. Range, and D. M. York. Accurate Proton Affinity and Gas-Phase Basicity Values for Molecules Important in Biocatalysis. *The Journal of Physical Chemistry B*, 114(43):13911–13921, 2010.

[11] G. Raabe, Y. Wang, and J. Fleischhauer. Calculation of the proton affinities of primary, secondary, and tertiary amines using semiempirical and ab initio methods. *Zeitschrift für Naturforschung A*, 55, 08 2000.

[12] M. Basheer, R. Custodio, P. Volpe, and R. Rittner. An Investigation of Chlorophenol Proton Affinities and Their Influence on the Biological Activity of Microorganisms. *The journal of physical chemistry. A*, 110:2021–2026, 03 2006.

[13] J. K. Labanowski, R. A. Hill, D. J. Heisterberg, D. D. Miller, C. F. Bender, and J. W. Andzelm. Proton Affinities Calculated by Traditional ab initio Approaches and by Density Functional Methods.

[14] A. K. Chandra and A. Goursot. Calculation of proton affinities using density functional procedures: A critical study. *The Journal of Physical Chemistry*, 100(28):11596–11599, 1996.

[15] P. Wilson, C. Freeman, and M. Mcewan. Reactions of small hydrocarbons with H_3O^+, O_2^+ and NO^+ ions. *International Journal of Mass Spectrometry*, 229:143–149, 10 2003.

[16] G. Francis, D. Milligan, and M. Mcewan. Gas-Phase Reactions and Rearrangements of Alkyl Esters with H_3O^+, O_2^+ and NO^+ : A Selected Ion Flow Tube Study. *The journal of physical chemistry. A*, 111:9670–9, 11 2007.

[17] A. G. Harrison. *Chemical Ionization Mass Spectrometry*, chapter 2, pages 7–41. Taylor & Francis, Canada, 2 edition, 1992.

[18] Y. Valadbeigi, H. Farrokhpour, and M. Tabrizchi. G4MP2, DFT and CBS-Q calculation of proton and electron affinities, gas phase basicities and ionization energies of hydroxylamines and alkanolamines. *Journal of Chemical Sciences*, 126:1209–1215, 07 2014.

[19] J. C. Delgado, Y. Ishikawa, and R. G. Selsby. The calculated ionization potential and electron affinity of cationic cyanine dyes. *Photochemistry and Photobiology*, 85(6):1286–1298, 2009.

[20] G. Amadei and B. Ross. The reactions of a series of terpenoids with H_3O^+, NO^+ and O_2^+ studied using Selected Ion Flow Tube Mass Spectrometry. *Rapid Communications in Mass Spectrometry*, 25:162–8, 01 2011.

[21] T. Fujii. *Ion-Molecule Attachment Reactions: Mass Spectrometry*. Springer US, 2015.

6

Predicted Rate Coefficients for Ion-Molecule Reactions

6.1 Introduction

IMRs are an extremely important class of reactions in organic chemistry [1–3]. Theoretical way of dealing IMRs are equally important because they provide an explanation to experimental observations and along with experimental results to explore various reaction mechanisms. IMRs in modern analytic mass spectrometry instruments, such as PTR-MS and SIFT-MS have been of continuous interest for many years [4, 5]. The core of these techniques for proper detection and accurate quantification is the database of rate coefficients and product ion distribution for the reactions of the precursor ions with each trace gas in

the sample. Since IMRs involved in the drift tube are fast, exothermic, and occur at almost every collision without any activation energy, therefore, traditional Arrhenius equation can not be applied. In this regard, capture collision cross-section based models dependent on dipole moment and polarizability have been very successful for the description of IMRs.

The collision models rely on the ion-dipole interactions and predict rate coefficients reminiscent to the experimental results to a larger extent [6–8]. This chapter deals with the rate coefficient estimation from various methods like Langevin collision model, ADO method and classical trajectory methods under PTR-MS and SIFT-MS working conditions. We also provide an extensive database of rate coefficients for the reactions of reagents ions such as H_3O^+, NH_4^+, NO^+ and O_2^+ with VOCs routinely occur in wine. The rate coefficients dependence on various parameters has been thoroughly investigated.

6.2 Computed Rate Coefficients

6.2.1 PTR-MS Conditions

In PTR-MS drift tube, the positive ions, H_3O^+ and NH_4^+, are deflected by the applied electric field [9]. As the applied electric field is uniform, the ion swarm establishes a constant drift velocity. Due to the high pressure in the drift tube, a constant velocity is maintained such that ion-molecule collisions occur in the drift tube. The resultant ions are unable to maintain constant velocity because of collisions with the neutral gas molecules and eventually gives rise to a steady-state velocity ($v_d = KE$, where K is the ion mobility and E is the applied field). It must be noted that the velocity represents here is the mean drift velocity of the ion swarm not the velocity of individual ions. Under normal working conditions of temperature and pressure (273.16 K and 760 Torr = 1.01325×10^5 Pa), the mobility[1] ($K_o = 2.81 cm^2V^{-1}s^{-1}$) of ion-neutral combination and gas number density ($N_o = 2.687 \times 10^{-19} cm^3$), the drift velocity[2] (v_d) comes out to be 906 ms^{-1} [9]. The value of reduced electric field E/N is usually $\sim$ 120 Td considered under normal PTR-MS

[1] Ion mobility is a function of temperature and pressure also depends on the cross-section of ion-molecule collisions called reduced mobility $K = (760 * T/P * 273) * K_o$

[2] $v_d = K_o * N_o * E/N$

experimental conditions at 298 K. Most of the experiments are performed under thermal conditions, however, T may vary from 300 K to 380 K [6, 10, 11]. Due to the energetics in the drift tube, the center-of-mass collision energy is critical to understand the impact of the ion kinetic energy on an ion-molecule reaction outcome. The quantity of interest in this case is the kinetic energy relative to the center-of-mass of the colliding system.

We computed rate coefficients for Langevin model (k_{Lang}), ADO (k_{ADO}) and classical trajectory method $k_{cap}(T,\ CT)$ and listed in the Tables 6.1– 6.6. The PTRs with ions H_3O^+, NH_4^+ under PTR-MS working conditions are presented in the Tables 6.1, 6.2, 6.5 and 6.6. All the values of rate coefficients are given in the unit of 10^{-9} cm^3s^{-1}. The rate coefficients data shows that the classical trajectory method evaluates higher values as compared to the other two methods and the rate coefficients decrease with an increase in the temperature from 300 K to 380 K, except k_{Lang} which is independent of temperature. Considering the fact that the effective temperature inside the drift tube is an uncertain quantity and could be higher than 1000 K, we also computed rate coefficients corresponding to center-of-mass kinetic energy, k_{cap}(COM), as listed in the tables. It is interesting to note that the k_{cap}(COM) values follow uncertain behavior at very high temperatures. Some of the values do not show any variation with temperature (for example, 2,4,6,-tribromophenol) while others found to be slightly increasing with the temperature (for example, 3-methylsulfanylpropan-1-ol). This shows that uncertainty of effective temperature inside the PTR-MS drift tube prevails in rate coefficients also.

6.2.2 SIFT-MS Conditions

It is the electric field that differentiate PTR-MS from SIFT-MS functioning. Noted that the electric field provides substantial additional energy to the reactive collisions in PTR-MS. While no such electric field is present in SIFT-MS and therefore, ion–molecule collision energies are primarily thermal. The SIFT-MS operates normally under thermal conditions with velocity given by $v_d = (3k_BT/m_{ion})^{1/2}$ and energy KE = $\frac{3}{2}k_BT$. Most of the SIFT-MS experimental results are available at 300 K. And, the corresponding theoretical rate coefficient calculations have been performed at 300 K. However, modern SIFT-MS instruments

are capable of working at different temperature conditions which may very from 80 K to 600 K in a typical instruments [12]. Su et al. have computed the rate coefficients using classical trajectory method at various temperature ranges and reported in [13] for SIFT-MS experiments. We have obtained our results at various temperatures as listed in the Table 6.3 and 6.4 for different ions under proton transfer and charge exchange reaction schemes.

We have computed rates for proton transfer and charge transfer reactions at different temperatures in 80 K–600 K range. Under SIFT-MS temperature conditions the rate coefficients are listed in the Tables 6.3, 6.4 and 6.7. All the reported values of rate coefficients decrease with increasing temperature. Our reported SIFT-MS data at 300 K agreed quite well with the available data in the literature (see Table 6.3). The symmetric molecules such as cis-3,6-dimethyl-1,2,4,5-tetrathiane and trans-3,6-dimethyl-1,2,4,5-tetrathiane contain zero dipole moment, so their rate coefficients contribution comes from k_{Lang} only. The charge transfer reaction rates with NO^+ and O_2^+ ions exhibit the same variation with temperature as shown in Figure 6.2. A comprehensive database has been established for SIFT-MS at thermal as well as varying temperature conditions for the reaction of VOCs and various ions: H_3O^+, NH_4^+, NO^+ and O_2^+. This data will be useful in supporting rapid non-invasive quality control for cork-taint in wine.

6.3 Variation of Rate Coefficients

The most important class of bi-molecular IMRs occur in the drift tube are fast reactions which proceed unit or near unit collision efficiency. Under this condition, the best-studied reactions are exothermic PTRs for which only one reaction channel persists. In other words, almost all exothermic reactions occur in virtually every capture collision. The progress and product of ion-polar molecule reactions are dependent on various factors such as temperature, pressure, and energy. To study the degree of accuracy, probably, relative to experimental results of ion-dipole collision theories, various comparisons should be made based on the theoretical results obtained at varying experimental conditions. Here we have made correspondence with experiments as well as the factors affecting the rate coefficients of IMRs.

Table 6.1: Ion-molecule reaction rate coefficients k_{Lang}, k_{ADO}, $k_{cap}(T,\ CT)$ and k_{cap}(COM) for proton transfer between H_3O^+ and cork-taint-related compounds at $T =$ 300 and 380 K drift tube temperature, and $E/N = 123$ Td in PTR-MS apparatus. The calculated reaction rate coefficients at corresponding T_{eff} are also reported in the last column.

Molecule name (Formula)	T **(K)**	**k** k_{Lang}	k_{ADO}	$k_{cap}(T,CT)$	T_{eff} **(K)**	k_{cap}**(COM)** T	T_{eff}
2,4,6-	300	2.59	2.91	3.12	1831	2.73	2.64
Trichloroanisole	380	2.59	2.84	3.03	1911	2.71	2.63
($C_7H_5Cl_3O$)							
2,4,6-	300	2.78	3.09	3.30	1881	2.91	2.83
Tribromoanisole	380	2.78	3.02	3.22	1961	2.89	2.83
($C_7H_5Br_3O$)							
Pentachlorophenol	300	2.79	3.32	3.60	1857	3.05	2.89
(C_6Cl_5OH)	380	2.79	3.22	3.46	1937	3.03	2.88
Pentabromophenol	300	2.99	3.55	3.85	1906	3.26	3.09
(C_6Br_5OH)	380	2.99	3.45	3.71	1986	3.24	3.09
2,4,6-	300	2.48	2.87	3.08	1822	2.66	2.55
Trichlorophenol	380	2.48	2.79	2.98	1902	2.64	2.55
($C_6H_2Cl_3OH$)							
2,4,6-	300	2.65	2.98	3.20	1878	2.79	2.70
Tribromophenol	380	2.65	2.91	3.11	1958	2.78	2.70
($C_6H_2Br_3OH$)							
2,3,4-	300	2.57	4.63	5.67	1830	4.57	3.40
Trichloroanisole	380	2.57	4.32	4.93	1911	4.39	3.37
($C_7H_5Cl_3O$)							
2,3,6-	300	2.56	2.97	3.20	1831	2.75	2.63
Trichloroanisole	380	2.56	2.89	3.09	1911	2.74	2.63
($C_7H_5Cl_3O$)							
2,3,4,5-	300	2.71	4.55	5.21	1849	4.41	3.36
Tetrachloroanisole	380	2.71	4.26	4.81	1929	4.25	3.34
($C_7H_4Cl_4O$)							
2,3,4,6-	300	2.70	3.21	3.48	1849	2.95	2.80
Tetrachloroanisole	380	2.70	3.11	3.35	1929	2.93	2.79
($C_7H_4Cl_4O$)							
2,3,5,6-	300	2.69	3.08	3.30	1849	2.86	2.76
Tetrachloroanisole	380	2.69	3.00	3.20	1929	2.85	2.75
($C_7H_4Cl_4O$)							
2,4-	300	2.46	4.00	4.53	1807	3.84	2.99
Dichloroanisole	380	2.46	3.75	4.20	1887	3.72	2.97
($C_7H_6Cl_2O$)							

Table 6.1: continued

Molecule name (Formula)	T **(K)**	**k** $\mathbf{k}_{\text{Lang}}$	$\mathbf{k}_{\text{ADO}}$	$\mathbf{k}_{\text{cap}}(T, CT)$	T_{eff} **(K)**	$\mathbf{k}_{\text{cap}}$**(COM)** T	T_{eff}
2,6-	300	2.42	3.18	3.53	1807	2.89	2.59
Dichloroanisole	380	2.42	3.05	3.34	1887	2.85	2.59
($C_7H_6Cl_2O$)							
Cis-1,5-	300	2.37	3.43	3.79	1747	3.18	2.68
octadien-3-one	380	2.37	3.25	3.67	1827	3.11	2.67
($C_8H_{12}O$)							
Cis-1,5-	300	2.39	2.89	3.15	1750	2.66	2.49
octadien-3-ol	380	2.39	2.80	3.02	1830	2.64	2.49
($C_8H_{14}O$)							
1-Octene-3-ol	300	2.37	2.83	3.06	1753	2.61	2.46
($C_8H_{16}O$)	380	2.37	2.74	2.95	1833	2.59	2.46
1-Octene-3-one	300	2.33	3.69	4.18	1750	3.56	2.80
($C_8H_{14}O$)	380	2.33	3.47	3.88	1830	3.45	2.79
Octanal	300	2.33	3.46	3.85	1753	3.22	2.67
($C_8H_{16}O$)	380	2.33	3.28	3.58	1833	3.14	2.66
2-Sec-butyl-3-	300	2.56	2.84	3.05	1797	2.69	2.61
methoxypyrazine	380	2.56	2.78	2.97	1877	2.68	2.61
($C_9H_{14}N_2O$)							
3-Iso-butyl-2-	300	2.54	2.89	3.85	1797	2.70	2.60
methoxypyrazine	380	2.54	2.82	3.62	1877	2.69	2.60
($C_9H_{14}N_2O$)							
2-Iso-propyl-3-	300	2.44	2.77	2.98	1783	2.60	2.50
methoxypyrazine	380	2.44	2.70	2.90	1863	2.58	2.50
($C_8H_{12}N_2O$)							
2-Methoxy-3,5-	300	2.34	2.60	2.79	1764	2.46	2.39
dimethylpyrazine	380	2.34	2.55	2.71	1847	2.45	2.38
($C_7H_{10}N_2O$)							
2-	300	2.54	2.92	3.13	1799	2.71	2.61
Methylisoborneol	380	2.54	2.84	3.03	1879	2.70	2.60
($C_{11}H_{20}O$)							
Geosmin	300	2.64	2.94	3.16	1811	2.78	2.69
($C_{12}H_{22}O$)	380	2.64	2.88	3.07	1891	2.76	2.69
Guaiacol	300	2.21	3.57	4.04	1747	3.45	2.69
($C_7H_8O_2$)	380	2.21	3.35	3.74	1827	3.34	2.67
4-Ethylguaiacol	300	2.48	3.49	3.83	1783	3.20	2.76
($C_9H_{12}O_2$)	380	2.48	3.32	3.71	1863	3.14	2.75

Table 6.1: continued

Molecule name (Formula)	T **(K)**	**k** $\mathbf{k}_{\text{Lang}}$	$\mathbf{k}_{\text{ADO}}$	$\mathbf{k}_{\text{cap}}(T, CT)$	T_{eff} **(K)**	$\mathbf{k}_{\text{cap}}$**(COM)** T	T_{eff}
4-Ethylphenol	300	2.29	2.79	3.04	1744	2.56	2.40
($C_8H_{10}O$)	380	2.29	2.70	2.91	1824	2.54	2.39
Eucalyptol	300	2.44	2.85	3.07	1785	2.64	2.52
($C_8H_{10}O$)	380	2.44	2.77	2.97	1865	2.62	2.51
4-Ethylcatechol	300	2.34	3.16	3.55	1767	2.89	2.55
($C_8H_{10}O_2$)	380	2.34	3.02	3.34	1847	2.84	2.54
4-Methylguaiacol	300	2.36	2.68	2.87	1767	2.51	2.42
($C_8H_{10}O_2$)	380	2.36	2.61	2.79	1847	2.49	2.41
Rotundone	300	2.97	4.73	5.35	1835	4.49	3.55
($C_{15}H_{22}O$)	380	2.97	4.45	4.96	1915	4.36	3.53
Geraniol	300	2.64	3.04	3.27	1785	2.83	2.71
($C_{10}H_{18}O$)	380	2.64	2.96	3.17	1865	2.81	2.71
Hotrienol	300	2.64	3.17	3.43	1783	2.91	2.74
($C_{10}H_{16}O$)	380	2.64	3.07	3.30	1863	2.89	2.74
Linalool	300	2.59	3.15	3.43	1785	2.88	2.70
($C_{10}H_{18}O$)	380	2.59	3.05	3.29	1865	2.86	2.69
Nerol	300	2.58	3.58	3.90	1785	3.27	2.84
($C_{10}H_{18}O$)	380	2.58	3.41	3.80	1865	3.21	2.84
$\alpha-$Terpineol	300	2.53	3.04	3.30	1785	2.80	2.63
($C_{10}H_{18}O$)	380	2.53	2.95	3.17	1865	2.77	2.63
Indole	300	2.31	3.29	3.62	1735	3.04	2.59
(C_8H_7N)	380	2.31	3.12	3.51	1815	2.98	2.58
1-Methylindole	300	2.45	3.60	3.99	1757	3.35	2.79
(C_9H_9N)	380	2.45	3.41	3.72	1837	3.27	2.78
2-	300	2.40	3.01	3.29	1763	2.75	2.53
Aminoacetophenone	380	2.40	2.90	3.14	1843	2.71	2.53
(C_8H_9NO)							
2-Chloro-6-	300	2.30	2.41	2.57	1772	2.35	2.32
methylphenol	380	2.30	2.38	2.53	1852	2.35	2.32
(C_7H_7ClO)							
3-Octanone	300	2.32	3.44	3.82	1753	3.24	2.67
($C_8H_{16}O$)	380	2.32	3.26	3.55	1833	3.16	2.64

Table 6.1: continued

Molecule name (Formula)	T **(K)**	**k** $\mathbf{k}_{\text{Lang}}$	$\mathbf{k}_{\text{ADO}}$	$\mathbf{k}_{\text{cap}}(T, CT)$	T_{eff} **(K)**	$\mathbf{k}_{\text{cap}}$**(COM)** T	T_{eff}
Fenchone	300	2.41	3.73	4.18	1783	3.57	2.84
($C_{10}H_{16}O$)	380	2.41	3.52	3.88	1863	3.46	2.83
Fenchol	300	2.44	2.74	2.94	1785	2.58	2.49
($C_{10}H_{18}O$)	380	2.44	2.67	2.86	1865	2.57	2.49
Trans-2-octen-1-ol	300	2.39	3.01	3.31	1753	2.75	2.53
($C_8H_{16}O$)	380	2.39	2.90	3.15	1833	2.72	2.53
Pentachloroanisole	300	2.82	3.49	3.81	1862	3.17	2.95
($C_7H_3Cl_5O$)	380	2.82	3.37	3.64	1942	3.14	2.95

Table 6.2: All parameters are same as in Table 6.1, but for PTR between NH_4^+ and cork-taint-related compounds.

Molecule name (Formula)	T **(K)**	**k** $\mathbf{k}_{Lang}$	$\mathbf{k}_{ADO}$	$\mathbf{k}_{cap}(T, CT)$	T_{eff} **(K)**	$\mathbf{k}_{cap}$**(COM)** T	T_{eff}
2,4,6-	300	2.65	2.99	3.20	1806	2.80	2.71
Trichloroanisole	380	2.65	2.91	3.11	1886	2.79	2.71
($C_7H_5Cl_3O$)							
2,4,6-	300	2.86	3.17	3.40	1853	3.00	2.91
Tribromoanisole	380	2.86	3.10	3.31	1933	2.98	2.91
($C_7H_5Br_3O$)							
Pentachlorophenol	300	2.87	3.41	3.70	1830	3.14	2.97
(C_6Cl_5OH)	380	2.2.87	3.30	3.56	1910	3.12	2.97
Pentabromophenol	300	3.07	3.65	3.95	1876	3.35	3.18
(C_6Br_5OH)	380	3.07	3.54	3.80	1956	3.33	3.17
2,4,6-	300	2.55	2.94	3.17	1797	2.74	2.62
Trichlorophenol	380	2.55	2.86	3.07	1877	2.74	2.62
($C_6H_2Cl_3OH$)							
2,4,6-	300	2.72	3.06	3.28	1850	2.87	2.78
Tribromophenol	380	2.72	2.99	3.19	1930	2.86	2.78
($C_6H_2Br_3OH$)							
2,3,4-	300	2.64	4.74	5.83	1806	4.71	3.51
Trichloroanisole	380	2.64	4.42	5.06	1886	4.52	3.48
($C_7H_5Cl_3O$)							
2,3,6-	300	2.63	3.04	3.28	1806	2.83	2.71
Trichloroanisole	380	2.63	2.96	3.18	1886	2.81	2.70
($C_7H_5Cl_3O$)							
2,3,4,5-	300	2.77	4.66	5.32	1822	4.52	3.45
Tetrachloroanisole	380	2.77	4.37	4.92	1902	4.36	3.43
($C_7H_4Cl_4O$)							
2,3,4,6-	300	2.76	3.29	3.56	1822	3.02	2.86
Tetrachloroanisole	380	2.76	3.19	3.42	1902	3.00	2.86
($C_7H_4Cl_4O$)							
2,3,5,6-	300	2.76	3.16	3.39	1822	2.94	2.83
Tetrachloroanisole	380	2.76	3.07	3.29	1902	2.93	2.83
($C_7H_4Cl_4O$)							
2,4-	300	2.52	4.09	4.64	1783	3.95	3.07
Dichloroanisole	380	2.52	3.84	4.30	1863	3.82	3.05
($C_7H_6Cl_2O$)							
2,6-	300	2.48	3.26	3.62	1783	2.96	2.66
Dichloroanisole	380	2.48	3.13	3.42	1863	2.92	2.66
($C_7H_6Cl_2O$)							

Table 6.2: continued

Molecule name (Formula)	T **(K)**	**k** $\mathbf{k}_{\text{Lang}}$	$\mathbf{k}_{\text{ADO}}$	$\mathbf{k}_{\text{cap}}(T,\ CT)$	T_{eff} **(K)**	$\mathbf{k}_{\text{cap}}$**(COM)** T	T_{eff}
Cis-1,5-	300	2.42	3.51	3.87	1727	3.26	2.74
octadien-3-one	380	2.42	3.33	3.75	1807	3.18	2.73
($C_8H_{12}O$)							
Cis-1,5-	300	2.44	2.96	3.21	1730	2.72	2.55
octadien-3-ol	380	2.44	2.86	3.08	1810	2.70	2.54
($C_8H_{14}O$)							
1-Octene-3-ol	300	2.43	2.89	3.14	1733	2.68	2.53
($C_8H_{16}O$)	380	2.43	2.81	3.02	1813	2.65	2.52
1-Octene-3-one	300	2.38	3.78	4.27	1730	3.65	2.87
($C_8H_{14}O$)	380	2.38	3.56	3.96	1810	3.53	2.85
Octanal	300	2.39	3.54	3.86	1733	3.31	2.74
($C_8H_{16}O$)	380	2.39	3.35	3.66	1813	3.23	2.73
2-Sec-butyl-3-	300	2.62	2.91	3.12	1774	2.75	2.67
methoxypyrazine	380	2.62	2.84	3.04	1854	2.74	2.67
($C_9H_{14}N_2O$)							
3-Iso-butyl-2-	300	2.60	2.96	3.94	1761	2.77	2.66
methoxypyrazine	380	2.60	2.88	3.71	1841	2.75	2.66
($C_9H_{14}N_2O$)							
2-Iso-propyl-3-	300	2.50	2.84	3.05	1761	2.66	2.56
methoxypyrazine	380	2.50	2.77	2.96	1841	2.65	2.56
($C_8H_{12}N_2O$)							
2-Methoxy-3,5-	300	2.40	2.67	2.86	1745	2.52	2.45
dimethylpyrazine	380	2.40	2.61	2.78	1825	2.51	2.45
($C_7H_{10}N_2O$)							
2-	300	2.61	2.99	3.21	1776	2.79	2.68
Methylisoborneol	380	2.61	2.91	3.11	1856	2.77	2.68
($C_{11}H_{20}O$)							
Geosmin	300	2.70	3.01	3.23	1787	2.84	2.75
($C_{12}H_{22}O$)	380	2.70	2.95	3.14	1867	2.83	2.75
Guaiacol	300	2.27	3.65	4.15	1727	3.56	2.77
($C_7H_8O_2$)	380	2.27	3.43	3.84	1807	3.44	2.75
4-Ethylguaiacol	300	2.54	3.58	3.92	1761	3.29	2.82
($C_9H_{12}O_2$)	380	2.54	3.40	3.80	1841	3.22	2.82
4-Ethylphenol	300	2.34	2.85	3.10	1724	2.62	2.45
($C_8H_{10}O$)	380	2.34	2.76	2.97	1804	2.60	2.45

Table 6.2: continued

Molecule name (Formula)	T **(K)**	**k** $\mathbf{k}_{\text{Lang}}$	$\mathbf{k}_{\text{ADO}}$	$\mathbf{k}_{\text{cap}}(T,\ CT)$	T_{eff} **(K)**	$\mathbf{k}_{\text{cap}}$**(COM)** T	T_{eff}
Eucalyptol	300	2.50	2.92	3.15	1763	2.71	2.58
($C_8H_{10}O$)	380	2.50	2.83	3.04	1843	2.69	2.58
4-Ethylcatechol	300	2.39	3.24	3.63	1745	2.96	2.61
($C_8H_{10}O_2$)	380	2.39	3.09	3.41	1825	2.91	2.61
4-Methylguaiacol	300	2.42	2.74	2.94	1745	2.57	2.48
($C_8H_{10}O_2$)	380	2.42	2.67	2.86	1825	2.56	2.48
Rotundone	300	3.04	4.85	5.48	1809	4.62	3.64
($C_{15}H_{22}O$)	380	3.04	4.56	5.08	1889	4.48	3.62
Geraniol	300	2.70	3.11	3.34	1763	2.90	2.78
($C_{10}H_{18}O$)	380	2.70	3.03	3.24	1843	2.88	2.77
Hotrienol	300	2.71	3.24	3.52	1761	2.99	2.81
($C_{10}H_{16}O$)	380	2.71	3.14	3.39	1841	2.97	2.81
Linalool	300	2.65	3.22	3.51	1763	2.96	2.77
($C_{10}H_{18}O$)	380	2.65	3.12	3.36	1843	2.93	2.76
Nerol	300	2.64	3.67	4.00	1763	3.36	2.92
($C_{10}H_{18}O$)	380	2.64	3.49	3.89	1843	3.30	2.91
$\alpha-$Terpineol	300	2.59	3.11	3.38	1763	2.87	2.70
($C_{10}H_{18}O$)	380	2.59	3.02	3.25	1843	2.84	2.69
Indole	300	2.36	3.36	3.69	1716	3.12	2.65
(C_8H_7N)	380	2.36	3.20	3.58	1796	3.05	2.64
1-Methylindole	300	2.50	3.68	4.07	1737	3.42	2.86
(C_9H_9N)	380	2.50	3.49	3.79	1817	3.34	2.84
2-	300	2.46	3.08	3.37	1742	2.82	2.60
Aminoacetophenone	380	2.46	2.97	3.22	1822	2.79	2.59
(C_8H_9NO)							
2-Chloro-6-	300	2.35	2.47	2.62	1751	2.40	2.37
methylphenol	380	2.35	2.44	2.58	1831	2.40	2.37
(C_7H_7ClO)							
3-Octanone	300	2.38	3.52	3.92	1733	3.30	2.73
($C_8H_{16}O$)	380	2.38	3.33	3.64	1813	3.22	2.72
Fenchone	300	2.47	3.82	4.29	1761	3.62	2.91
($C_{10}H_{16}O$)	380	2.47	3.60	3.98	1841	3.52	2.90

Table 6.2: continued

Molecule name (Formula)	T **(K)**	**k** $\mathbf{k}_{\text{Lang}}$	$\mathbf{k}_{\text{ADO}}$	$\mathbf{k}_{\text{cap}}(T,\ CT)$	T_{eff} **(K)**	$\mathbf{k}_{\text{cap}}$**(COM)** T	T_{eff}
Fenchol	300	2.50	2.80	3.01	1763	2.64	2.55
($C_{10}H_{18}O$)	380	2.50	2.74	2.93	1843	2.63	2.55
Trans-2-octen-1-ol	300	2.44	3.08	3.38	1733	2.82	2.58
($C_8H_{16}O$)	380	2.44	2.97	3.22	1813	2.78	2.58
Pentachloroanisole	300	2.90	3.58	3.92	1835	3.27	3.04
($C_7H_3Cl_5O$)	380	2.90	3.46	3.75	1915	3.24	3.04

Table 6.3: Ion-molecule reaction rate coefficients k_{ADO}, $k_{cap}(T)$ for PTR between H_3O^+ and NH_4^+ to organic compounds (cork-taint) at 80 K, 300 K and 600 K in SIFT-MS apparatus. Thermal drift tube velocity (634 m/s) and He as carrier gas is considered for the calculation of the rate coefficients.

Molecule name (Formula)	T **(K)**	$\mathbf{H_3O^+}$		$\mathbf{NH_4^+}$	
		$\mathbf{k}_{ADO}$	$\mathbf{k}_{cap}(T)$	$\mathbf{k}_{ADO}$	$\mathbf{k}_{cap}(T)$
2,4,6-	80	3.57	4.33	3.66	4.44
Trichloroanisole	300	2.91	3.43	2.99	3.53
($C_7H_5Cl_3O$)	600	2.75	2.97	2.82	3.05
2,4,6-	80	3.73	4.51	3.82	4.64
Tribromoanisole	300	3.09	3.59	3.17	3.70
($C_7H_5Br_3O$)	600	2.93	3.13	3.00	3.22
Pentachlorophenol	80	4.28	5.28	4.39	5.43
(C_6Cl_5OH)	300	3.32	3.93	3.41	4.04
	600	3.07	3.49	3.15	3.59
Pentabromophenol	80	4.58	5.65	4.70	5.80
(C_6Br_5OH)	300	3.55	4.21	3.65	4.32
	600	3.29	3.73	3.38	3.83
2,4,6-	80	3.60	4.38	3.69	4.51
Trichlorophenol	300	2.87	3.38	2.94	3.48
($C_6H_2Cl_3OH$)	600	2.68	2.95	2.75	3.04
2,4,6-	80	3.65	4.43	3.75	4.55
Tribromophenol	300	2.98	3.52	3.06	3.61
($C_6H_2Br_3OH$)	600	2.82	3.04	2.89	3.12
2,3,4-	80	7.23	9.90	7.41	10.17
Trichloroanisole	300	4.63	5.82	4.74	5.97
($C_7H_5Cl_3O$)	600	3.82	4.61	3.91	4.73
2,3,6-	80	3.74	4.57	3.83	4.70
Trichloroanisole	300	2.97	3.51	3.04	3.60
($C_7H_5Cl_3O$)	600	2.77	3.07	2.84	3.15
2,3,4,5-	80	6.96	9.49	7.14	9.70
Tetrachloroanisole	300	4.55	5.63	4.66	5.76
($C_7H_4Cl_4O$)	600	3.83	4.56	3.93	4.66
2,3,4,6-	80	4.14	5.11	4.24	5.23
Tetrachloroanisole	300	3.21	3.80	3.29	3.89
($C_7H_4Cl_4O$)	600	2.97	3.38	3.04	3.45

Table 6.3: continued

Molecule name (Formula)	T **(K)**	$\mathbf{H_3O^+}$ $\mathbf{k}_{\mathrm{ADO}}$	$\mathbf{k}_{\mathrm{cap}}(T)$	$\mathbf{NH_4^+}$ $\mathbf{k}_{\mathrm{ADO}}$	$\mathbf{k}_{\mathrm{cap}}(T)$
2,3,5,6-	80	3.83	4.66	3.93	4.78
Tetrachloroanisole	300	3.08	3.62	3.16	3.73
($C_7H_4Cl_4O$)	600	2.89	3.16	2.96	3.24
2,4-	80	6.06	8.19	6.21	8.39
Dichloroanisole	300	4.00	4.90	4.09	5.02
($C_7H_6Cl_2O$)	600	3.40	4.02	3.48	4.11
2,6-	80	4.39	5.62	4.50	5.76
Dichloroanisole	300	3.18	3.78	3.26	3.87
($C_7H_6Cl_2O$)	600	2.86	3.35	2.93	3.44
Cis-1,5-	80	4.97	6.57	5.09	6.71
octadien-3-one	300	3.43	4.12	3.51	4.21
($C_8H_{12}O$)	600	3.00	3.53	3.07	3.60
Cis-1,5-	80	3.78	4.70	3.87	4.80
octadien-3-ol	300	2.89	3.43	2.96	3.50
($C_8H_{14}O$)	600	2.66	3.08	2.72	3.14
1-Octene-3-ol	80	3.65	4.51	3.74	4.62
($C_8H_{16}O$)	300	2.83	3.34	2.89	3.43
	600	2.61	2.97	2.68	3.05
1-Octene-3-one	80	5.57	7.50	5.70	7.66
($C_8H_{14}O$)	300	3.69	4.52	3.78	4.62
	600	3.16	3.73	3.24	3.81
Octanal	80	5.08	6.76	5.20	6.90
($C_8H_{16}O$)	300	3.46	4.18	3.54	4.27
	600	3.02	3.55	3.09	3.62
2-Sec-butyl-3-	80	3.43	4.17	3.52	4.27
methoxypyrazine	300	2.84	3.33	2.91	3.41
($C_9H_{14}N_2O$)	600	2.69	2.90	2.76	2.96
3-Iso-butyl-2-	80	3.58	4.36	3.67	4.46
methoxypyrazine	300	2.89	3.42	2.96	3.50
($C_9H_{14}N_2O$)	600	2.71	2.96	2.78	3.03
2-Iso-propyl-3-	80	3.43	4.18	3.51	4.28
methoxypyrazine	300	2.77	3.28	2.84	3.36
($C_8H_{12}N_2O$)	600	2.60	2.84	2.67	2.91

Table 6.3: continued

Molecule name (Formula)	T **(K)**	$\mathbf{H_3O^+}$ $\mathbf{k}_{\mathrm{ADO}}$	$\mathbf{k}_{\mathrm{cap}}(T)$	$\mathbf{NH_4^+}$ $\mathbf{k}_{\mathrm{ADO}}$	$\mathbf{k}_{\mathrm{cap}}(T)$
2-Methoxy-3,5-dimethylpyrazine ($C_7H_{10}N_2O$)	80	3.15	3.81	3.23	3.91
	300	2.60	3.04	2.67	3.12
	600	2.47	2.65	2.53	2.71
2-Methylisoborneol ($C_{11}H_{20}O$)	80	3.63	4.42	3.72	4.54
	300	2.92	3.44	2.99	3.53
	600	2.73	2.99	2.80	3.07
Geosmin ($C_{12}H_{22}O$)	80	3.57	4.34	3.66	4.43
	300	2.94	3.46	3.01	3.53
	600	2.79	3.00	2.85	3.07
Guaiacol ($C_7H_8O_2$)	80	5.40	7.28	5.53	7.47
	300	3.57	4.37	3.65	4.49
	600	3.04	3.58	3.11	3.68
4-Ethylguaiacol ($C_9H_{12}O_2$)	80	5.01	6.56	5.13	6.72
	300	3.49	4.18	3.58	4.28
	600	3.08	3.62	3.15	3.70
4-Ethylphenol ($C_8H_{10}O$)	80	3.66	4.56	3.75	4.66
	300	2.79	3.30	2.85	3.38
	600	2.56	2.98	2.62	3.05
Eucalyptol ($C_8H_{10}O$)	80	3.61	4.42	3.69	4.53
	300	2.85[1]	3.37	2.92	3.45
	600	2.65	2.95	2.72	3.03
4-Ethylcatechol ($C_8H_{10}O_2$)	80	4.44	5.75	4.54	5.87
	300	3.16	3.77	3.24	3.86
	600	2.82	3.31	2.88	3.38
4-Methylguaiacol ($C_8H_{10}O_2$)	80	3.30	4.00	3.38	4.11
	300	2.68	3.16	2.74	3.24
	600	2.52	2.73	2.58	2.80
Rotundone ($C_{15}H_{22}O$)	80	7.15	9.61	7.32	9.84
	300	4.73	5.79	4.85	5.92
	600	4.05	4.77	4.15	4.88
Geraniol ($C_{10}H_{18}O$)	80	3.81	4.64	3.90	4.75
	300	3.04	3.59	3.11	3.67
	600	2.84	3.13	2.91	3.20

[1] 3.10: G. Amadei, B. M. Ross, 2011.

Table 6.3: continued

Molecule name (Formula)	T **(K)**	H_3O^+ k_{ADO}	H_3O^+ $k_{cap}(T)$	NH_4^+ k_{ADO}	NH_4^+ $k_{cap}(T)$
Hotrienol	80	4.11	5.10	4.21	5.21
($C_{10}H_{16}O$)	300	3.17	3.75	3.24	3.85
	600	2.92	3.35	3.00	3.43
Linalool	80	4.13	5.15	4.23	5.27
($C_{10}H_{18}O$)	300	3.15[2]	3.73	3.22	3.82
	600	2.89	3.36	2.96	3.44
Nerol	80	5.10	6.65	5.22	6.81
($C_{10}H_{18}O$)	300	3.58	4.28	3.67	4.38
	600	3.17	3.72	3.24	3.81
$\alpha-$Terpineol	80	3.95	4.90	4.05	5.02
($C_{10}H_{18}O$)	300	3.04	3.60	3.11	3.69
	600	2.80	3.22	2.87	3.30
Indole	80	4.74	6.23	4.85	6.37
(C_8H_7N)	300	3.29[3]	3.94	3.36	4.03
	600	2.89	3.40	2.95	3.47
1-Methylindole	80	5.25	6.97	5.38	7.11
(C_9H_9N)	300	3.60	4.33	3.68	4.42
	600	3.14	3.69	3.21	3.76
2-	80	4.03	5.06	4.12	5.19
Aminoacetophenone	300	3.01	3.56	3.08	3.65
(C_8H_9NO)	600	2.74	3.21	2.81	3.29
2-Chloro-6-	80	2.70	3.28	2.76	3.35
methylphenol	300	2.41	2.60	2.47	2.66
(C_7H_7ClO)	600	2.34	2.43	2.40	2.48
3-Octanone	80	5.05	6.68	5.16	6.86
($C_8H_{16}O$)	300	3.44	4.14	3.52	4.25
	600	3.00	3.51	3.07	3.60
Fenchone	300	5.57	7.44	5.71	7.63
($C_{10}H_{16}O$)	300	3.73	4.53	3.82	4.64
	600	3.21	3.78	3.29	3.87

[2] 3.20: G. Amadei, B. M. Ross, 2011.

[3] 3.30: B. M. Ross, Volatile bio-markers: non-invasive diagnosis in physiology and medicine, 2013.

Table 6.3: continued

Molecule name (Formula)	T **(K)**	$\mathbf{H_3O^+}$ $\mathbf{k}_{\mathrm{ADO}}$	$\mathbf{k}_{\mathrm{cap}}(T)$	$\mathbf{NH_4^+}$ $\mathbf{k}_{\mathrm{ADO}}$	$\mathbf{k}_{\mathrm{cap}}(T)$
Fenchol	80	3.34	4.06	3.42	4.16
($C_{10}H_{18}O$)	300	2.74	3.23	2.80	3.31
	600	2.59	2.79	2.65	2.86
Trans-2-octen-1-ol	80	4.05	5.12	4.14	5.22
($C_8H_{16}O$)	300	3.01	3.57	3.08	3.65
	600	2.74	3.22	2.80	3.28
Pentachloroanisole	80	4.64	5.80	4.76	5.97
($C_7H_3Cl_5O$)	300	3.49	4.13	3.58	4.25
	600	3.19	3.74	3.27	3.85

Table 6.4: Charge transfer reaction rate coefficients (in units of 10^{-9} cm^3s^{-1}) between reagent ions (NO^+ and O_2^+) and cork-taint molecules as computed from Langevin model (k_{Lang}), ADO theory (k_{ADO}) and classical trajectory method (k_{cap}) at different range of temperature 80–600 K.

Molecule name	*T*	$\mathbf{k_{Lang}}$		$\mathbf{k_{ADO}}$		$\mathbf{k_{cap}}$	
	(K)	$\mathbf{NO^+}$	$\mathbf{O_2^+}$	$\mathbf{NO^+}$	$\mathbf{O_2^+}$	$\mathbf{NO^+}$	$\mathbf{O_2^+}$
2,4,6-	80	1.95	1.90	2.95	2.87	3.35	3.27
Trichloroanisole	150			2.60	2.52	2.89	2.81
($C_7H_5Cl_3O$)	300			2.30	2.24	2.49	2.43
	450			2.19	2.13	2.35	2.29
	600			2.14	2.08	2.27	2.21
2,4,6-	80	2.09	2.03	2.99	2.91	3.35	3.25
Tribromoanisole	150			2.66	2.59	2.93	2.84
($C_7H_5Br_3O$)	300			2.40	2.33	2.58	2.50
	450			2.30	2.23	2.45	2.38
	600			2.25	2.18	2.38	2.31
Pentachlorophenol	80	2.03	1.97	3.20	3.11	3.66	3.56
(C_6Cl_5OH)	150			2.79	2.71	3.13	3.04
	300			2.45	2.38	2.66	2.58
	450			2.32	2.25	2.49	2.42
	600			2.25	2.19	2.40	2.33
Pentabromophenol	80	2.24	2.18	3.09	3.00	3.43	3.34
(C_6Br_5OH)	150			2.78	2.69	3.03	2.95
	300			2.52	2.45	2.70	2.63
	450			2.43	2.36	2.58	2.51
	600			2.38	2.31	2.52	2.45
2,4,6-	80	1.86	1.81	2.80	2.71	3.17	3.09
Trichlorophenol	150			2.46	2.39	2.74	2.66
($C_6H_2Cl_3OH$)	300			2.19	2.13	2.36	2.30
	450			2.08	2.03	2.23	2.17
	600			2.03	1.98	2.16	2.10
2,4,6-	80	2.00	1.95	2.80	2.72	3.11	3.03
Tribromophenol	150			2.51	2.43	2.74	2.67
($C_6H_2Br_3OH$)	300			2.27	2.21	2.43	2.37
	450			2.18	2.12	2.32	2.26
	600			2.14	2.08	2.26	2.20
2,3,4-	80	1.95	1.90	5.89	5.73	8.43	8.21
Trichloroanisole	150			4.70	4.57	6.32	6.16
($C_7H_5Cl_3O$)	300			3.72	3.62	4.65	4.53
	450			3.29	3.20	3.75	3.66
	600			3.03	2.94	3.41	3.37

Table 6.4: continued

Molecule name	T (K)	k_{Lang} NO^+	k_{Lang} O_2^+	k_{ADO} NO^+	k_{ADO} O_2^+	k_{cap} NO^+	k_{cap} O_2^+
2,3,6-	80	1.94	1.90	3.28	3.19	3.99	3.88
Trichloroanisole	150			2.82	2.74	3.11	3.03
($C_7H_5Cl_3O$)	300			2.44	2.37	2.68	2.61
	450			2.30	2.23	2.47	2.41
	600			2.22	2.16	2.37	2.31
2,3,4,5-	80	2.04	1.98	5.22	5.07	7.22	7.01
Tetrachloroanisole	150			4.23	4.11	5.45	5.29
($C_7H_4Cl_4O$)	300			3.41	3.32	3.89	3.77
	450			3.06	2.98	3.41	3.31
	600			2.88	2.80	3.12	3.03
2,3,4,6-	80	2.03	1.98	3.42	3.33	3.97	3.87
Tetrachloroanisole	150			2.94	2.86	3.24	3.16
($C_7H_4Cl_4O$)	300			2.55	2.48	2.79	2.72
	450			2.40	2.33	2.58	2.52
	600			2.32	2.26	2.47	2.41
2,3,5,6-	80	2.03	1.98	3.03	2.95	3.44	3.35
Tetrachloroanisole	150			2.68	2.60	2.97	2.90
($C_7H_4Cl_4O$)	300			2.38	2.32	2.57	2.51
	450			2.27	2.21	2.43	2.37
	600			2.22	2.15	2.35	2.29
2,4-	80	1.87	1.82	4.81	4.68	6.66	6.49
Dichloroanisole	150			3.90	3.80	5.03	4.89
($C_7H_6Cl_2O$)	300			3.14	3.06	3.58	3.49
	450			2.82	2.75	3.14	3.05
	600			2.65	2.58	2.87	2.80
2,6-	80	1.86	1.81	3.38	3.29	4.25	4.14
Dichloroanisole	150			2.87	2.79	3.22	3.13
($C_7H_6Cl_2O$)	300			2.45	2.38	2.72	2.65
	450			2.28	2.22	2.48	2.42
	600			2.19	2.14	2.36	2.29
Cis-1,5-	80	1.85	1.80	4.50	4.39	6.15	5.99
octadien-3-one	150			3.67	3.57	4.65	4.53
($C_8H_{12}O$)	300			2.98	2.90	3.37	3.28
	450			2.69	2.62	2.96	2.88
	600			2.54	2.48	2.83	2.75

Table 6.4: continued

Molecule name	T (K)	k_{Lang} NO^+	k_{Lang} O_2^+	k_{ADO} NO^+	k_{ADO} O_2^+	k_{cap} NO^+	k_{cap} O_2^+
Cis-1,5-	80	1.88	1.83	3.40	3.32	4.29	4.17
octadien-3-ol	150			2.89	2.82	3.25	3.16
($C_8H_{14}O$)	300			2.46	2.40	2.75	2.68
	450			2.30	2.24	2.51	2.44
	600			2.21	2.16	2.38	2.32
1-Octene-3-ol	80	1.86	1.81	2.81	2.74	3.20	3.12
($C_8H_{16}O$)	150			2.47	2.41	2.76	2.68
	300			2.19	2.14	2.38	2.31
	450			2.09	2.03	2.24	2.18
	600			2.03	1.98	2.17	2.11
1-Octene-3-one	80	1.82	1.77	4.62	4.50	6.40	6.23
($C_8H_{14}O$)	150			3.75	3.65	4.83	4.70
	300			3.03	2.95	3.45	3.36
	450			2.72	2.65	3.03	2.94
	600			2.56	2.49	2.77	2.70
Octanal	80	1.82	1.78	4.81	4.68	6.69	6.54
($C_8H_{16}O$)	150			3.89	3.79	5.04	4.93
	300			3.12	3.04	3.57	3.49
	450			2.79	2.72	3.12	3.05
	600			2.62	2.55	2.85	2.79
2-Sec-butyl-3-	80	1.99	1.93	2.77	2.69	3.08	2.99
methoxypyrazine	150			2.48	2.41	2.72	2.64
($C_9H_{14}N_2O$)	300			2.25	2.19	2.42	2.34
	450			2.16	2.10	2.30	2.24
	600			2.12	2.06	2.25	2.18
3-Iso-butyl-2-	80	1.99	1.93	2.85	2.78	3.20	3.10
methoxypyrazine	150			2.54	2.47	2.79	2.71
($C_9H_{14}N_2O$)	300			2.28	2.22	2.46	2.38
	450			2.18	2.13	2.33	2.26
	600			2.14	2.08	2.27	2.20
2-Iso-propyl-3-	80	1.91	1.86	2.77	2.69	3.12	3.04
methoxypyrazine	150			2.46	2.39	2.71	2.64
($C_8H_{12}N_2O$)	300			2.20	2.15	2.37	2.31
	450			2.11	2.05	2.25	2.19
	600			2.06	2.01	2.19	2.13

Table 6.4: continued

Molecule name	T (K)	k_{Lang} NO^+	k_{Lang} O_2^+	k_{ADO} NO^+	k_{ADO} O_2^+	k_{cap} NO^+	k_{cap} O_2^+
2-Methoxy-3,5-dimethylpyrazine ($C_7H_{10}N_2O$)	80	1.83	1.78	2.47	2.40	2.84	2.76
	150			2.23	2.17	2.44	2.37
	300			2.03	1.98	2.19	2.13
	450			1.96	1.91	2.09	2.04
	600			1.93	1.88	2.04	1.99
2-Methylisoborneol ($C_{11}H_{20}O$)	80	2.00	1.95	2.97	2.89	3.36	3.28
	150			2.62	2.55	2.91	2.84
	300			2.34	2.28	2.52	2.46
	450			2.23	2.17	2.38	2.33
	600			2.18	2.12	2.31	2.25
Geosmin ($C_{12}H_{22}O$)	80	2.07	2.02	2.92	2.84	3.26	3.18
	150			2.61	2.54	2.86	2.79
	300			2.36	2.29	2.53	2.47
	450			2.26	2.20	2.41	2.35
	600			2.21	2.15	2.35	2.29
Guaiacol ($C_7H_8O_2$)	80	1.73	1.69	4.26	4.15	5.84	5.71
	150			3.47	3.38	4.42	4.31
	300			2.81	2.74	3.19	3.11
	450			2.53	2.47	2.80	2.73
	600			2.39	2.33	2.67	2.61
4-Ethylguaiacol ($C_9H_{12}O_2$)	80	1.93	1.88	2.60	2.53	2.97	2.90
	150			2.35	2.29	2.56	2.49
	300			2.15	2.09	2.30	2.24
	450			2.07	2.02	2.20	2.15
	600			2.04	1.98	2.15	2.10
4-Ethylphenol ($C_8H_{10}O$)	80	1.81	1.76	2.79	2.72	3.19	3.11
	150			2.45	2.38	2.74	2.66
	300			2.16	2.10	2.34	2.28
	450			2.05	2.00	2.20	2.14
	600			2.00	1.95	2.12	2.07
Eucalyptol ($C_8H_{10}O$)	80	1.92	1.87	2.94	2.87	3.36	3.27
	150			2.58	2.51	2.88	2.81
	300			2.28	2.22	2.47	2.41
	450			2.17	2.11	2.32	2.26
	600			2.11	2.06	2.25	2.19

Table 6.4: continued

Molecule name	T (K)	k_{Lang} NO^+	k_{Lang} O_2^+	k_{ADO} NO^+	k_{ADO} O_2^+	k_{cap} NO^+	k_{cap} O_2^+
4-Ethylcatechol	80	1.83	1.78	3.76	3.66	4.93	4.79
($C_8H_{10}O_2$)	150			3.12	3.05	3.75	3.65
	300			2.61	2.54	2.87	2.79
	450			2.40	2.34	2.66	2.59
	600			2.29	2.24	2.49	2.42
4-Methylguaiacol	80	1.84	1.79	2.56	2.49	2.85	2.77
($C_8H_{10}O_2$)	150			2.29	2.23	2.51	2.44
	300			2.08	2.03	2.23	2.17
	450			2.00	1.95	2.13	2.07
	600			1.96	1.91	2.08	2.02
Rotundone	80	2.32	2.26	5.66	5.51	7.74	7.54
($C_{15}H_{22}O$)	150			4.61	4.48	5.85	5.70
	300			3.74	3.64	4.23	4.12
	450			3.38	3.28	3.72	3.62
	600			3.19	3.10	3.55	3.46
Geraniol	80	2.05	2.00	3.96	3.86	5.08	4.95
($C_{10}H_{18}O$)	150			3.33	3.24	3.77	3.68
	300			2.81	2.73	3.16	3.08
	450			2.61	2.54	2.85	2.78
	600			2.49	2.43	2.68	2.62
Hotrienol	80	2.08	2.02	3.25	3.16	3.73	3.62
($C_{10}H_{16}O$)	150			2.84	2.76	3.19	3.10
	300			2.50	2.43	2.72	2.64
	450			2.37	2.31	2.54	2.47
	600			2.30	2.24	2.45	2.38
Linalool	80	2.03	1.97	3.40	3.32	3.96	3.84
($C_{10}H_{18}O$)	150			2.93	2.85	3.23	3.14
	300			2.54	2.47	2.79	2.71
	450			2.39	2.33	2.58	2.51
	600			2.31	2.25	2.47	2.40
Nerol	80	2.01	1.96	4.14	4.03	5.41	5.28
($C_{10}H_{18}O$)	150			3.44	3.35	4.13	4.02
	300			2.87	2.79	3.15	3.07
	450			2.64	2.57	2.92	2.85
	600			2.52	2.46	2.73	2.66

Table 6.4: continued

Molecule name	T (K)	k_{Lang} NO^+	k_{Lang} O_2^+	k_{ADO} NO^+	k_{ADO} O_2^+	k_{cap} NO^+	k_{cap} O_2^+
$\alpha-$Terpineol	80	1.98	1.92	3.10	3.02	3.55	3.45
($C_{10}H_{18}O$)	150			2.71	2.63	3.04	2.95
	300			2.38	2.32	2.59	2.51
	450			2.26	2.20	2.42	2.35
	600			2.19	2.14	2.34	2.27
Indole	80	1.83	1.79	3.57	3.48	4.58	4.48
(C_8H_7N)	150			3.00	2.92	3.39	3.32
	300			2.52	2.46	2.84	2.78
	450			2.34	2.28	2.55	2.50
	600			2.24	2.18	2.41	2.35
1-Methylindole	80	1.93	1.88	3.96	3.86	5.16	5.02
(C_9H_9N)	150			3.30	3.21	3.76	3.66
	300			2.75	2.68	3.01	2.93
	450			2.54	2.47	2.79	2.72
	600			2.42	2.36	2.61	2.55
2-	80	1.89	1.84	3.37	3.28	4.19	4.08
Aminoacetophenone	150			2.87	2.79	3.20	3.11
(C_8H_9NO)	300			2.45	2.39	2.72	2.64
	450			2.30	2.24	2.49	2.42
	600			2.21	2.15	2.37	2.30
2-Chloro-6-	80	1.78	1.73	2.19	2.13	2.46	2.39
methylphenol	150			2.03	1.98	2.20	2.13
(C_7H_7ClO)	300			1.90	1.85	2.03	1.97
	450			1.85	1.80	1.97	1.91
	600			1.83	1.78	1.93	1.88
3-Octanone	80	1.81	1.76	4.18	4.07	5.62	5.46
($C_8H_{16}O$)	150			3.42	3.33	4.26	4.14
	300			2.80	2.72	3.13	3.05
	450			2.54	2.47	2.77	2.69
	600			2.41	2.35	2.65	2.58
Fenchone	80	1.90	1.85	4.57	4.45	6.22	6.05
($C_{10}H_{16}O$)	150			3.72	3.62	4.70	4.58
	300			3.03	2.95	3.42	3.33
	450			2.74	2.66	3.01	2.93
	600			2.59	2.52	2.87	2.80

Table 6.4: continued

Molecule name	*T* **(K)**	$\mathbf{k}_{\mathrm{Lang}}$ $\mathbf{NO}^+$	$\mathbf{O}_2^+$	$\mathbf{k}_{\mathrm{ADO}}$ $\mathbf{NO}^+$	$\mathbf{O}_2^+$	$\mathbf{k}_{\mathrm{cap}}$ $\mathbf{NO}^+$	$\mathbf{O}_2^+$
Fenchol	80	1.92	1.87	2.86	2.78	3.23	3.14
($C_{10}H_{18}O$)	150			2.52	2.46	2.79	2.72
	300			2.25	2.19	2.42	2.36
	450			2.15	2.09	2.29	2.23
	600			2.09	2.04	2.22	2.16
Trans-2-octen-1-ol	80	1.87	1.82	3.13	3.05	3.63	3.54
($C_8H_{16}O$)	150			2.69	2.62	2.97	2.89
	300			2.34	2.28	2.56	2.49
	450			2.20	2.14	2.37	2.31
	600			2.13	2.07	2.27	2.21
Pentachloroanisole	80	2.11	2.05	3.58	3.48	4.35	4.23
($C_7H_3Cl_5O$)	150			3.08	2.99	3.39	3.29
	300			2.66	2.58	2.92	2.83
	450			2.50	2.43	2.70	2.62
	600			2.42	2.35	2.58	2.51

Table 6.5: Reaction rate coefficients (k_{Lang},k_{ADO}, $k_{cap}(T, CT)$ and k_{cap}(COM)) for proton transfer between H_3O^+ and cork-taint compounds related to sulfur at 300, 380 and T_{eff} drift tube temperature, and E/N = 120 Td in PTR-MS apparatus.

Molecule name (Formula)	T **(K)**	**k** k_{Lang}	**k** k_{ADO}	T_{eff} **(K)**	k_{cap}**(COM)** T	k_{cap}**(COM)** T_{eff}
Hydrogen Sulfide	300	1.29	1.70	1316	1.65	1.56
(H_2S)	380	1.29	1.63	1396	1.61	1.54
Methanethiol	300	1.49	2.21	1435	2.18	1.98
(CH_4S)	380	1.49	2.09	1515	2.12	1.97
Ethanethiol	300	1.67	2.39	1512	2.29	2.12
(C_2H_6S)	380	1.67	2.27	1592	2.23	2.09
Dimethyl Sulfide	300	1.67	2.34	1512	2.22	2.07
(C_2H_6S)	380	1.67	2.23	1592	2.17	2.04
Diethyl Sulfide	300	1.98	2.57	1608	2.37	2.26
($C_4H_{10}S$)	380	1.98	2.47	1688	2.34	2.25
Dimethyl Disulfide	300	1.93	2.76	1618	2.61	2.41
($C_2H_6S_2$)	380	1.93	2.62	1698	2.54	2.39
Diethyl Disulfide	300	2.20	3.03	1670	2.79	2.62
($C_4H_{10}S_2$)	380	2.20	2.89	1750	2.74	2.60
Methyl Thioacetate	300	1.83	2.28	1608	2.11	2.03
(C_3H_6OS)	380	1.83	2.20	1688	2.09	2.02
3-Mercaptohexan-1-ol	300	2.24	2.78	1687	2.55	2.46
($C_6H_{14}OS$)	380	2.24	2.68	1767	2.52	2.45
4-Mercapto-4-	300	2.20	3.09	1684	2.86	2.67
methylpentan-2-one	380	2.20	2.95	1764	2.80	2.64
($C_6H_{12}OS$)						
4-Mercapto-4-	300	2.24	3.28	1687	3.08	2.83
methylpentan-2-ol	380	2.24	3.11	1767	3.00	2.80
($C_6H_{14}OS$)						
Benzothiazole	300	2.28	2.63	1688	2.46	2.41
(C_7H_5NS)	380	2.28	2.56	1768	2.44	2.40
2-Furanmethanethiol	300	2.07	2.80	1657	2.59	2.44
(C_5H_6OS)	380	2.07	2.67	1737	2.54	2.42
2-Mercaptoethanol	300	1.70	2.94	1574	2.30	2.12
(C_2H_6OS)	380	1.70	2.74	1654	2.29	2.14
Benzenemethanethiol	300	2.28	2.70	1673	2.51	2.44
(C_7H_8S)	380	2.28	2.62	1753	2.49	2.43
2-Mercaptoethyl acetate	300	1.99	2.66	1667	2.46	2.32
($C_4H_8O_2S$)	380	1.99	2.55	1747	2.42	2.30
3-mercaptopropyl acetate	300	2.14	2.65	1687	2.44	2.35
($C_5H_{10}O_2S$)	380	2.14	2.56	1767	2.42	2.34

Table 6.5: continued

Molecule name (Formula)	T **(K)**	**k** $\mathbf{k}_{\text{Lang}}$	$\mathbf{k}_{\text{ADO}}$	T_{eff} **(K)**	$\mathbf{k}_{\text{cap}}$**(COM)** T	T_{eff}
Cis-3,6-dimethyl-	300	2.50	2.50	1735	2.50	2.50
1,2,4,5-tetrathiane	380	2.50	2.50	1815	2.50	2.50
($C_4H_8S_4$)						
Prenyl-mercaptan	300	2.13	2.76	1635	2.55	2.43
($C_5H_{10}S$)	380	2.13	2.65	1715	2.51	2.41
Trans-3,6-dimethyl-	300	2.45	2.45	1735	2.45	2.45
1,2,4,5-tetrathiane	380	2.45	2.45	1815	2.45	2.45
($C_4H_8S_4$)						
2-Methyl-3-furanthiol	300	2.04	2.21	1657	2.12	2.10
(C_5H_6OS)	380	2.04	2.17	1737	2.12	2.10
2-Methylthiolane-3-ol	300	2.05	2.90	1664	2.69	2.50
($C_5H_{10}OS$)	380	2.05	2.76	1744	2.63	2.48
3-Mercapto-3-	300	2.12	2.77	1667	2.55	2.43
methylbutan-1-ol	380	2.12	2.66	1747	2.52	2.41
($C_5H_{12}OS$)						
Ethyl-3-	300	2.13	3.35	1687	3.06	2.79
mercaptopropionate	380	2.13	3.15	1767	3.04	2.80
($C_5H_{10}O_2S$)						
5-2-hydroxyethyl-	300	2.22	3.43	1698	3.22	2.93
4-methylthiazole	380	2.22	3.23	1778	3.17	2.92
(C_6H_9NOS)						
2-Methyltetrahydro	300	2.01	2.62	1661	2.41	2.29
thiophen-3-one	380	2.01	2.52	1744	2.37	2.28
(C_5H_8OS)						
3-Methylsulfanyl	300	2.01	3.49	1643	2.74	2.52
propan-1-ol	380	2.01	3.26	1723	2.73	2.54
($C_4H_{10}OS$)						
3-Mercaptohexylacatate	300	2.47	2.85	1729	2.66	2.60
($C_8H_{16}O_2S$)	380	2.47	2.78	1809	2.64	2.59
Ethylthioacetate	300	1.98	2.42	1639	2.24	2.17
(C_4H_8OS)	380	1.98	2.35	1719	2.22	2.16

Table 6.6: All the parameters are same as in Table 6.5 except the reagent ion in this case is NH_4^+.

Molecule name (Formula)	T **(K)**	**k** $\mathbf{k}_{Lang}$	**k** $\mathbf{k}_{ADO}$	T_{eff} **(K)**	$\mathbf{k}_{cap}$**(COM)** T	$\mathbf{k}_{cap}$**(COM)** T_{eff}
Hydrogen Sulfide (H_2S)	300	1.31	1.73	1314	1.67	1.58
	380	1.31	1.66	1394	1.64	1.56
Methanethiol (CH_4S)	300	1.52	2.25	1428	2.23	2.02
	380	1.52	2.13	1508	2.16	2.01
Ethanethiol (C_2H_6S)	300	1.70	2.44	1502	2.34	2.16
	380	1.70	2.32	1582	2.28	2.13
Dimethyl Sulfide (C_2H_6S)	300	1.70	2.39	1502	2.26	2.11
	380	1.70	2.27	1582	2.21	2.08
Diethyl Sulfide ($C_4H_{10}S$)	300	2.03	2.63	1593	2.44	2.32
	380	2.03	2.53	1673	2.40	2.31
Dimethyl Disulfide ($C_2H_6S_2$)	300	1.97	2.83	1602	2.67	2.47
	380	1.97	2.69	1682	2.60	2.44
Diethyl Disulfide ($C_4H_{10}S_2$)	300	2.25	3.10	1652	2.86	2.69
	380	2.25	2.96	1732	2.81	2.66
Methyl Thioacetate (C_3H_6OS)	300	1.87	2.33	1592	2.16	2.08
	380	1.87	2.25	1672	2.13	2.07
3-Mercaptohexan-1-ol ($C_6H_{14}OS$)	300	2.30	2.85	1667	2.62	2.53
	380	2.30	2.75	1747	2.59	2.52
4-Mercapto-4-methylpentan-2-one ($C_6H_{12}OS$)	300	2.26	3.17	1665	2.95	2.75
	380	2.26	3.02	1745	2.88	2.72
4-Mercapto-4-methylpentan-2-ol ($C_6H_{14}OS$)	300	2.29	3.36	1667	3.16	2.90
	380	2.29	3.18	1747	3.08	2.87
Benzothiazole (C_7H_5NS)	300	2.33	2.70	1668	2.51	2.46
	380	2.33	2.62	1748	2.50	2.45
2-Furanmethanethiol (C_5H_6OS)	300	2.12	2.87	1639	2.65	2.50
	380	2.12	2.74	1719	2.61	2.48
2-Mercaptoethanol (C_2H_6OS)	300	1.74	3.00	1560	2.35	2.17
	380	1.74	2.81	1640	2.34	2.19
Benzenemethanthiol (C_2H_6OS)	300	2.33	2.77	1654	2.54	2.50
	380	2.33	2.69	1734	2.49	2.44
2-Mercaptoethyl acetate ($C_4H_8O_2S$)	300	2.03	2.73	1649	2.51	2.37
	380	2.03	2.61	1729	2.47	2.35
3-mercaptopropyl acetate ($C_5H_{10}O_2S$)	300	2.19	2.71	1667	2.50	2.41
	380	2.19	2.62	1747	2.47	2.40

Table 6.6: continued

Molecule name (Formula)	T **(K)**	**k** $\mathbf{k}_{\text{Lang}}$	$\mathbf{k}_{\text{ADO}}$	T_{eff} **(K)**	$\mathbf{k}_{\text{cap}}$**(COM)** T	T_{eff}
Cis-3,6-dimethyl-	300	2.56	2.56	1713	2.56	2.56
1,2,4,5-tetrathiane	380	2.56	2.56	1793	2.56	2.56
($C_4H_8S_4$)						
Prenyl-mercaptan	300	2.18	2.83	1618	2.61	2.49
($C_5H_{10}S$)	380	2.18	2.72	1698	2.57	2.47
Trans-3,6-dimethyl-	300	2.52	2.52	1713	2.52	2.52
1,2,4,5-tetrathiane	380	2.52	2.52	1793	2.52	2.52
($C_4H_8S_4$)						
2-Methyl-3-furanthiol	300	2.09	2.27	1639	2.18	2.15
(C_5H_6OS)	380	2.09	2.23	1719	2.17	2.15
2-Methylthiolane-3-ol	300	2.10	2.97	1646	2.76	2.57
($C_5H_{10}OS$)	380	2.10	2.82	1726	2.70	2.54
3-Mercapto-3-	300	2.17	2.84	1649	2.62	2.49
methylbutan-1-ol	380	2.17	2.73	1729	2.58	2.47
($C_5H_{12}OS$)						
Ethyl-3-	300	2.18	3.43	1667	3.13	2.85
mercaptopropionate	380	2.18	3.23	1747	3.11	2.86
($C_5H_{10}O_2S$)						
5-2-hydroxyethyl-	300	2.28	3.51	1678	3.30	3.00
4-methylthiazole	380	2.28	3.31	1758	3.27	3.01
(C_6H_9NOS)						
2-Methyltetrahydro	300	2.06	2.68	1643	2.47	2.36
thiophen-3-one	380	2.06	2.58	1723	2.44	2.34
(C_5H_8OS)						
3-Methylsulfanyl	300	2.06	3.57	1626	2.80	2.58
propan-1-ol	380	2.06	3.34	1706	2.79	2.60
($C_4H_{10}OS$)						
3-Mercaptohexylacatate	300	2.54	2.93	1707	2.73	2.68
($C_8H_{16}O_2S$)	380	2.54	2.85	1787	2.72	2.67
Ethylthioacetate	300	2.02	2.48	1622	2.29	2.21
(C_4H_8OS)	380	2.02	2.40	1702	2.27	2.20

Table 6.7: SIFT-MS reaction rate coefficients (k_{ADO} and k_{cap}) for the reaction between reagent ions (H_3O^+, NH_4^+, NO^+ and O_2^+) and cork-taint compounds related to sulfur at different temperatures.

Molecule name (Formula)	T **(K)**	$\mathbf{k_{ADO}}$ $\mathbf{H_3O^+}$	$\mathbf{NH_4^+}$	$\mathbf{NO^+}$	$\mathbf{O_2^+}$	$\mathbf{k_{cap}}$ $\mathbf{H_3O^+}$	$\mathbf{NH_4^+}$	$\mathbf{NO^+}$	$\mathbf{O_2^+}$
Hydrogen Sulfide	80	2.36	2.41	2.07	2.03	2.98	3.03	2.59	2.57
(H_2S)	150	2.00	2.04	1.75	1.72	2.25	2.29	1.96	1.94
	300	1.70	1.73	1.49	1.46	1.90	1.93	1.65	1.64
	450	1.59	1.62	1.39	1.37	1.73	1.76	1.50	1.49
	600	1.53	1.55	1.33	1.31	1.64	1.67	1.43	1.41
Methanethiol	80	3.24	3.31	2.78	2.73	4.30	4.39	3.70	3.61
(CH_4S)	150	2.68	2.73	2.30	2.25	3.27	3.34	2.81	2.74
	300	2.21	2.25	1.90	1.86	2.45	2.50	2.11	2.06
	450	2.02	2.06	1.73	1.70	2.26	2.30	1.94	1.89
	600	1.92	1.96	1.65	1.62	2.10	2.14	1.80	1.76
Ethanethiol	80	3.45	3.52	2.93	2.86	4.53	4.61	3.82	3.74
(C_2H_6S)	150	2.87	2.93	2.43	2.38	3.45	3.51	2.91	2.85
	300	2.39	2.44	2.03	1.98	2.63	2.68	2.22	2.17
	450	2.20	2.24	1.86	1.82	2.44	2.48	2.06	2.01
	600	2.10	2.14	1.78	1.74	2.28	2.32	1.92	1.88
Dimethyl Sulfide	80	3.34	3.41	2.83	2.77	4.33	4.41	3.68	3.60
(C_2H_6S)	150	2.79	2.85	2.37	2.32	3.18	3.24	2.70	2.65
	300	2.34	2.39	1.98	1.94	2.55	2.60	2.17	2.12
	450	2.16	2.21	1.83	1.79	2.38	2.42	2.02	1.98
	600	2.06	2.11	1.75	1.71	2.23	2.27	1.90	1.86
Diethyl Sulfide	80	3.52	3.60	2.94	2.87	4.33	4.48	3.64	3.58
($C_4H_{10}S$)	150	3.00	3.07	2.51	2.45	3.34	3.43	2.78	2.73
	300	2.57	2.63	2.15	2.10	2.84	2.91	2.37	2.32
	450	2.41	2.46	2.01	1.96	2.60	2.67	2.17	2.13
	600	2.32	2.37	1.94	1.90	2.48	2.54	2.06	2.03
Dimethyl Disulfide	80	4.00	4.09	3.33	3.25	5.24	5.35	4.37	4.27
($C_2H_6S_2$)	150	3.32	3.40	2.77	2.70	3.99	4.08	3.33	3.25
	300	2.76	2.83	2.30	2.25	3.05	3.11	2.54	2.48
	450	2.54	2.60	2.12	2.07	2.82	2.88	2.35	2.29
	600	2.43	2.48	2.02	1.79	2.63	2.69	2.20	2.14

Table 6.7: continued

Molecule name (Formula)	*T* **(K)**	$\mathbf{k_{ADO}}$ $\mathbf{H_3O^+}$	$\mathbf{NH_4^+}$	$\mathbf{NO^+}$	$\mathbf{O_2^+}$	$\mathbf{k_{cap}}$ $\mathbf{H_3O^+}$	$\mathbf{NH_4^+}$	$\mathbf{NO^+}$	$\mathbf{O_2^+}$
Diethyl Disulfide	80	4.28	4.39	3.54	3.45	5.49	5.62	4.55	4.42
($C_4H_{10}S_2$)	150	3.60	3.68	2.97	2.90	4.07	4.16	3.37	3.28
	300	3.03	3.10	2.51	2.44	3.41	3.49	2.82	2.74
	450	2.81	2.87	2.32	2.26	3.07	3.14	2.54	2.47
	600	2.68	2.75	2.22	2.16	2.89	2.96	2.39	2.32
Methyl Thioacetate	80	3.05	3.12	2.55	2.49	3.54	3.62	2.96	2.88
(C_3H_6OS)	150	2.63	2.69	2.19	2.14	2.89	2.96	2.42	2.35
	300	2.28	2.33	1.90	1.86	2.50	2.56	2.09	2.04
	450	2.15	2.20	1.79	1.75	2.32	2.37	1.94	1.89
	600	2.08	2.13	1.74	1.70	2.22	2.27	1.86	1.81
3-Mercaptohexan-1-ol	80	3.69	3.79	3.05	2.97	4.26	4.38	3.52	3.43
($C_6H_{14}OS$)	150	3.19	3.27	2.63	2.56	3.49	3.58	2.88	2.80
	300	2.78	2.85	2.29	2.23	3.03	3.11	2.50	2.44
	450	2.62	2.69	2.16	2.11	2.82	2.89	2.32	2.26
	600	2.54	2.61	2.09	2.04	2.70	2.77	2.23	2.17
4-Mercapto-4-	80	4.43	4.54	3.65	3.56	5.73	5.89	4.74	4.61
methylpentan-2-one	150	3.70	3.79	3.05	2.97	4.20	4.32	3.48	3.38
($C_6H_{12}OS$)	300	3.09	3.17	2.55	2.49	3.37	3.46	2.79	2.71
	450	2.86	2.93	2.36	2.30	3.14	3.22	2.60	2.52
	600	2.73	2.80	2.25	2.19	2.94	3.02	2.44	2.37
4-Mercapto-4-	80	4.79	4.91	3.95	3.84	6.33	6.47	5.20	5.09
methylpentan-2-ol	150	3.96	4.06	3.27	3.18	4.81	4.92	3.95	3.87
($C_6H_{14}OS$)	300	3.28	3.36	2.70	2.63	3.63	3.71	2.98	2.92
	450	3.01	3.08	2.48	2.41	3.35	3.42	2.75	2.69
	600	2.87	2.94	2.36	2.30	3.12	3.19	2.56	2.51
Benzothiazole	80	3.30	3.38	2.72	2.65	3.71	3.79	3.06	2.98
(C_7H_5NS)	150	2.93	3.00	2.41	2.35	3.23	2.33	2.67	2.59
	300	2.63	2.70	2.17	2.11	2.83	2.89	2.33	2.27
	450	2.51	2.58	2.07	2.02	2.69	2.75	2.21	2.16
	600	2.46	2.52	2.03	1.97	2.61	2.67	2.15	2.09

Table 6.7: continued

Molecule name (Formula)	T **(K)**	$\mathbf{k_{ADO}}$ $\mathbf{H_3O^+}$	$\mathbf{NH_4^+}$	$\mathbf{NO^+}$	$\mathbf{O_2^+}$	$\mathbf{k_{cap}}$ $\mathbf{H_3O^+}$	$\mathbf{NH_4^+}$	$\mathbf{NO^+}$	$\mathbf{O_2^+}$
2-Furanmethanethiol	80	3.93	4.02	3.26	3.17	5.01	5.14	4.14	4.05
(C_5H_6OS)	150	3.31	3.39	2.74	2.67	3.74	3.83	3.09	3.02
	300	2.80	2.87	2.32	2.26	3.14	3.22	2.60	2.54
	450	2.60	2.66	2.15	2.10	2.84	2.91	2.35	2.29
	600	2.49	2.55	2.06	2.01	2.68	2.75	2.22	2.17
2-Mercaptoethanol	80	4.53	4.63	3.80	3.72	6.33	6.47	5.32	5.21
(C_2H_6OS)	150	3.66	3.74	3.07	3.00	4.76	4.88	4.01	3.92
	300	2.94	3.00	2.47	2.41	3.53	3.61	2.97	2.90
	450	2.62	2.68	2.20	2.15	2.94	3.01	2.47	2.42
	600	2.45	2.51	2.06	2.01	2.69	2.75	2.26	2.21
Benzenemethanethiol	80	3.48	3.56	2.87	2.80	3.97	4.05	3.27	3.18
(C_7H_8S)	150	3.05	3.13	2.52	2.46	3.41	3.48	2.81	2.74
	300	2.70	2.77	2.23	2.18	2.93	2.99	2.41	2.35
	450	2.57	2.63	2.12	2.07	2.76	2.82	2.27	2.21
	600	2.50	2.56	2.07	2.02	2.66	2.72	2.20	2.14
2-Mercaptoethyl acetate	80	3.73	3.81	3.08	3.00	4.73	4.82	3.90	3.80
($C_4H_8O_2S$)	150	3.14	3.22	2.60	2.53	3.55	3.62	2.92	2.85
	300	2.66	2.73	2.20	2.15	2.98	3.04	2.46	2.40
	450	2.48	2.54	2.05	2.00	2.71	2.76	2.23	2.18
	600	2.38	2.44	1.97	1.92	2.56	2.61	2.11	2.06
3-mercaptopropyl acetate	80	3.53	3.62	2.91	2.83	4.09	4.19	3.37	3.27
($C_5H_{10}O_2S$)	150	3.05	3.12	2.51	2.45	3.35	3.43	2.75	2.68
	300	2.65	2.71	2.18	2.13	2.90	2.97	2.39	2.32
	450	2.50	2.56	2.06	2.01	2.70	2.76	2.22	2.15
	600	2.42	2.48	1.99	1.94	2.59	2.65	2.13	2.07
Cis-3,6-dimethyl-	80	2.50	2.56	2.04	1.99	same as k_{Lang}			
1,2,4,5-tetrathiane	150	2.50	2.56	2.04	1.99	same as k_{Lang}			
($C_4H_8S_4$)	300	2.50	2.56	2.04	1.99	same as k_{Lang}			
	450	2.50	2.56	2.04	1.99	same as k_{Lang}			
	600	2.50	2.56	2.04	1.99	same as k_{Lang}			

Table 6.7: continued

Molecule name (Formula)	*T* **(K)**	$\mathbf{k_{ADO}}$ $\mathbf{H_3O^+}$	$\mathbf{NH_4^+}$	$\mathbf{NO^+}$	$\mathbf{O_2^+}$	$\mathbf{k_{cap}}$ $\mathbf{H_3O^+}$	$\mathbf{NH_4^+}$	$\mathbf{NO^+}$	$\mathbf{O_2^+}$
Prenyl-mercaptan	80	3.78	3.87	3.15	3.07	4.71	4.82	3.91	3.82
($C_5H_{10}S$)	150	3.22	3.30	2.68	2.62	3.60	3.68	2.99	2.92
	300	2.76	2.83	2.29	2.24	3.06	3.13	2.54	2.48
	450	2.58	2.64	2.15	2.10	2.80	2.87	2.33	2.27
	600	2.49	2.55	2.07	2.02	2.67	2.73	2.21	2.16
Trans-3,6-dimethyl-	80	2.45	2.52	2.01	1.95	same as k_{Lang}			
1,2,4,5-tetrathiane	150	2.45	2.52	2.01	1.95	same as k_{Lang}			
($C_4H_8S_4$)	300	2.45	2.52	2.01	1.95	same as k_{Lang}			
	450	2.45	2.52	2.01	1.95	same as k_{Lang}			
	600	2.45	2.52	2.01	1.95	same as k_{Lang}			
2-Methyl-3-furanthiol	80	2.61	2.68	2.17	2.11	2.95	3.02	2.44	2.38
(C_5H_6OS)	150	2.39	2.45	1.98	1.93	2.59	2.65	2.15	2.09
	300	2.21	2.27	1.83	1.79	2.37	2.42	1.96	1.91
	450	2.15	2.20	1.78	1.74	2.28	2.34	1.89	1.85
	600	2.12	2.17	1.76	1.71	2.24	2.29	1.86	1.81
2-Methylthiolane-3-ol	80	4.15	4.25	3.44	3.35	5.38	5.52	4.47	4.36
($C_5H_{10}OS$)	150	3.47	3.55	2.87	2.80	3.94	4.04	3.27	3.19
	300	2.90	2.97	2.40	2.34	3.16	3.24	2.62	2.56
	450	2.67	2.74	2.21	2.16	2.94	3.01	2.44	2.38
	600	2.55	2.61	2.11	2.06	2.75	2.82	2.28	2.23
3-Mercapto-3-	80	3.82	3.92	3.16	3.08	4.79	4.91	3.96	3.87
methylbutan-1-ol	150	3.25	3.33	2.69	2.62	3.64	3.73	3.00	2.94
($C_5H_{12}OS$)	300	2.77	2.84	2.29	2.24	3.08	3.16	2.55	2.49
	450	2.59	2.65	2.14	2.09	2.82	2.88	2.32	2.27
	600	2.49	2.55	2.06	2.01	2.68	2.74	2.21	2.16
Ethyl-3-	80	5.03	5.16	4.15	4.04	6.80	6.96	5.62	5.46
mercaptopropionate	150	4.11	4.21	3.38	3.30	5.15	5.27	4.25	4.13
($C_5H_{10}O_2S$)	300	3.35	3.43	2.76	2.69	3.76	3.85	3.11	3.02
	450	3.03	3.11	2.50	2.44	3.32	3.39	2.74	2.66
	600	2.87	2.94	2.37	2.31	3.17	3.25	2.62	2.55

Table 6.7: continued

Molecule name (Formula)	T **(K)**	$\mathbf{k_{ADO}}$ $\mathbf{H_3O^+}$	$\mathbf{NH_4^+}$	$\mathbf{NO^+}$	$\mathbf{O_2^+}$	$\mathbf{k_{cap}}$ $\mathbf{H_3O^+}$	$\mathbf{NH_4^+}$	$\mathbf{NO^+}$	$\mathbf{O_2^+}$
5-2-hydroxyethyl-	80	5.12	5.24	4.21	4.10	6.86	7.04	5.65	5.50
4-methylthiazole	150	4.19	4.29	3.45	3.36	5.20	5.34	4.28	4.17
(C_6H_9NOS)	300	3.43	3.51	2.82	2.75	3.83	3.94	3.16	3.07
	450	3.12	3.19	2.56	2.50	3.38	3.47	2.79	2.71
	600	2.96	3.03	2.43	2.37	3.24	3.33	2.67	2.60
2-Methyltetrahydro	80	3.60	3.69	2.98	2.91	4.49	4.60	3.71	3.62
thiophen-3-one	150	3.07	3.14	2.54	2.47	3.42	3.51	2.83	2.76
(C_5H_8OS)	300	2.62	2.68	2.17	2.11	2.90	2.98	2.40	2.34
	450	2.45	2.51	2.03	1.98	2.66	2.72	2.19	2.14
	600	2.36	2.42	1.95	1.90	2.53	2.59	2.09	2.04
3-Methylsulfanyl	80	5.39	5.52	4.47	4.36	7.53	7.71	6.25	6.10
propan-1-ol	150	4.35	4.45	3.61	3.52	5.67	5.81	4.71	4.60
($C_4H_{10}OS$)	300	3.49	3.57	2.90	2.83	4.19	4.30	3.48	3.40
	450	3.12	3.19	2.59	2.52	3.49	3.58	2.90	2.83
	600	2.91	2.98	2.42	2.36	3.19	3.27	2.65	2.59
3-Mercaptohexylacatate	80	3.58	3.67	2.93	2.85	4.01	4.12	3.28	3.20
($C_8H_{16}O_2S$)	150	3.18	3.26	2.60	2.53	3.49	3.59	2.86	2.79
	300	2.85	2.93	2.34	2.27	3.06	3.15	2.51	2.44
	450	2.73	2.80	2.23	2.17	2.91	2.99	2.38	2.32
	600	2.67	2.73	2.18	2.12	2.82	2.90	2.31	2.25
Ethylthioacetate	80	3.20	3.28	2.66	2.60	3.69	3.77	3.06	2.98
(C_4H_8OS)	150	2.78	2.84	2.31	2.25	3.03	3.09	2.51	2.45
	300	2.42	2.48	2.01	1.96	2.64	2.70	2.19	2.14
	450	2.29	2.35	1.90	1.86	2.46	2.51	2.04	1.99
	600	2.22	2.28	1.85	1.80	2.37	2.42	1.96	1.91

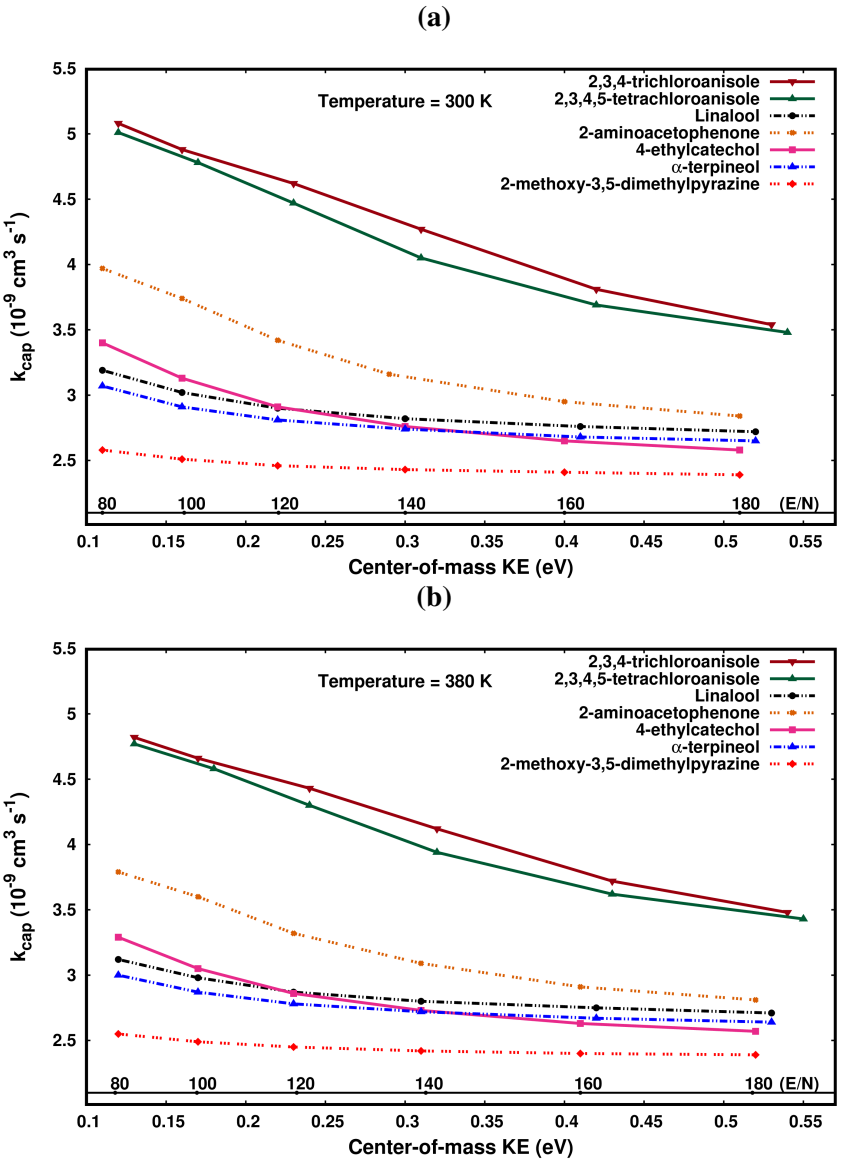

Figure 6.1: Variation of the capture collision rate coefficient with the center-of- mass kinetic energy for proton transfer reaction between H_3O^+ and VOCs at 6.1a 300 K and 6.1b 380 K. The second horizontal scale provides the calibration in terms of reduced electric field E/N

Figure 6.2: Variation of ADO rate coefficients as a function of temperature for the reaction of NO^+ and O_2^+ ions with VOCs.

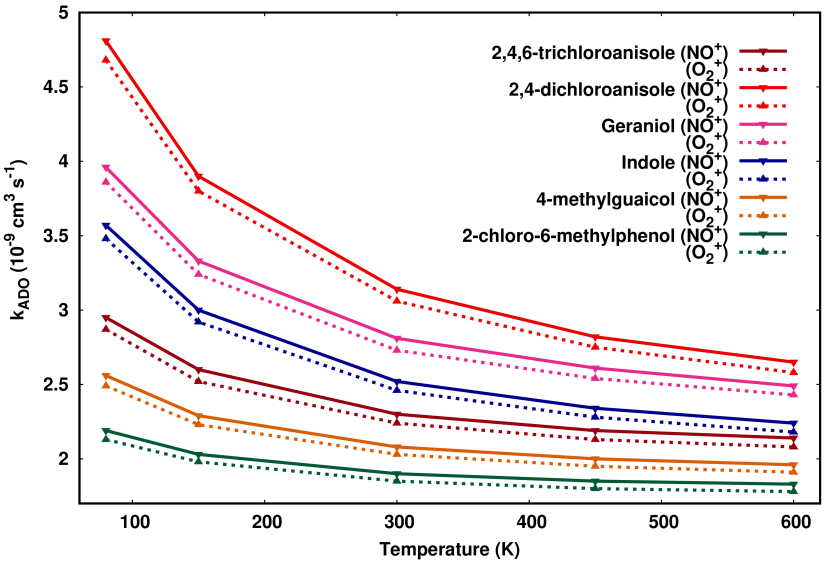

Figure 6.3: The dipole locking constant C as a function of $\mu_D/\alpha^{1/2}$ at temperatures ranging from 80 K to 600 K.

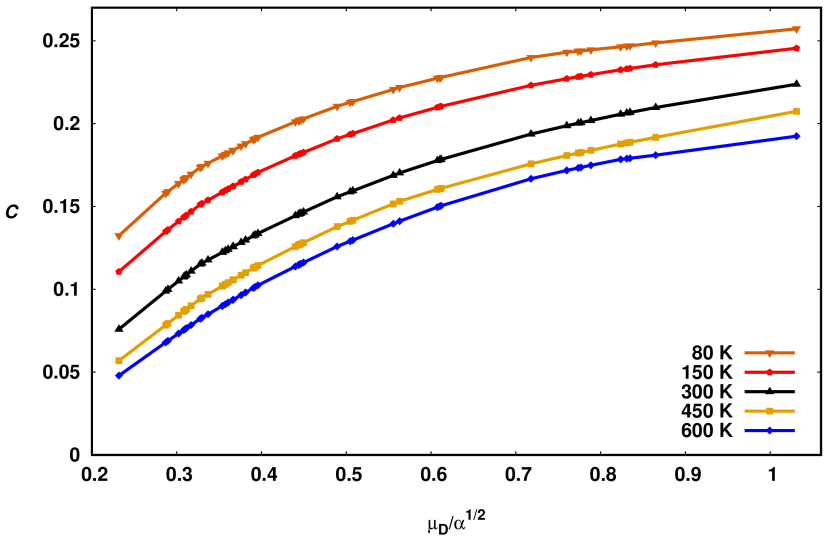

6.3.1 Dipole Moment Dependent Rate Coefficients

The models we discussed here predominately depend on the ion and molecule interactions. The dipole moment plays a very crucial role in determining the reaction outcome and consequently the rate coefficients of the IMRs. The rate coefficient, k_{Lang}, in the Langevin model derived from the long range interaction between a point charge and a non-polar molecule (ion-induced dipole interaction). However, results were unsatisfactory for reactions involving polar neutral molecules because its derivation neglects the interaction between the positive charge and the permanent electric dipole moment of the neutral molecule.

The ADO theory considered ion-dipole interactions in addition to the ion-induced dipole interaction and introducing a parameter C (a function of μ_D and α) which reflects the extent to which the dipole of the molecule orients itself with the incoming charge with orientation from 0 (no alignment) to 1 (locked dipole). Su et al. [14] pointed out that for a very large value of $\mu_D/\sqrt{\alpha}$, C can vary maximum up to 0.26. Thus, the effect of ion-dipole interactions is much less than predicted from the simple model involving locking-in of the dipole ($C = 1$), although it has been observed that rate coefficient may increase 2 to 4 times of the ion-induced dipole value for molecules having large dipole moments [4]. The summary of the results has shown that ion-permanent dipole contribution to the rate coefficient varies with the dipole moment of the neutral molecules and for the most polar molecule, it can be as large as ion-induced dipole contribution. Hence, the overall rate coefficient increases with the dipole moment of the neutral molecule.

Our calculated rate coefficients values in Table 6.1 validate the above statement. The table shows that the molecules like 2,3,4-trichloroanisole (4.34 μ_D), 2,3,4,5-tetrachloroanisole (4.09 μ_D), and rotundone (4.06 μ_D) have the highest rate coefficients respectively. Similarly, molecules such as 2-chloro-6-methylphenol and 2-Methyl-3-furanthiol possess lower rate coefficients because of their low dipole moment values. It is worth noting that the rate of cis-3,6-dimethyl-1,2,4,5-tetrathiane and trans-3,6-dimethyl-1,2,4,5-tetrathiane is Langevin dependent only because these molecules have zero dipole moment.

6.3.2 Absolute Rate Coefficients at Thermal Energies

Most of the experimental study of IMRs has been done at thermal energy conditions and obtained results are available for comparison with theoretical results at thermal energies. Smith and Španěl have studied SIFT-MS reactions and established a comprehensive set of thermal reaction rates data at 300 K for PTRs with H_3O^+ ion. Many other contributors: Viggiano and co-workers [15, 16] and Arijs and co-workers [17, 18] have collected kinetic data using either SIFT-MS or flowing afterglow measurements. This database is derived from thermal energy reagent ions and common to ion-molecule reactions used by both techniques i.e. PTR-MS and SIFT-MS at thermal energies. Theoretical rate coefficients obtained by ADO theory agree best with the experimental rate coefficients. Lidinger et al. have also observed that the thermal energy rate coefficients are in good agreement with the ADO theory predictions.

However, at higher relative energies the experimental results were considerably higher than ADO. Our rate coefficients at 300 K are in good agreement with the available experimental results both by ADO and classical trajectory methods for proton transfer as well as charge transfer reactions (see Tables 6.3, and 6.4). Although, not much experimental data is available on cork-taint and off-flavor compounds in wine, our calculated rate coefficients would serve as a reliable source of information to perform PTR-MS and SIFT-MS experiments on wine compounds at thermal temperature and higher energy conditions.

6.3.3 Relative Kinetic Energy Dependence of Rate Coefficients

There has been a continuous surge of interest to investigate ion-polar molecules reactions experimentally and theoretically at higher kinetic energy. The growing need for the ion-molecule collision theory that able to describe the kinetic energy dependence of the reaction kinetics when the neutral molecule remains at a given temperature. The point of interest in the polar molecule is to understand how ion orient the dipole during the collision and the effect of relative translational energy on the orientation operation. Bowers and Su (1975) [19, 20] and Dugan (1973) [21] have made comparisons of various theories

with the experimental kinetic energy dependence of rate coefficients and established that the average dipole orientation theory agrees best with the experimental results[1], both in magnitude and shape of the curves as reported in [19, 22].

Alternatively, parametrization based on trajectory calculations given by Su provides capture rate coefficients within 5% error at center-of-mass energies ranging from thermal to several eV. As the kinetic energy increases corresponding rotational energy also increases at some equilibrium temperature. Consequently, elevated rotational energy decreases the effectiveness of the charge "locking in" the dipole and lower the rate coefficients. We performed kinetic energy dependent calculations of the rate coefficients for some selected molecules to examine the nature of the known experimental and theoretical results. Our results (graphical curves) follow the same pattern, although for different molecules (see Fig. 6.1).

Currently, no experimental results are available to make a comprehensive comparison with our theoretically obtained results. The center-of-mass kinetic energy remains well below (0.55 eV) the experimental limit i.e. $\approx$ 0.7 eV. It must also be noted that the energy above $\approx$ 1 eV, the average dipole orientation theory limits in applications. Also, E/N values are marked horizontally in Figure 6.1. We have also observed that the internal temperature does not make any significant difference in rate vs center-of-mass kinetic energy plot.

6.3.4 Temperature Dependence of Rate Coefficients

ADO theory provides substantial evidence for the temperature dependence of rate coefficients. From ADO expression (3.25), a negative temperature dependence comes from the second part and dipole locking parameter C also decreases with the temperature, refer Figure 6.3. The corresponding rates vary proportionally as $T^{-1/2}$. However, since $0 < C < 1$, the contribution of the second term of equation (3.25) to k will be smaller than in the locked dipole model ($C = 1$), and the overall temperature dependence predicted by the two models remains comparable. The predictions of collision theory concerning the temper-

[1]Results were limited to 0.7 eV due to experimental complications. Additionally, higher energies above $\sim$ 0.7 eV ion-polar molecule cross-section approaches the gas kinetic cross-section and current dipole theory does not remain valid.

ature dependence of collision rates may be tested by the measurements on fast exchange reactions. The exothermic proton transfer and charge exchange reactions should be especially suitable, since Bohme (1975) [23] showed that the majority of exothermic reactions proceeds at unit collision efficiency at 300 K. Thus, the temperature dependence of fast reactions should reflect the temperature dependence of the collision rates. Many experiments are performed at temperatures higher than 300 K [14, 24, 25].

We obtained ADO rate coefficients for the proton transfer and charge exchange reactions between H_3O^+, NH_4^+, NO^+ and O_2^+ ions to the polar molecules at the different temperature range from 80 K to 600 K and are plotted for some selected molecules in Figure 6.2. We also obtained rates under PTR-MS experimental conditions at higher effective temperatures (above 1000 K) and the results are also reported in Tables 6.1, 6.2, 6.5 and 6.6 respectively.

In summary, the data on the temperature dependent ion-molecule collision rate coefficients is limited. The existing data is generally in qualitative agreement with the predictions of collision theory, wherein negative temperature dependence is observed. More experimental data is required in order to make quantitative validation of theoretical predictions.

6.4 Center-of-Mass KE variation with E/N

It is evident that ions move along the drift tube are provided an additional drift by the electric field. Kinetic energy expression in equation (2.4) represents the mean kinetic energy of the ions. The effective collision energy contribution comes from the 3rd term of equation (2.4) which depicts the collisions between the ions and buffer gas molecules. In order to fully understand the effect of the ion kinetic energy on the ion-molecule reaction outcome, the relative kinetic energy of the colliding species is critical.

This relative kinetic energy, in the prerequisite to conserve linear momentum, is different and much higher than the average thermal kinetic energy ($3k_BT/2$) at 300 K. As an example, 2,4,6-Trichloroanisole molecule in our calculations from equation (2.5) found to have center-of-mass kinetic energy: KE_{com} = 0.23 eV with the reaction of H_3O^+ at buffer

Figure 6.4: The center-of-mass kinetic energy KE_{com} dependence on the E/N ratios at $T = 300$ K for a few of the species considered in the present work.

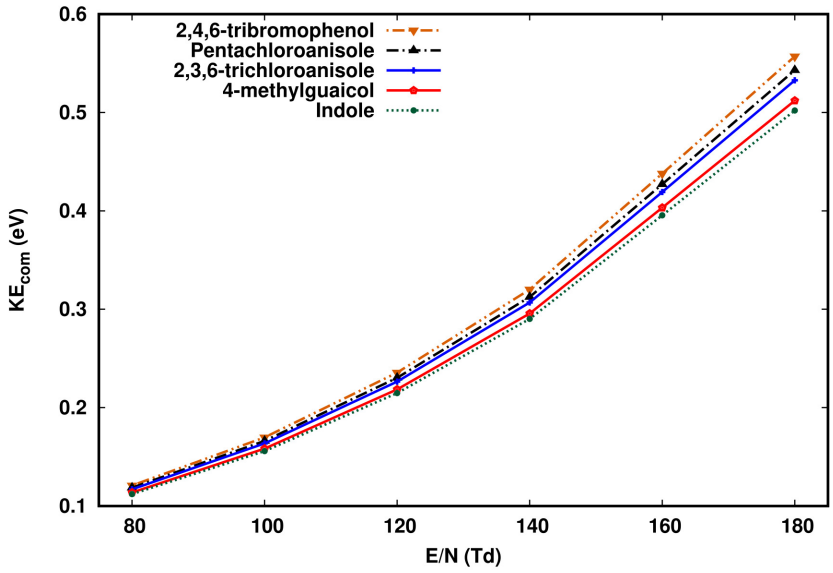

gas mass 28.8 (weighted average of N_2 and O_2); and operating electric field is E/N = 123 Td (refer Table 6.8). We report KE_{com} at several experimentally sensible E/N values ranging from 80 Td to 180 Td for other molecules in the Table 6.8. The KE_{com} of the colliding system is notably higher than the thermal energy and illustrates the effect of applied electric field on the reactive collisions occurring in PTR-MS measurements. A graph showing the variation of KE_{com} with the reduced electric field (E/N) is shown in Figure 6.4. Although, KE_{com} is mass-dependent the Figure 6.4 shows that the difference in KE_{com} among different compounds is quite small, especially at small E/N, in qualitative agreement with the experimental curve for the collision of H_3O^+ with acetone and trinitrotoluene [26].

Table 6.8: Center-of-mass kinetic energy and rate coefficients for the proton-transfer reaction from H_3O^+ to VOCs in PTR-MS conditions ($T = 300$K) at various E/N values.

Molecule name	E/N					
	80	**100**	**120**	**140**	**160**	**180**
2,4,6-Trichloroanisole	0.12[4]	0.17	0.23	0.31	0.42	0.53
($C_7H_5Cl_3O$)	2.87[5]	2.79	2.73	2.69	2.66	2.64
2,4,6-Tribromoanisole	0.12	0.17	0.23	0.32	0.43	0.55
($C_7H_5Br_3O$)	3.04	2.97	2.92	2.88	2.85	2.84
Pentachlorophenol	0.12	0.17	0.23	0.31	0.43	0.54
(C_6Cl_5OH)	3.31	3.16	3.06	2.99	2.94	2.90
Pentabromophenol	0.12	0.17	0.24	0.32	0.44	0.56
(C_6Br_5OH)	3.54	3.38	3.27	3.20	3.14	3.11
2,4,6-Trichlorophenol	0.12	0.16	0.23	0.31	0.42	0.53
($C_6H_2Cl_3OH$)	2.84	2.74	2.67	2.62	2.58	2.56
2,4,6-Tribromophenol	0.12	0.17	0.23	0.32	0.43	0.55
($C_6H_2Br_3OH$)	2.94	2.86	2.80	2.76	2.73	2.71
2,3,4-Trichloroanisole	0.12	0.16	0.23	0.31	0.42	0.53
($C_7H_5Cl_3O$)	5.08	4.88	4.62	4.27	3.81	3.54
2,3,6-Trichloroanisole	0.12	0.16	0.23	0.31	0.42	0.53
($C_7H_5Cl_3O$)	2.94	2.84	2.76	2.71	2.67	2.65
2,3,4,5-Tetrachloroanisole	0.12	0.17	0.23	0.31	0.42	0.54
($C_7H_4Cl_4O$)	5.01	4.78	4.47	4.05	3.69	3.48
2,3,4,6-Tetrachloroanisole	0.12	0.17	0.23	0.31	0.42	0.54
($C_7H_4Cl_4O$)	3.31	3.07	2.96	2.89	2.84	2.81
2,3,5,6-Tetrachloroanisole	0.12	0.17	0.23	0.31	0.42	0.54
($C_7H_4Cl_4O$)	3.04	2.94	2.87	2.82	2.79	2.77
2,4-Dichloroanisole	0.12	0.16	0.22	0.30	0.41	0.52
($C_7H_6Cl_2O$)	4.40	4.19	3.89	3.53	3.24	3.08
2,6-Dichloroanisole	0.12	0.16	0.22	0.30	0.41	0.52
($C_7H_6Cl_2O$)	3.36	3.09	2.91	2.78	2.68	2.63
Cis-1,5-octadien-3-one	0.11	0.16	0.22	0.29	0.40	0.51
($C_8H_{12}O$)	3.75	3.51	3.22	3.00	2.83	2.73
Cis-1,5-octadien-3-ol	0.11	0.16	0.22	0.29	0.40	0.51
($C_8H_{14}O$)	2.93	2.78	2.67	2.60	2.54	2.51
1-Octene-3-ol	0.11	0.16	0.22	0.29	0.40	0.51
($C_8H_{16}O$)	2.85	2.71	2.67	2.55	2.50	2.48

[4]Here, 1st row represents, KE_{com}.

[5]2nd row represents, rate coefficient, k_{cap}(COM) and so on....

Table 6.8: continued

Molecule name	E/N					
	80	**100**	**120**	**140**	**160**	**180**
1-Octene-3-one	0.11	0.16	0.22	0.29	0.40	0.51
($C_8H_{14}O$)	4.08	3.89	3.60	3.28	3.03	2.88
Octanal	0.11	0.16	0.22	0.29	0.40	0.51
($C_8H_{16}O$)	3.81	3.58	3.28	3.03	2.85	2.74
2-Sec-butyl-3-	0.12	0.16	0.22	0.30	0.41	0.52
methoxypyrazine	2.82	2.75	2.69	2.66	2.63	2.62
($C_9H_{14}N_2O$)						
3-Iso-butyl-2-	0.12	0.16	0.22	0.30	0.41	0.52
methoxypyrazine	3.67	3.38	3.15	2.99	2.87	2.80
($C_9H_{14}N_2O$)						
2-Iso-propyl-3-	0.11	0.16	0.22	0.30	0.41	0.52
methoxypyrazine	2.75	2.66	2.60	2.56	2.53	2.51
($C_8H_{12}N_2O$)						
2-Methoxy-3,5-	0.11	0.16	0.22	0.30	0.40	0.51
dimethylpyrazine	2.58	2.51	2.46	2.43	2.41	2.39
($C_7H_{10}N_2O$)						
2-Methylisoborneol	0.12	0.16	0.22	0.30	0.41	0.52
($C_{11}H_{20}O$)	2.89	2.79	2.72	2.67	2.64	2.62
Geosmin	0.12	0.16	0.22	0.30	0.41	0.53
($C_{12}H_{22}O$)	2.92	2.84	2.78	2.75	2.72	2.70
Guaiacol	0.11	0.16	0.22	0.29	0.40	0.51
($C_7H_8O_2$)	3.93	3.75	3.49	3.17	2.92	2.77
4-Ethylguaiacol	0.11	0.16	0.22	0.30	0.41	0.52
($C_9H_{12}O_2$)	3.79	3.52	3.23	3.04	2.89	2.80
4-Ethylphenol	0.11	0.16	0.22	0.29	0.40	0.50
($C_8H_{10}O$)	2.84	2.68	2.58	2.50	2.45	2.41
Eucalyptol	0.11	0.16	0.22	0.30	0.41	0.52
($C_8H_{10}O$)	2.84	2.73	2.65	2.59	2.55	2.53
4-Ethylcatechol	0.12	0.16	0.22	0.30	0.40	0.51
($C_8H_{10}O_2$)	3.40	3.13	2.91	2.76	2.65	2.58
4-Methylguaiacol	0.11	0.16	0.22	0.30	0.40	0.51
($C_8H_{10}O_2$)	2.65	2.57	2.51	2.47	2.44	2.43
Rotundone	0.12	0.16	0.23	0.31	0.42	0.53
($C_{15}H_{22}O$)	5.20	4.94	4.56	4.14	3.83	3.64
Geraniol	0.11	0.16	0.22	0.30	0.41	0.52
($C_{10}H_{18}O$)	3.03	2.92	2.84	2.79	2.75	2.73

Table 6.8: continued

Molecule name	E/N					
	80	**100**	**120**	**140**	**160**	**180**
Hotrienol	0.11	0.16	0.22	0.30	0.41	0.52
($C_{10}H_{16}O$)	3.19	3.03	2.92	2.85	2.79	2.76
Linalool	0.11	0.16	0.22	0.30	0.41	0.52
($C_{10}H_{18}O$)	3.19	3.02	2.90	2.82	2.76	2.72
Nerol	0.11	0.16	0.22	0.30	0.41	0.52
($C_{10}H_{18}O$)	3.87	3.58	3.30	3.11	2.97	2.89
$\alpha-$Terpineol	0.11	0.16	0.22	0.30	0.41	0.52
($C_{10}H_{18}O$)	3.07	2.91	2.81	2.74	2.68	2.65
Indole	0.11	0.16	0.21	0.29	0.40	0.50
(C_8H_7N)	3.59	3.35	3.07	2.87	2.72	2.64
1-Methylindole	0.11	0.16	0.22	0.29	0.40	0.51
(C_9H_9N)	3.95	3.70	3.38	3.14	2.96	2.85
2-Aminoacetophenone	0.11	0.16	0.22	0.29	0.40	0.51
(C_8H_9NO)	3.09	2.90	2.76	2.67	2.60	2.55
2-Chloro-6-methylphenol	0.11	0.16	0.22	0.30	0.40	0.51
(C_7H_7ClO)	2.40	2.37	2.35	2.34	2.33	2.32
3-Octanone	0.11	0.16	0.22	0.29	0.40	0.51
($C_8H_{16}O$)	3.77	3.55	3.24	3.00	2.82	2.71
Fenchone	0.11	0.16	0.22	0.30	0.41	0.52
($C_{10}H_{16}O$)	4.10	3.88	3.57	3.26	3.04	2.90
Fenchol	0.11	0.16	0.22	0.30	0.41	0.52
($C_{10}H_{18}O$)	2.71	2.64	2.58	2.54	2.52	2.50
Trans-2-octen-1-ol	0.11	0.16	0.22	0.29	0.40	0.51
($C_8H_{16}O$)	3.12	2.91	2.77	2.67	2.60	2.55
Pentachloroanisole	0.12	0.17	0.23	0.31	0.43	0.54
($C_7H_3Cl_5O$)	3.54	3.33	3.19	3.09	3.02	2.98

6.5 Suitability of Different Collision Models to Specific Experiments

The Langevin model based on pure polarization theory predicts rate coefficients for ion and non-polar molecule collisions and agrees rather good for some simple low energy IMRs.

However, the Langevin model could not provide temperature and energy dependence of rates, although the model provides enough information to address experimental issues related to IMRs. Later, the locked dipole model which predicts rate coefficients based on the assumption that the ion 'locks in' the dipole completely. The locked dipole models seriously overestimate the experimental rate coefficients. The ADO and trajectory models have provided results fairly close to experimental values. The models we discussed throughout the chapter can be used under different experimental conditions specific to PTR-MS and SIFT-MS instruments. With some caveats, the models suitable for particular experimental conditions have been discussed below.

6.5.1 Thermal Conditions

The IMRs involving polar molecules were studied in detail using ADO theory. The ADO theory provide much-required information about temperature dependence and kinetic energy dependence of rate coefficients in close agreement to experiments. At thermal conditions ADO rate coefficients best fit with experimental conditions for PTR-MS and more preferably to SIFT-MS instrument. Various comparisons of the rate coefficients with experimental values have shown that ADO underestimate the rates typically by 10–20% seems pretty good considering the fact that the dipole moment and polarizability values calculated with theoretical methods may incur some errors [27, 28].

A much more refined model based on the classical trajectory method later presented by Su et al. produces thermal rate coefficients with margin of error $\sim$3% to experimental rate coefficients [29]. This model was successful for evaluating rates at thermal as well as very low-temperature limits. In practice, at thermal conditions both for PTR-MS and SIFT-MS, ADO results should be considered where experimental values are not known. However, at very low and high-temperature conditions typical to SIFT-MS, the classical trajectory method should be preferred. Appropriate DFT functionals should be used, preferably hybrid with large basis sets, to calculate dipole moment and polarizability values to minimize the error where experimental values are not available.

6.5.2 High-Temperature Conditions

It is usually assumed that rate coefficients obtained at room temperature using SIFT-MS are suitable for PTR-MS instrument. Often flow tube kinetics are employed for quantitative analysis in PTR-MS. This is strictly not recommended since collisions inside PTR-MS drift tube could be more energetic due to the applied electric field. As a result, the temperature inside the drift tube could be much higher even more than 1000 K. Equation (2.6) can be used to estimate the effective ion translational temperature. With the varying electric field (E/N) the effective temperature may increase to higher values as estimated in Table 6.1 and 6.2. Thereby, for varying field and effective temperature conditions in the PTR-MS instrument, the recommended model to calculate rate coefficients should be the parameterized trajectory method within the kinetic energy dependence approach. This model gives capture rate coefficients within 5% error for ion-molecule systems with center-of-mass kinetic energies ranging from thermal to several eV and temperatures ranging from 50 K to 1000 K [30]. We have provided extensive information on rate coefficients under different experimental conditions in [31].

6.6 Summary

The rate coefficients for proton transfer of H_3O^+ and NH_4^+ ions and charge exchange IMRs of NO^+ and O_2^+ ions with cork-taint and off-flavor compounds in wine have been presented. We use ion-molecule collision models where dipole moment and polarizability of the neutral molecule are the input ingredients. The basic collision model, Langevin model, largely underestimate the corresponding experimental values and yields low rate coefficients. With ADO theory, one can predict capture rate coefficients fairly accurately for many ion-molecule encounters. Although, much less experimental results for these particular classes of compounds are available. The predicted rate coefficients agree quite closely with the available rate coefficients as reported in the tables. Various theoretically reported data have established that ADO generally underestimate experimental values close to 10–20%. While the classical trajectory method predicts rates within 3% of error.

The ADO theory was successful for predicting thermal rate coefficients whereas the trajectory method made significant progress in predicting rates at the various temperatures ranging from 1 K to 1000 K as well as the kinetic energy dependency has been predicted. We have provided data for the rate coefficients at effected temperature conditions as confronting in PTR-MS with varying electric fields. Both PTRs and charge exchange reactions rate coefficients are listed in the corresponding tables. It is known that various experimental complexities that limit the quantitative analysis are: availability of kinetic data, appropriate gas standards, an accurate estimation of elevated temperature conditions. Due to the insufficiency of experimental data for cork-taint and off-flavor compounds reaction kinetics, this database will certainly incentivize research in the field of wine research.

Bibliography

[1] J. H. Futrell and F. P. Abramson. *Effect of Translational Energy on Ion-Molecule Reaction Rates*, volume 58, chapter 8, pages 107–130. 1967.

[2] W. L. Hase. *Dynamics of Ion-Molecule Complexes*. Elsevier, 2016.

[3] J. Meyer and R. Wester. Ion-Molecule Reaction Dynamics. *Annual Review of Physical Chemistry*, 68(1):333–353, 2017.

[4] A. G. Harrison. *Chemical Ionization Mass Spectrometry, Second Edition*. Taylor & Francis, 2017.

[5] D. K. Böhme. Ion-molecule reactions in mass spectrometry. In John C. Lindon, George E. Tranter, and David W. Koppenaal, editors, *Encyclopedia of Spectroscopy and Spectrometry*, pages 338–346. Academic Press, Oxford, 3 edition, 2017.

[6] P. Španěl, T. Wang, and D. Smith. A selected ion flow tube, SIFT, study of the reactions of H_3O^+, NO^+ and O_2^+ ions with a series of diols. *International Journal of Mass Spectrometry*, 218(3):227–236, 2002.

[7] L. Iachetta, L. Malek, and B. M. Ross. The reactions of H_3O^+, NO^+ and O_2^+ with

several flavourant esters studied using Selected Ion Flow Tube Mass Spectrometry. *Rapid Communications in Mass Spectrometry*, 24(6):815–822, 2010.

[8] D. Smith, T. Chippendale, and P. Spanel. Selected ion flow tube, SIFT, studies of the reactions of H_3O^+, NO^+ and O_2^+ with some biologically active isobaric compounds in preparation for SIFT-MS analyses. *International Journal of Mass Spectrometry*, 303:81–89, 06 2011.

[9] *Experimental: Components and Principles*, chapter 3, pages 49–109. John Wiley & Sons, Ltd, 2013.

[10] D. Smith and P. Španěl. On–line measurement of the absolute humidity of air, breath and liquid headspace samples by Selected Ion Flow Tube Mass Spectrometry. *Rapid Communications in Mass Spectrometry*, 15(8):563–569, 2001.

[11] P. Spanel and D. Smith. SIFT studies of the reactions of H_3O^+, NO^+ and O_2^+ with a series of alcohols. *International Journal of Mass Spectrometry and Ion Processes*, 167–168:375–388, 1997.

[12] D. Smith and P. Španěl. SIFT-MS and FA-MS methods for ambient gas phase analysis: developments and applications in the UK. *Analyst*, 140:2573–2591, 2015.

[13] T. Su. Erratum: Trajectory calculations of ion-polar molecule capture rate constants at low temperatures [j. chem. phys. 88, 4102 (1988)]. *The Journal of Chemical Physics*, 89(8):5355–5355, 1988.

[14] Timothy Su and Michael T. Bowers. Parameterization of the average dipole orientation theory: temperature dependence. *International Journal of Mass Spectrometry and Ion Processes*, 17(2):211–212, June 1975.

[15] S. T. Arnold, J. M. Thomas, and A. A. Viggiano. Reactions of $H_3O^+(H_2O)_n$ and $H^+(H_2O)_n(CH_3COCH_3)_m$ with CH_3SCH_3. *International Journal of Mass Spectrometry*, 179–180:243–251, 1998.

[16] S. T. Arnold, A. A. Viggiano, and R. A. Morris. Rate constants and product branching fractions for the reactions of H_3O^+ and NO^+ with C_2–C_{12} alkanes. *The Journal of Physical Chemistry A*, 102(45):8881–8887, 1998.

[17] N. Schoon, C. Amelynck, L. Vereecken, H. Coeckelberghs, and E. Arijs. A selected ion flow tube study of the reactions of H_3O^+, NO^+ and O_2^+ with some monoterpene oxidation products. *International Journal of Mass Spectrometry*, 239(1):7–16, 2004.

[18] C. Amelynck, N. Schoon, T. Kuppens, P. Bultinck, and E. Arijs. A selected ion flow tube study of the reactions of H_3O^+, NO^+ and O_2^+ with some oxygenated biogenic volatile organic compounds. *International Journal of Mass Spectrometry*, 247(1):1–9, 2005.

[19] M. T. Bowers, T. Su, and V. G. Anicich. Theory of ion-polar molecule collisions. kinetic energy dependence of ion-polar molecule reactions: $CH_3OH^+ + CH_3OH \longrightarrow CH_3OH_2^+ + CH_3O$. *The Journal of Chemical Physics*, 58(11):5175–5176, 1973.

[20] T. Su and M. T. Bowers. Theory of ion–polar molecule collisions. comparison with experimental charge transfer reactions of rare gas ions to geometric isomers of difluorobenzene and dichloroethylene. *The Journal of Chemical Physics*, 58(7):3027–3037, 1973.

[21] J. V. Dugan. A useful approximation and simple scaling laws for predicting ion-dipole capture cross sections and rate coefficients. *Chemical Physics Letters*, 21(3):476–482, 1973.

[22] W. Lindinger, D. L. Albritton, F. C. Fehsenfeld, A. L. Schmeltekopf, and E. E. Ferguson. Flow-drift tube measurements of kinetic energy dependences of some exothermic proton transfer rate constants. *The Journal of Chemical Physics*, 62(9):3549–3553, 1975.

[23] H. I. Schiff and D. K. Bohme. Flowing afterglow studies at York University. *International Journal of Mass Spectrometry and Ion Physics*, 16(1):167–189, 1975.

[24] T. Mikoviny, L. Kaser, and A. Wisthaler. Development and characterization of a high-temperature proton-transfer-reaction mass spectrometer (HT-PTR-MS). *Atmospheric Measurement Techniques*, 3, 01 2010.

[25] N. G. Adams and L. M. Babcock. *Advances in Gas Phase Ion Chemistry*, volume 1 of *Advances in Gas Phase Ion Chemistry*. JAI Press, 1992.

[26] *Experimental: Components and Principles*, chapter 3, pages 49–109. John Wiley & Sons, Ltd, 2013.

[27] G. I. Mackay, K. Tanaka, and D. K. Bohme. Rate constants at 297 K for proton-transfer reactions with C_2H_2: An assessment of the average quadrupole orientation theory. *International Journal of Mass Spectrometry and Ion Physics*, 24(2):125–136, 1977.

[28] T. Su and M. T. Bowers. Ion-polar molecule collisions: the effect of ion size on ion-polar molecule rate constants; the parameterization of the average-dipole-orientation theory. *International Journal of Mass Spectrometry and Ion Physics*, 12(4):347–356, 1973.

[29] T. Su and W. J. Chesnavich. Parametrization of the ion-polar molecule collision rate constant by trajectory calculations. *The Journal of Chemical Physics*, 76(10):5183–5185, 1982.

[30] T. Su. Parametrization of kinetic energy dependences of ion-polar molecule collision rate constants by trajectory calculations. *The Journal of Chemical Physics*, 100(6):4703–4703, 1994.

[31] M. Bhatia, F. Biasioli, L. Cappellin, P. Piseri, and N. Manini. Ab initio calculation of the proton transfer reaction rate coefficients to volatile organic compounds related to cork taint in wine. *Journal of Mass Spectrometry*, 55(11):e4592, 2020.

7

Thermodynamic and Chemical Reactivity Descriptors

7.1 Introduction

Electronic structure methods have been the forefront methods in the calculations of many molecular properties. The majority of the chemical and physical properties of a molecule can be defined by the response functions [1–3]. DFT methods provide an efficient way to calculate response properties of the system to the change in the independent variable. Usually, reactivity parameters are connected with these response functions and can be represented by derivatives of electronic properties. DFT methods within the Born–Oppenheimer approximation, allow calculating the Hamiltonian operator which interns determine the

properties of the system. Most of the properties may be defined as the response of a wave function, energy or expectation value of an operator to a perturbation, where the perturbation may be of any type for example electric field, magnetic field, and change in the molecular geometry.

There are mainly three methods to calculate the perturbation effects viz derivative methods, perturbation based on energy, and perturbation theory based on expectation values of properties. The derivative methods are very handy in calculating the response functions. In this chapter, we discuss different molecular properties such as hardness, softness, electronic chemical potential, electronegativity, and electrophilic index obtained from the response of the energy and chemical potential to the number of electrons [4–6]. The interconnection between HOMO-LUMO energy gap to the molecular properties established by Koopmans is also being explored [7]. That sort of treatment, reactivity parameters calculation, can be used to follow the reaction mechanism a short part of the whole reaction pathway. Further, it can be useful to predict relative reactivity based on the properties of the reactants.

7.2 HOMO-LUMO Analysis

The study of HOMO-LUMO orbitals of any system is one of the essential parts of molecular dynamic calculations [8, 9]. The HOMO-LUMO orbitals are also known as frontier molecular orbitals due to their location at the outermost boundary of the electrons in a molecule. The information about frontier molecular orbitals is vital in any molecular system for its chemical stability and reactivity point of view. The energy gap between HOMO-LUMO orbitals ($\varepsilon_{\text{HOMO}}$-$\varepsilon_{\text{LUMO}}$) determines the molecular reactivity [7, 10, 11]. It is also a measure of the excitability of a molecule such that electron can easily be excited from HOMO to LUMO when $\varepsilon_{\text{HOMO}}$-$\varepsilon_{\text{LUMO}}$ gap is small. In other words, eventual charge-transfer interaction within the molecule occurs more frequently as compared to the molecules with large $\varepsilon_{\text{HOMO}}$-$\varepsilon_{\text{LUMO}}$ gap. Thus, larger the energy gap lower will be the chemical reactivity of a molecule because the situation will be unfavorable to add an electron to high lying LUMO and similarly removing an electron from low lying HOMO states. The formation of an activated complex of any potential reaction can be easily achieved in

low energy gap systems in comparison to systems with a large energy gap. The DFT method with 6-31+(d,p) basis set is used to compute $\varepsilon_{\text{HOMO}}$-$\varepsilon_{\text{LUMO}}$ energy gap and obtained results are listed in the Table 7.1.

7.3 Measures of Chemical Reactivity

Usually, reactivity parameters have been associated with the response of the electronic properties of the system to the changes in the independent variables. Then the reactivity parameters are identified with response functions and they are represented by derivatives of electronic properties. The parameters obtained from the response functions are called global reactivity parameters because they determine the collective chemical reactivity of the molecule as a whole. The global reactivity parameters like chemical hardness (η), chemical softness (σ), chemical potential (μ), and electrophilic index (ω) have been addressed below.

7.3.1 Chemical Hardness

Chemical hardness is one of the important properties that helps in determining the chemical reactivity of a molecule. It is the response of the chemical potential to the change in the number of electrons and represented by

$$\eta = \left(\frac{\partial^2 \mathrm{E}}{\partial \mathrm{N}^2}\right)_{v(\vec{r})} = \left(\frac{\partial \mu}{\partial \mathrm{N}}\right)_{v(\vec{r})}. \tag{7.1}$$

In terms of $\varepsilon_{\text{HOMO}}$-$\varepsilon_{\text{LUMO}}$ energy, η can be expressed as,

$$\eta = \frac{1}{2}\left(\mathrm{I} - \mathrm{A}\right), \tag{7.2}$$

where I $\approx$ -$\varepsilon_{\text{HOMO}}$ and A $\approx$ -$\varepsilon_{\text{LUMO}}$ as approximated using Koopmans theorem [7]. Generally, molecules with large $\varepsilon_{\text{HOMO}}$-$\varepsilon_{\text{LUMO}}$ energy gap have high hardness values as compared to low energy gap molecules. Due to the large energy gap, charge transfer interactions are much more difficult and makes the molecules chemically less active. A hard

molecule thus has a large HOMO-LUMO gap, and is expected to be chemically nonreactive, i.e. hardness is directly associated with the chemical stability. A high η value corresponds to how hard the molecule is for chemical reaction to take place. If the electron transfer or rearrangement is necessary for the reaction to take place hard molecules are less reactive or nonreactive. Hard molecules are very difficult to polarize as a result these molecules possess small polarizability values as can be seen from the calculations in Table 7.1. We observed that molecules such as pentabromoohenol and rotundone have high polarizability values and accordingly low chemical hardness values.

7.3.2 Chemical Softness

The softness, inverse of chemical hardness, is a property of any molecule attributed to the $\varepsilon_{\text{HOMO}}$-$\varepsilon_{\text{LUMO}}$ energy gap within the molecules. Softness (σ) of the molecule is defined as

$$\sigma = \frac{1}{2\eta}\,. \tag{7.3}$$

Molecules with a smaller energy gap $\varepsilon_{\text{HOMO}}$-$\varepsilon_{\text{LUMO}}$ would exhibit eventual charge-transfer interactions, to add an electron to a high lying LUMO and to remove an electron from low lying HOMO, taking place within the molecule generally responsible for the bioactivity of the molecules and therefore favors activated complex formation in any potential chemical reaction. A small HOMO-LUMO gap indicates a soft molecule. It can be followed from second-order perturbation theory that a small gap between occupied and unoccupied orbitals will give a large contribution to the polarizability, i.e. softness is a measure of how easily the electron density can be distorted by external fields, for example, generated by another molecule. Our computed values of σ for the respective molecules are listed in the Table 7.1.

7.3.3 Chemical Potential

An important concept that can be connected with DFT is the electronic chemical potential μ given by the first derivative of the energy E with respect to the number of electrons N.

$$\mu = \left(\frac{\partial \mathrm{E}}{\partial \mathrm{N}}\right)_{v(\vec{r})} , \tag{7.4}$$

In terms of ionization potential and electron affinity,

$$\mu = -\frac{1}{2}\left(\mathrm{I}+\mathrm{A}\right). \tag{7.5}$$

$$\mu = \frac{1}{2}\left(\varepsilon_{\mathrm{LUMO}} + \varepsilon_{\mathrm{HOMO}}\right) . \tag{7.6}$$

Equation (7.6) represents μ in terms of HOMO-LUMO energy. It can also be written in terms of electronegativity (Mullikens electronegativity) [12], (χ = -μ). The χ value determines whether a given molecule is a Lewis acid or base. Large χ corresponds to acids while small χ represents bases. It helps to establish the fact that in molecules electron will be partially transferred from low electronegativity to high electronegativity (χ) (electron from high chemical potential to low chemical potential) values. It should be noted that there are several other definitions of electronegativity, which do not necessarily agree on the ordering of the elements.

7.3.4 Electrophilic Index

Knowing the nucleophilic site (highly electrons concentrated region) and electrophilic site (probable electrons attachment site) permits us to predict different available sites where the reagent can attack a molecule. One molecule may have several such acid or basic sites. The electrophilic index [13] in the present context is important to identify available sites for proton transfer to the particular molecule of interest. The global electrophilic index, which measures the energy stabilization in the system on acquiring additional charge, can be written in terms of chemical hardness η and electronic chemical potential μ, electrophilic

index (ω) of the molecule,

$$\omega = \frac{\mu^2}{2\eta} \quad \text{or} \quad \omega = \mu^2\sigma\,. \tag{7.7}$$

The electrophilic index represents two characteristics from the above equation: first, the propensity of the electrophile to acquire additional electronic charge as given by the square of the electronegativity (chemical potential in terms of electronegativity, χ = -μ) and resistance of the system to exchange the electronic charge as represented by η. Hence, the characteristics of a good electrophile are: a high value of μ and a low value of η. From the listed values of η, μ and ω from the Table 7.1, it is worth noting that the molecules such as pentachlorophenol, pentabromophenol, cis-1,5-octadien-3-one and 1-octen-3one are among many other compounds investigated contain high values of μ and low values of η ultimately increasing ω that makes them good electrophiles. Moreover, the molecules for instance guaiacol and 4-ethylguiaicol are the least electrophiles among the listed compounds.

7.4 Comparison and Validation

7.4.1 Chemical Hardness vs Polarizability

Conceptual DFT has been very successful in predicting various aspects of chemical bonding and reactivity of the molecules based on response functions. Basically these functions are the response of the chemical system upon some perturbations by the number of electrons, external chemical potential, and other external forces. For example, chemical potential (μ) and hardness (η) appear to the response of an atom or molecule to the change in the number of electrons at the fixed external potential. On a similar note, the response function corresponds to the change in external potential at a fixed number of electrons determines polarizability. The relation between these two different response functions (change in N and v(r)) through DFT and efficient schemes have been very popular in establishing an inverse connection between polarizability and chemical hardness [14].

The principle of maximum hardness and minimum polarizability has been widely as-

sociated with greater molecular stability. Pearson stated that the molecular systems at equilibrium tend to acquire the state of maximum hardness [15]. On the basis of inverse relationship between hardness and polarizability, Chattaraj and Sengupta stated that the natural evolution of any system is towards a state of minimum polarizability [16]. Our calculated results on hardness and polarizability follow the maximum hardness and minimum polarizability principle for a large number of compounds. Clearly, there is breakdown in MHP and MPP especially for some aromatic compounds. Recently, an in-depth review of MHP and MPP breakdown was provided in the bond length alternation (BLA) mode of molecules such as benzene and pyradine [17]. BLA distortions in aromatic rings lead to the reduction of delocalization of the π-electron and consequently the polarizability of the molecule. As a result, non totally symmetric BLA vibrational modes should disobey the MPP and, likely, the MHP. The breakdown of MPP is an indicator of the most aromatic center in the molecule. A detailed review of MHP and MPP, those interested in further reading, can be found in many reports [17, 18].

7.4.2 Ionization Energy by Koopmans Theorem

One way to calculate IE of a molecular system has been discussed in chapter 5. Another way to calculate IE within the 'frozen molecular orbital' approximation simply given by the orbital energy known as Koopmans theorem [7]. In Koopmans approximation, originally applied in HF theory, if orbitals of the system are unaffected by loss of electron then the vertical ionization energy[1] of an electron is given by the negative of the HOMO energy ($I_i \approx -\varepsilon_i$). However, implementing Kohn-Sham orbitals ($I_i \approx -\varepsilon_{\text{highest,KS}}$) to the higher level of accuracy has been a subject of considerable analysis and discussion agreed by many authors [19, 20] and concern for others [21, 22]. In practice, it has been found that HF and typical Kohn–Sham procedures using hybrid functionals produce valence orbital energies having magnitudes that tend to be larger and smaller, respectively, than the experimental

[1]For vertical transitions, both energies are computed for the same geometry, optimized for the starting state. For adiabatic potentials, the geometry of both ions is optimized.

ionization energies of the electrons.

$$|\varepsilon_{i,\mathrm{KS}}| < \mathrm{IE} < |\varepsilon_{\mathrm{i,HF}}|\,. \tag{7.8}$$

It is worth mentioning that our computed IE_i energies (= -$\varepsilon_{\mathrm{HOMO}}$) as listed in the Table 7.1 were lower by $\approx$ 1 to 1.5 eV than those obtained from equation (5.6) listed in the Table 5.3. However, the reported theoretical results of $|\varepsilon_{i,\mathrm{KS}}|$ deviate more than $|\varepsilon_{i,\mathrm{HF}}|$ to IE, usually fall below 2 to 3 eV (with BP86, B3PW91, etc.) [23]. We have reported improved results using B_3LYP $\approx 1-1.5$ eV deviation when compared with the IE from Table 7.1. Interestingly, (IE - IE_i) difference fairly uniform for all of the valence orbitals in the molecules, suggesting that the error is somewhat systematic around 14% in the calculations.

7.5 Enthalpy Change of the Reaction

The enthalpy change of any reaction is a decisive factor that determines whether a reaction can occur or not. The negative enthalpy change indicates that the reaction is exothermic and thermodynamically feasible. Thermodynamic parameters (free energy and enthalpy of the reaction) are important to understand the interactions of binding partners. Considering reaction dynamics, both sign and magnitude become crucial in order to express the likelihood of any bi-molecular reaction to proceed.

The enthalpy change of charge transfer reaction of NO^+ and O_2^+ ions with targeted cork-taint molecules are listed in Table 7.2. The negative values represent that the binding will occur spontaneously without any extra energy loss and the reaction will proceed through exothermic charger transfer. Greater negative values of ΔH also indicate improved thermodynamic properties. All the listed molecules show negative ΔH, indicative of exothermic reactions with NO^+ and O_2^+ ions occurring in SIFT-MS flow tube. Since ion-molecule reactions in the flow (drift) tube are exceedingly of complex nature, thermodynamic parameters are indispensable in determining the nature of the reaction and reaction products in PTR-MS and SIFT-MS flow (drift) tubes.

Table 7.1: Computed chemical reactivity parameters: energy of frontier molecular orbitals (ε_{HOMO}, ε_{LUMO}), hardness (η), softness (σ), chemical potential (μ), and electrophilic index (ω) of cork-taint molecules in gas phase. (Note: all quantities are in eV).

Molecule name	ε_{HOMO}	ε_{LUMO}	η	σ	μ	ω
2,4,6-Trichloroanisole ($C_7H_5Cl_3O$)	-7.0994	-1.3660	2.8667	0.1747	-4.2327	3.1248
2,4,6-Tribromoanisole ($C_7H_5Br_3O$)	-6.9906	-1.4013	2.7946	0.1789	-4.1959	3.1500
Pentachlorophenol (C_6Cl_5OH)	-7.3715	-1.7741	2.7986	0.1786	-4.5728	3.7358
Pentabromophenol (C_6Br_5OH)	-7.1647	-2.3129	2.4258	0.2061	-4.7388	4.6285
2,4,6-Trichlorophenol ($C_6H_2Cl_3OH$)	-7.1620	-1.3306	2.9157	0.1714	-4.2463	3.0921
2,4,6-Tribromophenol ($C_6H_2Br_3OH$)	-7.0668	-1.4422	2.8122	0.1777	-4.2545	3.2181
2,3,4-Trichloroanisole ($C_7H_5Cl_3O$)	-6.6042	-1.1836	2.7102	0.1844	-3.8939	2.7973
2,3,6-Trichloroanisole ($C_7H_5Cl_3O$)	-7.0450	-1.1836	2.9306	0.1706	-4.1143	2.8880
2,3,4,5-Tetrachloroanisole ($C_7H_4Cl_4O$)	-6.7783	-1.3687	2.7048	0.1848	-4.0735	3.0674
2,3,4,6-Tetrachloroanisole ($C_7H_4Cl_4O$)	-7.1321	-1.5075	2.8122	0.1777	-4.3198	3.3177
2,3,5,6-Tetrachloroanisole ($C_7H_4Cl_4O$)	-7.1348	-1.4340	2.8503	0.1754	-4.2844	3.2199
2,4-Dichloroanisole ($C_7H_6Cl_2O$)	-6.4354	-1.0394	2.6980	0.1853	-3.7374	2.5887

Table 7.1: continued

Molecule name	ε_{HOMO}	ε_{LUMO}	η	σ	μ	ω
2,6-Dichloroanisole ($C_7H_6Cl_2O$)	-7.0967	-0.9877	3.0544	0.1636	-4.0422	2.6747
Cis-1,5-octadien-3-one ($C_8H_{12}O$)	-6.7674	-1.9428	2.4122	0.2072	-4.3551	3.9314
Cis-1,5-octadien-3-ol ($C_8H_{14}O$)	-6.9144	-0.3646	3.2748	0.1526	-3.6395	2.0223
1-Octene-3-ol ($C_8H_{16}O$)	-7.3443	-0.3918	3.4762	0.1438	-3.8681	2.1520
1-Octene-3-one ($C_8H_{14}O$)	-7.0640	-1.9456	2.5592	0.1953	-4.5048	3.9647
Octanal ($C_8H_{16}O$)	-7.1321	-1.0748	3.0286	0.1650	-4.1034	2.7798
2-Sec-butyl-3-methoxypyrazine ($C_9H_{14}N_2O$)	-6.6395	-1.3986	2.6204	0.1908	-4.0191	3.0821
3-Iso-butyl-2-methoxypyrazine ($C_9H_{14}N_2O$)	-6.6314	-1.4095	2.6109	0.1915	-4.0204	3.0955
2-Iso-propyl-3-methoxypyrazine ($C_8H_{12}N_2O$	-6.6423	-1.4068	2.6177	0.1910	-4.0245	3.0937
2-Methoxy-3,5-dimethylpyrazine ($C_7H_{10}N_2O$)	-6.4028	-1.2353	2.5837	0.1935	-3.8191	2.8226
2-Methylisoborneol ($C_{11}H_{20}O$)	-7.2844	-0.0489	3.6177	0.1382	-3.6667	1.8581
Geosmin ($C_{12}H_{22}O$)	-7.0804	-0.1360	3.4721	0.1440	-3.6082	1.8748
Guaiacol ($C_7H_8O_2$)	-5.9048	-0.2149	2.8449	0.1757	-3.0599	1.6455
4-Ethylguaiacol ($C_9H_{12}O_2$)	-5.6735	-0.2204	2.7265	0.1833	-2.9469	1.5926

Table 7.1: continued

Molecule name	ε_{HOMO}	ε_{LUMO}	η	σ	μ	ω
4-Ethylphenol ($C_8H_{10}O$)	-6.0871	-0.4489	2.8191	0.1773	-3.2680	1.8942
Eucalyptol ($C_8H_{10}O$)	-6.5171	-0.0408	3.2381	0.1544	-3.2789	1.6601
4-Ethylcatechol ($C_8H_{10}O_2$)	-5.8939	-0.3836	2.7551	0.1814	-3.1388	1.7879
4-Methylguaiacol ($C_8H_{10}O_2$)	-5.6762	-0.2340	2.7211	0.1837	-2.9551	1.6046
Rotundone ($C_{15}H_{22}O$)	-6.6259	-1.3605	2.6327	0.1899	-3.9932	3.0284
Geraniol ($C_{10}H_{18}O$)	-6.4082	-0.2857	3.0612	0.1633	-3.3470	1.8296
Hotrienol ($C_{10}H_{16}O$)	-6.0953	-0.8136	2.6408	0.1893	-3.4544	2.2593
Linalool ($C_{10}H_{18}O$)	-6.4463	-0.2857	3.0803	0.1623	-3.3660	1.8391
Nerol ($C_{10}H_{18}O$)	-6.6423	-0.2204	3.2109	0.1557	-3.4313	1.8334
$\alpha-$Terpineol ($C_{10}H_{18}O$)	-6.2096	-0.1795	3.0150	0.1658	-3.1946	1.6924
Indole (C_8H_7N)	-5.7388	-0.5659	2.5864	0.1933	-3.1524	1.9211
1-Methylindole (C_9H_9N)	-5.6001	-0.5523	2.5238	0.1981	-3.0762	1.8747
2-Aminoacetophenone (C_8H_9NO)	-5.8395	-1.6598	2.0898	0.2392	-3.7497	3.3640
2-Chloro-6-methylphenol (C_7H_7ClO)	-6.4436	-0.6449	2.8993	0.1724	-3.5442	2.1663
3-Octanone ($C_8H_{16}O$)	-6.8790	-0.6013	3.1388	0.1592	-3.7402	2.2283
Fenchone ($C_{10}H_{16}O$)	-6.5008	-0.6340	2.9333	0.1704	-3.5674	2.1692
Fenchol ($C_{10}H_{18}O$)	-7.1729	-0.1115	3.5306	0.1416	-3.6422	1.8786
Trans-2-octen-1-ol ($C_8H_{16}O$)	-6.8844	-0.2966	3.2939	0.1517	-3.5905	1.9569
Pentachloroanisole ($C_7H_3Cl_5O$)	-7.2600	-1.6517	2.8041	0.1783	-4.4558	3.5402

Table 7.2: Enthalpy change of charge transfer reactions: $NO^+(O_2^+)$+M $\longrightarrow$ M^+ + $NO(O_2)$. Where, M represents volatile organic compound related to cork-taint. ΔH is represented in kcal/mol.

Molecule name	ΔH	
	NO^+	O_2^+
2,4,6-Trichloroanisole ($C_7H_5Cl_3O$)	-38.1896	-64.4584
2,4,6-Tribromoanisole ($C_7H_5Br_3O$)	-40.8647	-67.1335
Pentachlorophenol (C_6Cl_5OH)	-31.9471	-58.2159
Pentabromophenol (C_6Br_5OH)	-37.8137	-64.0825
2,4,6-Trichlorophenol ($C_6H_2Cl_3OH$)	-26.9904	-53.2592
2,4,6-Tribromophenol ($C_6H_2Br_3OH$)	-30.9801	-57.2464
2,3,4-Trichloroanisole ($C_7H_5Cl_3O$)	-41.3447	-67.6135
2,3,6-Trichloroanisole ($C_7H_5Cl_3O$)	-36.1063	-62.2496
2,3,4,5-Tetrachloroanisole ($C_7H_4Cl_4O$)	-39.4496	-65.7184
2,3,4,6-Tetrachloroanisole ($C_7H_4Cl_4O$)	-36.6597	-62.9285
2,3,5,6-Tetrachloroanisole ($C_7H_4Cl_4O$)	-29.6561	-55.9249
2,4-Dichloroanisole ($C_7H_6Cl_2O$)	-43.6445	-69.9133
2,6-Dichloroanisole ($C_7H_6Cl_2O$)	-37.7616	-64.0304
Cis-1,5-octadien-3-one ($C_8H_{12}O$)	-36.0366	-62.3054
Cis-1,5-octadien-3-ol ($C_8H_{14}O$)	-38.9194	-65.1882
1-Octene-3-ol ($C_8H_{16}O$)	-24.8695	-51.1383
1-Octene-3-one ($C_8H_{14}O$)	-22.6506	-48.9194
Octanal ($C_8H_{16}O$)	-19.4773	-45.7461
2-Sec-butyl-3-methoxypyrazine ($C_9H_{14}N_2O$)	-38.6151	-64.8839

Table 7.2: continued

Molecule name	ΔH	
	NO^+	O_2^+
3-Iso-butyl-2-methoxypyrazine ($C_9H_{14}N_2O$)	-39.1114	-65.3802
2-Iso-propyl-3-methoxypyrazine ($C_8H_{12}N_2O$	-37.2615	-63.5303
2-Methoxy-3,5-dimethylpyrazine ($C_7H_{10}N_2O$)	-42.9254	-69.1942
2-Methylisoborneol ($C_{11}H_{20}O$)	-39.7904	-66.0592
Geosmin ($C_{12}H_{22}O$)	-37.5012	-63.7700
Guaiacol ($C_7H_8O_2$)	-52.2395	-78.3797
4-Ethylguaiacol ($C_9H_{12}O_2$)	-60.5327	-86.8015
4-Ethylphenol ($C_8H_{10}O$)	-47.7434	-74.0122
Eucalyptol ($C_8H_{10}O$)	-39.5915	-65.8603
4-Ethylcatechol ($C_8H_{10}O_2$)	-53.4663	-79.7351
4-Methylguaiacol ($C_8H_{10}O_2$)	-60.0621	-86.3309
Rotundone ($C_{15}H_{22}O$)	-41.9126	-68.1839
Geraniol ($C_{10}H_{18}O$)	-51.2211	-77.4899
Hotrienol ($C_{10}H_{16}O$)	-51.3171	-77.5859
Linalool ($C_{10}H_{18}O$)	-44.8105	-71.0793
Nerol ($C_{10}H_{18}O$)	-48.6577	-74.9265
$\alpha-$Terpineol ($C_{10}H_{18}O$)	-47.4742	-73.7430
Indole (C_8H_7N)	-55.8364	-82.1052

Table 7.2: continued

Molecule name	ΔH	
	NO^+	O_2^+
1-Methylindole (C_9H_9N)	-60.6982	-86.9590
2-Aminoacetophenone (C_8H_9NO)	-53.8033	-80.0721
2-Chloro-6-methylphenol (C_7H_7ClO)	-40.3062	-66.5447
3-Octanone ($C_8H_{16}O$)	-24.7427	-51.0115
Fenchone ($C_{10}H_{16}O$)	-38.5234	-64.7922
Fenchol ($C_{10}H_{18}O$)	-38.5172	-64.7860
Trans-2-octen-1-ol ($C_8H_{16}O$)	-34.1604	-60.4292
Pentachloroanisole ($C_7H_3Cl_5O$)	-34.6297	-60.8985

7.6 Summary

The chemical reactivity of the molecular systems of interest is calculated directly from the response functions. The ground state energy and chemical potential are certainly pivotal in any molecular system and many other molecular properties that can be calculated by electronic structure methods. Most of the chemical properties may be defined as the response of a wave function. In the DFT framework, we have predicted chemical reactivity descriptors such as HOMO-LUMO energy, electronegativity, hardness, and electrophilicity index of the molecules of interest. We have presented a brief overview of MHP and MPP principles and the instances where these principles fail. Although, most of the molecules in this work follow the MHP and MPP principles but there is a number of aromatic, π-conjugated, non-π-conjugated, or even non-π-bonded organic and inorganic molecules that possess non totally symmetric molecular distortions that not necessarily follow these two principles. More rigorous work is needed to be performed in order to obtain a comprehensive con-

clusion on the validity of hardness and polarizability principles. The IE values predicted by Koopmans frozen orbital method predicts IE fairly in agreement with as calculated in chapter 5 shows that the hybrid DFT functional B_3LYP performs better to obtain $\varepsilon_{i,\mathrm{KS}}$ IEs. Furthermore, the exothermicity of the charge transfer reactions has been predicted by calculating the enthalpy change of the reaction. These computed chemical properties are useful to predict and interpret the outcome of a potential chemical reaction.

Bibliography

[1] P. Geerlings, F. De Proft, and P. W. Ayers. Chapter 1 chemical reactivity and the shape function. In Alejandro Toro-Labbé, editor, *Theoretical Aspects of Chemical Reactivity*, volume 19 of *Theoretical and Computational Chemistry*, pages 1–17. Elsevier, 2007.

[2] P. Geerlings, F. De Proft, and W. Langenaeker. Conceptual Density Functional Theory. *Chemical Reviews*, 103(5):1793–1874, 2003.

[3] F. Jensen. *Introduction to Computational Chemistry*. Wiley, 2007.

[4] A. Cedillo. Chapter 2 density functional theory models of reactivity based on an energetic criterion. In Alejandro Toro-Labbé, editor, *Theoretical Aspects of Chemical Reactivity*, volume 19 of *Theoretical and Computational Chemistry*, pages 19–30. Elsevier, 2007.

[5] G. Makov. Chemical hardness in density functional theory. *The Journal of Physical Chemistry*, 99(23):9337–9339, 1995.

[6] R. G. Pearson. Chemical hardness and density functional theory. *Journal of Chemical Sciences*, 117(5):369–377, 2005.

[7] T. Koopmans. Ordering of wave functions and eigenvalues to the individual electrons of an atom. *Physica*, 1(1):104–110, 1934.

[8] V. Dixit and R. Yadav. DFT-B3LYP computations of electro and thermo molecular characteristics and mode of action of fungicides (Chlorophenols). *International journal of pharmaceutics*, 491, 07 2015.

[9] V. Balachandran, S. Rajeswari, and S. Lalitha. Vibrational spectral analysis, computation of thermodynamic functions for various temperatures and NBO analysis of 2,3,4,5-tetrachlorophenol using ab initio HF and DFT calculations. *Spectrochimica Acta Part A: Molecular and Biomolecular Spectroscopy*, 101:356–369, 2013.

[10] R. G. Pearson. Absolute electronegativity and hardness correlated with molecular orbital theory. *Proceedings of the National Academy of Sciences*, 83(22):8440–8441, 11 1989.

[11] M. Torrent-Sucarrat, L. Blancafort, M. Duran, J. M. Luis, and M. Solà. Chapter 3 the breakdown of the maximum hardness and minimum polarizability principles for non-totally symmetric vibrations. In Alejandro Toro-Labbé, editor, *Theoretical Aspects of Chemical Reactivity*, volume 19 of *Theoretical and Computational Chemistry*, pages 31–45. Elsevier, 2007.

[12] R. S. Mulliken. A new electroaffinity scale; together with data on valence states and on valence ionization potentials and electron affinities. *The Journal of Chemical Physics*, 2(11):782–793, 1934.

[13] P. Pérez, L. R. Domingo, A. Aizman, and R. Contreras. Chapter 9 the electrophilicity index in organic chemistry. In Alejandro Toro-Labbé, editor, *Theoretical Aspects of Chemical Reactivity*, volume 19 of *Theoretical and Computational Chemistry*, pages 139–201. Elsevier, 2007.

[14] M. Torrent-Sucarrat, L. Blancafort, M. Duran, J. M. Luis, and M. Solà. Chapter 3 the breakdown of the maximum hardness and minimum polarizability principles for non-totally symmetric vibrations. In Alejandro Toro-Labbé, editor, *Theoretical Aspects of Chemical Reactivity*, volume 19 of *Theoretical and Computational Chemistry*, pages 31–45. Elsevier, 2007.

[15] R. G. Pearson. Recent advances in the concept of hard and soft acids and bases. *Journal of Chemical Education*, 64(7):561, 1987.

[16] P. K. Chattaraj and S. Sengupta. Popular electronic structure principles in a dynamical context. *The Journal of Physical Chemistry*, 100(40):16126–16130, 1996.

[17] M. Torrent-Sucarrat, J. M. Luis, M. Duran, and M. Solà. The hardness profile as a tool to detect spurious stationary points in the potential energy surface. *The Journal of Chemical Physics*, 120(23):10914–10924, 2004.

[18] A. Toro-Labbe. *Theoretical Aspects of Chemical Reactivity*. ISSN. Elsevier Science, 2006.

[19] L. Kleinman. Significance of the highest occupied kohn-sham eigenvalue. *Physical Review B*, 56:12042–12045, 11 1997.

[20] M. K. Harbola. Relationship between the highest occupied Kohn-Sham orbital eigenvalue and ionization energy. *Physical Review B*, 60:4545–4550, 08 1999.

[21] D. P. Chong, O. V. Gritsenko, and E. J. Baerends. Interpretation of the Kohn-Sham orbital energies as approximate vertical ionization potentials. *The Journal of Chemical Physics*, 116(5):1760–1772, 2002.

[22] O. V. Gritsenko, B. Braïda, and E. J. Baerends. Physical interpretation and evaluation of the Kohn-Sham and Dyson components of the ε-I relations between the Kohn-Sham orbital energies and the ionization potentials. *The Journal of Chemical Physics*, 119(4):1937–1950, 2003.

[23] P. Politzer and J. S. Murray. Chapter 8 the average local ionization energy: concepts and applications. In A. Toro-Labbé, editor, *Theoretical Aspects of Chemical Reactivity*, volume 19 of *Theoretical and Computational Chemistry*, pages 119–137. Elsevier, 2007.

8

Conclusions

We study a total of 74 volatile compounds that play a very important role to maintain wine aroma and flavor and thus the wine quality. The compounds we investigated can be considered as a wine fault when present above their threshold limits and are not limited to wine, but commonly occur in other food items. We studied a broad class of volatile compounds which include: alcohols, esters, phenols, chloro and bromo-anisoles, aldehydes, and sulfur compounds causing cork-taint and off-flavor in wine. Direct injection mass spectrometry-based standard techniques such as PTR-MS and SIFT-MS are largely used for the identification and quantification of these compounds through IMRs usually occur in the drift tube. The absolute concentration of a compound can be obtained for the reaction of H_3O^+ to the VOCs concerned without the need for calibration if the reaction kinetics are already known.

We compute rate coefficients of the IMRs occurring in the drift or flow tubes. We use capture collision cross-section models to calculate rate coefficients of proton transfer and charge transfer reactions occur through the following reagent ions: H_3O^+, NH_4^+, NO^+ and O_2^+. These collision models need dipole moment and polarization for their implementation. We compute dipole moment and polarizability of the targeted molecules from the first principle calculations using DFT. First, we apply the Langevin model based on pure polarization theory to compute rate coefficients for IMRs. The Langevin model includes long-range ion-induced dipole interactions and generally considered suitable for low energy collisions, though it provides useful initial information for IMRs.

Then we considered ADO theory because it includes crucial temperature dependence of rate coefficients and ion-dipole interaction along with ion-induced dipole interaction. Here, we did not consider locked dipole theory because earlier studies have shown that it seriously overestimates the rate coefficients compared to experimental results. Our computed rate coefficients from ADO theory at 300 K were in good agreement with fewer available results. This shows that ADO results can be safely accepted for PTR-MS as well as SIFT-MS experiments at thermal conditions when experimental results are not available. We provide a large data for ADO rate coefficients for the IMRs with H_3O^+, NH_4^+, NO^+ and O_2^+ ions to the VOCs at thermal conditions.

However, the IMRs inside the PTR-MS drift tube are not the same as that at thermal conditions. Due to the applied electric field in PTR-MS the effective collisions are far more energetic than collisions at thermal conditions. Thereby, the effective temperature could be much higher than 300 K. In most of the cases the effective temperature could be higher than 1000 K. We computed the effective temperature dependence and kinetic energy-dependent rate coefficients using the parameterized classical trajectory method given by Su and Chesnavich. This model predicts rate coefficients even more accurately within 5% error on considering the energy from thermal to several eV and temperature ranging from 50 K to 1000 K. We computed rate coefficients for the similar IMRs but for center-of-mass kinetic energy and effective temperature conditions. Similarly for SIFT-MS working environment usually thermal, where temperature can vary from 80 K to 600 K in a typical SIFT-MS

instrument, we have obtained rate coefficients using ADO and classical trajectory calculations. All the calculations have been obtained for four reagent ions to the corresponding analyte molecules via proton transfer and charge transfer reactions. We have also made an in-depth investigation of the dependence of rate coefficients upon various parameters such as dipole moment, temperature, thermal energy, and center-of-mass kinetic energy.

We then proceed to study the PA and IE of the VOCs. The motive for this study was to determine the likelihood of the IMRs to proceed through proton transfer and charge transfer. Because they proceed via PTR from H_3O^+ or NH_4^+ to the neutral molecule only if the molecule possesses higher PA than the corresponding ion. And on a similar note, there will be effective charge transfer from ions NO^+ and O_2^+ if the neutral molecule has IE less than the corresponding ion. We report PAs and IEs of the molecules and observed that all the molecules possess sufficiently higher PAs in order to have effective PTRs. Likewise, IEs of all the investigated molecules are lower enough to have charge transfer reactions with the respective ions. However, applications of NH_4^+ and O_2^+ ions are limited due to their respective higher PA and IE values. We thoroughly studied and discussed their targeted areas of application.

Since we are dealing with IMRs, DFT offers an elegant way to predict and interpret the outcome of a chemical reaction in terms of the properties of the reactants. Having this in mind, we also studied and computed chemical reactivity parameters such as chemical hardness, chemical softness, chemical potential, electronegativity, and electrophilic index of the VOCs. The HOMO-LUMO energy gap determines these parameters owing to the Koopmans theorem. Chemical hardness and softness are the indicators of the chemical reactivity and stability of the molecules, whereas negative of the chemical potential (electronegativity) measures the resistance of the chemical species to deliver electrons. The electrophilic index determines the stability in energy when the molecule acquires an additional charge. The identification of the electrophilic and nucleophilic regions of the molecule is very useful in the prediction of the initial steps of chemical reactions.

The wine analysis, knowing concentration of individual components of a gas sample, using PTR-MS and SIFT-MS will provide a great deal of information about a wine and the

present results will help to improve the analytic outcome. After PTR-MS and SIFT-MS analysis of wine sample one can know the amount of alcohol by volume, the levels of free and total sulfur dioxide, total acidity, residual sugar, the amount of dissolved oxygen, and whether the wine contains disastrous spoilage compounds such as 2,4,6-trichloroanisole or 2,4,6-tribromoanisole in a wine. An effective strategy to track the presence of individual cork-taint compounds and their precursors (e.g. sodium hypochlorite, calcium chloride, chlorine, chloro- and bromo-phenols) at various stages during the winemaking and bottling process could involve PTR-MS and SIFT-MS applied to the individual involved vessels including barrels, bottles, and corks themselves. With a systematic application of these methods, the wine-taint concentration can be restricted below human sensory threshold.

Presently, a thorough analysis of the VOCs related to wine is absent, and limited experimental results are available in the literature for the reactions between our investigated ions and compounds responsible for cork-taint and off-flavor in wine. The rate coefficients calculated here will be useful for the PTR-MS and SIFT-MS quantitation, in the measurement of the concentrations of VOCs, in view of future wine-related analytic investigations. Our provided data will be useful in supporting rapid non-invasive quality control for cork-taint in wine. The database of reaction kinetics will serve as input for IMRs and will be useful to conduct experiments in PTR-MS/SIFT-MS and promote research in food science.

Furthermore, wine is a complex mixture of hundreds of compounds and the presence of excessive ethanol content in the wine (sample) head space depletes the H_3O^+ ions and hence the mass spectra. A large number of VOCs are still to be identified and calibrated. A limited data is known for IMR kinetics related to the reactions in wine components, especially ethanol clusters. Many useful reactions such as ion cluster formation and fragmentation are vital in PTR-MS and need intensive research. The numerical evaluations of physical and chemical properties of VOCs related to food and alcoholic beverages will help extending the role of mass spectrometry for quality and anti-fraud control in food science and industry.

Appendices

A

Determination of the Dipole Locking Parameter *C*

The dipole locking parameter C depends on the degree that the dipole is aligned with the ionic charge during the collision. C ranges between 0 (no-alignment) to 1 (locked dipole). The C parameter depends on the electric dipole moment μ_D and polarizability α of the neutral molecule. The parameter C is also a function of temperature. We extended the values for the dipole locking parameter C to temperatures in the 80 K–600 K range and to our computed values of $\mu_D/\sqrt{\alpha}$, based on the values computed and reported by Su [1] for a few temperatures in 150 K–500 K range. C values at 450 K in Figure (A.1) and 380 in Figure (A.2) are obtained by linear interpolation of corresponding published values between 150 to 500 K. In contrast, the values at 80 K and 600 K are obtained by linearly extrapolating the published C values relative to the two closest temperatures. See extrapolated data in Figures (A.1) and (A.2) below.

Bibliography

[1] T. Su and M. T. Bowers. Parameterization of the average dipole orientation theory: temperature dependence. *International Journal of Mass Spectrometry and Ion Processes*, 17(2):211–212, 06 1975.

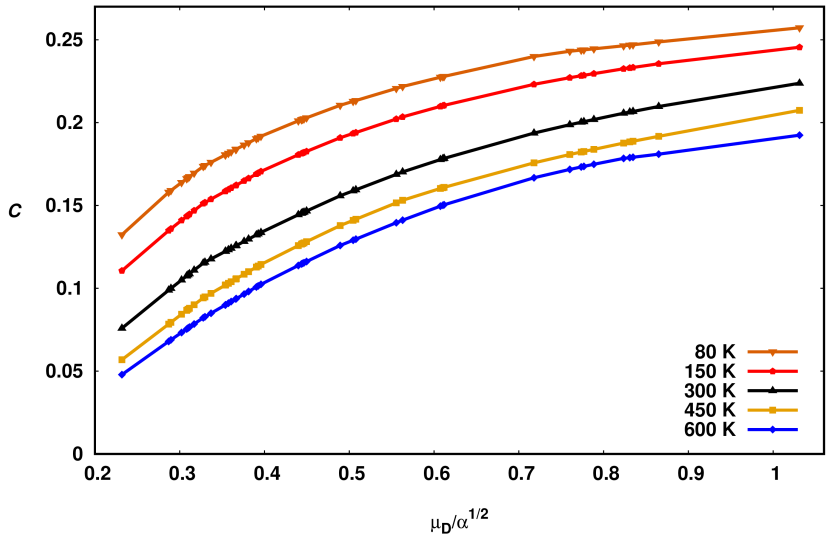

Figure A.1: The dipole locking constant C as a function of $\mu_D/\sqrt{\alpha}$ at temperatures 80 K to 600 K. The dipole moment and polarizability values are obtained by Gaussian.

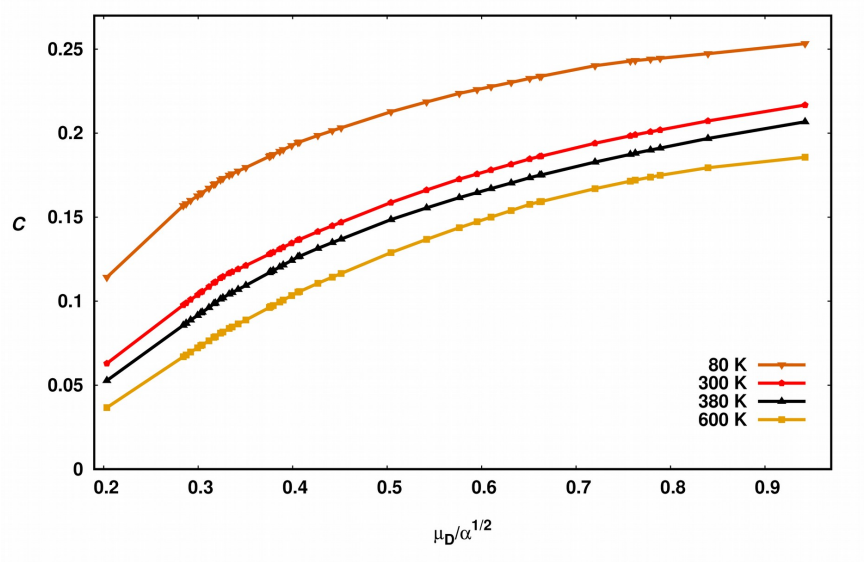

Figure A.2: Same as in A.1, except the dipole moment and polarizability values as obtained using QuantumEspresso.

List of Figures

List of Tables

List of Symbols

k_{ADO}	ADO rate coefficient, $10^{-9}cm^3s^{-1}$
k_{cap}	capture collision rate coefficient, $10^{-9}cm^3s^{-1}$
μ	chemical potential, eV
k_c	collision rate coefficient, $10^{-9}cm^3s^{-1}$
μ_D	dipole moment, Debye
v_d	drift velocity of ions, ms^{-1}
T_{eff}	effective temperature, K
ω	electrophilic index, eV
η	Hardness parameter, eV
k_{Lang}	Langevin rate coefficient, $10^{-9}cm^3s^{-1}$
α	polarizability, $Å^3$
τ	reaction time, μs
μ	reduced mass, a.m.u.
σ	softness parameter, eV

List of Publications

As of September 30, 2020

Refereed publications

1. M. Bhatia, F. Biasioli, L. Cappellin, P. Piseri and N. Manini. Ab initio calculation of the proton transfer reaction rate coefficients to volatile organic compounds related to cork taint in wine, *Journal of Mass Spectrometry*, **55(11)**, e4592, 2020.

Publications in preparation

1. M. Bhatia, N. Manini, F. Biasioli, L. Cappellin and P. Piseri, Reactivity of Compounds Causing Cork-taint andOff-flavor in Wine and Food: A DFT Evaluation.

2. M. Bhatia, F. Biasioli, L. Cappellin, P. Piseri and N. Manini, DFT study of SIFT-MS reactions of NO^+ and O_2^+ with cork-taint and off-flavour compounds in wine.

3. M. Bhatia, F. Biasioli, L. Cappellin, P. Piseri and N. Manini, Ab initio investigations of gas phase reactions of Sulfur compounds with H_3O^+, NH_4^+, NO^+ and O_2^+ ions in food and alcoholic beverages.

Conference Abstracts/Posters/Presentations

1. Manjeet Kumar, Luca Cappellin, Franco Biasioli, Paolo Piseri and Nicola Manini, Ab initio study of proton transfer reaction rates under PTR-MS/SIFT experimental conditions, *TUMIEE Training School*, Rethymno, Crete (Greece), 23 Sep-04 Oct 2019.

2. Manjeet Kumar, Franco Biasioli, Paolo Piseri and Nicola Manini, Ab initio study of proton transfer reaction between H_3O^+ ion and volatile organic compounds (VOCs) related to cork-taint in wine, *QUANTUM ESPRESSO Summer School on Advanced Materials and Molecular Modelling*, J. Stefan Institute, Ljubljana, Slovenia, 16-20 Sep 2019.

Schools/Workshops

1. *QUANTUM ESPRESSO Summer School on Advanced Materials and Molecular Modelling*, J. Stefan Institute, Ljubljana, Slovenia, 16-20 Sep 2019.

2. *TUMIEE Training School*, Rethymno, Crete (Greece), 23 Sep-04 Oct 2019.

3. *Introduction to Gaussian: Theory and Practice*, Hyderabad, India, 20-24 January 2020.

Acknowledgments

I would like to acknowledge my indebtedness and render my warmest thank to my supervisor, Professor Nicola Manini, who made this work possible. Your friendly guidance and expert advice have been invaluable for me throughout all stages of this work. Thank you for all the advice, ideas, moral support, and patience in guiding me through this project. Your worth of knowledge in the field of Physics of matter is inspiring. I have earned the greatest understanding of the research field during my Ph.D. period.

A special thank goes to my co-supervisors, Dr. Franco Biasioli and Professor Paolo Piseri, for providing me an opportunity to work on this interesting research project. Your guidance and support are exceptional throughout the research period. Thank you for creating various opportunities in the project and letting me work freely. I would like to express my heartful appreciation to Professor Paolo Piseri for arranging everything during my initial days in Milan. I also like to thank Dr. Franco Biasioli for arranging my trips and stay at Fondazione Edmund Mach (FEM), San Michele. I would like to acknowledge the training provided by Julia Khomenko on PTR-MS sample preparation and calibration. I like to thank the staff and researchers of FEM whom I interacted with.

This project is partially funded by FEM with the grant ADP-2018. I would like to thank the FEM, San Michelle for providing excellent working conditions and financial support.

I would also wish to express my gratitude to Professor Luca Cappellin for extended discussions and valuable suggestions that have contributed greatly to the improvement of my thesis.

This thesis has also benefited from comments and suggestions made by Dr. Jonathan Beauchamp and Professor Giorgio Benedek who have read through the manuscript. I take this opportunity to thank them.

My thanks are extended to the SSPTG group in Milan for stimulating discussions and helping me directly or indirectly during my years at the University of Milan. I would also like to express my thanks to the administrative staff of the Physics department, especially Andrea Zanzani for all the paperwork and administrative support.

Further, I would like to give special thanks to Dr. K. K. Panjaje and many other friends for inspiring me through my journey in research.

Last but not least, I would like to thank my parents for their unconditional love and support. Thank you for your constant encouragement and motivation.

Milan, November 30th, 2020
Manjeet Kumar